

POLITECNICO DI TORINO

Department of Structural, Geotechnical and Building Engineering



Master's Degree in Civil Engineering – Structures

**BUCKLING AND PROGRESSIVE COLLAPSE OF DIAGRID
SPACE STRUCTURES**

Supervisors:

Prof. Giuseppe Lacidogna

Dr. Gianfranco Piana

Candidate:

Gianluca Ferrigno

A.Y. 2024 – 2025

To Livia and my family

*Few joys are comparable to the one you feel when,
after a long wait, you finally reach the goal that
few thought you were capable of achieving.*

TABLE OF CONTENTS

ABSTRACT	7
1. INTRODUCTION.....	9
2. HISTORICAL ASPECTS OF HIGH-RISE BUILDINGS.....	11
3. FUNDAMENTAL PRINCIPLES OF HIGH-RISE BUILDING DESIGN	15
3.1 Site conditions	15
3.2 Material properties	16
3.3 Structural systems	16
3.4 Characteristics of the structural system and the effect of external forces.....	22
4. DIAGRID STRUCTURES	23
4.1 History of diagrid structures.....	23
4.2 Structural behaviour of a diagrid structure.....	25
4.3 Geometry-driven performance optimization of diagrid structures	28
4.4 Preliminary design of diagrid structures	54
4.5 Structural Analysis Methodologies for Diagrid Tall Buildings.....	61
4.5.1 Finite Element Method (FEM).....	61
5. REQUIREMENTS AND PRELIMINARY FRAMEWORK FOR DIAGRID MODEL DEVELOPMENT	77
5.1. Methodological Framework, Geometric and Structural Assumptions.....	77
5.2. Tall Building Strength and Stiffness Requirements	78
5.2.1. Compressive Strength	78
5.2.2. Buckling Critical Load	79
5.2.3. Tensile Strength	84
5.3. External Actions	84
5.3.1. Wind Load	84
5.3.2. ASCE 7-10 Procedure for Evaluating Wind Loads.....	85

5.4. Strength- and Stiffness-Based Preliminary Design	91
6. CRITICAL LOAD ANALYSIS AND PROGRESSIVE COLLAPSE OF DIAGRID SYSTEMS	97
6.1. Stability Analysis of Diagrid Members	97
6.2. Structural Stability Analysis, Conditions, and Verification Methods	100
6.3. Methodology	106
6.4. Validation of the Methodology	111
6.4.1. FEM Analysis Model and Assumptions	111
6.4.2. Results Comparison	112
7. RESULTS	119
7.1. Results Introduction	119
7.2. Results for Uniform-Angle Diagrid Systems	120
7.3. Results for Varying-Angle Diagrid Systems	129
7.4. Progressive Collapse Behavior of Uniform- and Varying-Angle Diagrid Systems: Insights from DCR Analysis	137
8. CONCLUSIONS	141
ACKNOWLEDGMENTS	143
REFERENCES	145

ABSTRACT

The growing demand for sustainable, efficient and aesthetically innovative tall buildings has led to the development of advanced structural systems. Among these, diagrid structures have emerged as a prominent solution due to their geometric efficiency, structural performance and architectural flexibility.

This thesis analyses the buckling behavior of spatial diagrid structures, focusing on their stability and resistance in the case of extreme situations, studied by means of a progressive collapse analysis to highlight the resilience of such structures. The following study involves the development of a model based on numerical analysis for the efficient and effective description of these behaviors. Thus, compared to existing methodologies based on the definition of the structure's shear and bending stiffness, and on finite element models, the proposed approach is based on the direct calculation of the structure's stiffness matrix. This methodology is named Matrix-Based Method (MBM) and was used as the foundation for the preliminary design of the structures to be analyzed. The relevant numerical procedure was implemented in a MATLAB code. In addition, the proposed model was validated using a FEM-based analysis, comparing the results obtained with theoretical predictions to ensure its accuracy and reliability. The results highlight the crucial role of stability analysis in the design of diagrid structures, demonstrating their ability to withstand significant compressive and tensile forces while maintaining structural integrity even under extreme conditions, in order to demonstrate the importance of geometry-based optimization to improve the performance of diagrid systems.

This thesis contributes to the field of structural engineering by providing an effective tool for the preliminary design and analysis of spatial diagrid structures, offering insights into their stability, efficiency and application potential in modern tall building architecture. The results provide a basis for future research and practical applications in the design of innovative and resilient buildings.

1. INTRODUCTION

The advent of tall buildings became one of the major features of urban places starting in the late 1800s, especially in the United States. In the early days of skyscrapers, taller buildings relied on conventional moment-resisting frame systems, but as these buildings got taller, several limitations arose, in part from structural efficiency and part as a result of resource consumption. This created an opportunity for change in tall building design, and one of the major innovations in this field is the diagrid system, which is a triangulated system of steel or concrete members that efficiently transfer gravity loads and lateral loads in ways which minimize the use of the internal vertical columns, making space on the floors available for other purposes, and providing for greater architectural flexibility [1].

Additionally, the new diagrid system uses less material than an equivalent frame system, allowing for lighter and slender structural members. As less material is used (reducing construction costs) and the amount of material needed to produce, transport and assemble is less, then the lower is the environmental impact.

However, looking at tall buildings, it is common to find that they need complex models in order to look at the structural behavior under loads. The Matrix-Based Method (MBM) procedure, can be a very useful thing to make some design alternatives and to use in place of complex models to see changes in the structural behavior of diagrid systems, in a simplified and fairly accurate form [30]. MBM can be used to easily assess the axial forces of the members and the displacements of the structure. However, apparently no current MBM method has yet included the determination of critical load factors for buckling or progressive collapse analysis. Therefore, the main purpose of this study is to extend the MBM framework so that either or both of these can be analyzed for a better understanding of the stability and resilience of diagrid systems. In addition, some of the diagrid systems that will be analyzed in this study are based on a multi-response framework approach that also uses the MBM framework [26], meaning that the chosen diagrid configurations will also fit with the MBM core framework in this study. By analyzing these outcomes, the modeled and assessed configurations would then be consistent with the same method applied in this study, reinforcing its consistency.

The results of the study show the potential use of the extended MBM framework so that it can accurately assess critical load factors as well as the progressive collapse behaviors of diagrid structures, with the validation of the results from a three-dimensional FEM based analysis. By establishing the advanced analysis capabilities of the MBM framework to make sure there is continuity between the preliminary design and analysis methods, this study makes a significant contribution to the study of structural engineering, which would advocate for establishing a strong methodical framework for the design and analysis of diagrid systems, which can establish stability, resilience and also could be applied and explored in the development of innovative, sustainable, resilient tall buildings.

2. HISTORICAL ASPECTS OF HIGH-RISE BUILDINGS

Modern tall buildings were born in the 19th century in the United States of America, but ancient civilizations had already conceived the idea of tall buildings, such as the Egyptian pyramids, the Mesopotamian Ziggurat and the Tower of Babel, all monumental structures that far exceed the height of the average buildings of the time. These structures symbolized power and grandeur, reflecting the ambitions of those who commissioned them [2].



Figure 1: Pyramids of Gyzah [43]



Figure 2: Ancient Ziggurat at Ali Air Base Iraq [44]

In more recent centuries, the global population has grown exponentially, with projections indicating it will soon reach 9 billion. This rapid growth has exposed the unsustainability of current urban development models, which rely on the flawed assumption of unlimited resources such as land, water, and energy. These resources, however, are finite and are being depleted at an alarming rate. Additionally, buildings and transportation systems are responsible for approximately two-thirds of global carbon dioxide emissions, making them major contributors to climate change [2]. This is largely due to the way cities are designed and how people move within them. As a result, the future of the planet depends on our ability to create cities that are not only attractive and liveable but also carefully planned with sustainability and efficient urban design in mind. One of the key solutions to this challenge

lies in an invention from 19th-century America: the skyscraper. Initially constructed using reinforced concrete and later with steel and glass, skyscrapers revolutionized architecture and urban development, offering a way to build upward rather than outward, thus addressing some of the pressing issues of resource scarcity and urban sprawl [3].

The first practical application of these new technologies for high-rise construction took place in Chicago after the devastating fire of 1871, which destroyed much of the city.



Figure 3: The Great Chicago Fire, an artists rendering, Chicago in Flames - The Rush for Lives Over Randolph Street Bridge [45]

At the time, Chicago was a key trading center connecting the East and West and was experiencing rapid economic growth. This created an urgent need to rebuild the city quickly while maximizing the use of valuable downtown land. These circumstances provided the perfect conditions for the emergence of a new architectural form: the skyscraper. One of the main problems of the time for the construction of tall buildings was the type of material used, i.e. wood and masonry. These materials were widely used, in fact traditional construction techniques and methods were based on them, but wood and masonry imposed limits on the height of buildings because, as the number of floors increased, the thickness of the walls of the lower floors also increased, and this made these buildings economically inefficient. With the arrival of steel, the first structures formed by beams and columns were born that replaced the load-bearing walls, and the amount of glass incorporated into the design increased, as the external walls were replaced with thin closing panels directly fixed to the frame. Therefore, the need to update the methods of structural analysis and design, as well as construction, has also developed. Thanks to this technological advance, in 1885, the architect William Le Baron Jenney designed the Home Insurance Building in Chicago, a 10-story building whose height reached 42.1 meters, widely considered the first modern skyscraper as it consisted of an

2. HISTORICAL ASPECTS OF HIGH-RISE BUILDINGS

internal steel frame and therefore laid the foundations for the construction of today's modern skyscrapers [4].



Figure 4: Home Insurance Building, Chicago [46]

Significant advancements occurred in the 1970s with the advent of the first supercomputers, which provided the computational power necessary to design and model increasingly complex structures. This period also saw the rise of new fields, such as wind engineering and geotechnical engineering, which allowed for the development of more ambitious and innovative solutions. At the same time, alternatives to structural steel emerged with the expanded use of reinforced concrete. Improved knowledge of the physical and mechanical properties of concrete, along with advancements in its compressive strength, made it a cost-effective and viable alternative for constructing tall buildings. Since then, skyscraper construction has spread globally, driven by continuous innovations in technology, materials, and design, enabling the creation of taller and architecturally significant buildings. Engineers and architects continue to push the boundaries of what is possible, as for the Burj Khalifa in Dubai (2009, 829.8 m), which remains the tallest skyscraper in the world [2].



Figure 5: Burj Khalifa [47]

3. FUNDAMENTAL PRINCIPLES OF HIGH-RISE BUILDING DESIGN

Tall buildings, like all types of structures, must have sufficient strength and be capable of fulfilling the purpose for which they are designed. This requires a thorough assessment of various factors, including [5]:

- Magnitude of lateral displacements;
- Accelerations caused by wind;
- Damping properties;
- Elastic shortening;
- Viscosity and shrinkage.

The factors that influence the design of tall buildings, and consequently determine their maximum achievable height, can be categorized as follows [5]:

1. Site conditions;
2. Material properties;
3. Structural systems;
4. Characteristics of the structural system and the effect of external forces;

3.1 Site conditions

Site conditions include all the natural aspects that influence the area where the building is to be constructed. These include the geotechnical properties of the foundation soil, exposure to wind, and susceptibility to seismic activity. Tall buildings are typically highly flexible and have a long fundamental period of vibration, often exceeding 5 seconds. As a result, during an earthquake, these structures generally experience much smaller inertia forces compared to shorter buildings, which have a shorter fundamental period of vibration. Consequently, for buildings taller than 200 meters located in highly seismic regions, wind effects tend to have a greater influence on structural behavior than seismic forces [4].

Regarding soil properties, these primarily determine the type of foundation required for the building. Key considerations include soil consolidation, the potential for differential

settlement, and the risk of liquefaction during a strong earthquake. Due to the variability of soil conditions, a range of foundation types can be employed for tall buildings. Common examples include surface slab foundations and deep pile foundations, the latter being used when it is necessary to reach a stable, load-bearing soil layer at greater depths [4].

The methods most commonly used in the past for the design of foundations were based on empirical formulas that led to oversized, expensive and frequently approximate solutions, therefore which did not allow to study well the interaction between the soil and the structure, which plays a critical role in the distribution of vertical loads and internal stresses, without forgetting the influence on the dynamic behavior of the building subjected to lateral forces like the wind and the earthquake. In fact, over time, the measurements have greatly improved thanks to the advancement of in situ test methods, thus allowing for obtaining more precise geotechnical parameters for the design of foundations [6].

3.2 Material properties

Other factors that influence the design of tall buildings are the mechanical properties of the materials and the overall behavior of the structure under the applied loads, as they are essential to verify that the design is feasible. In fact, thanks to innovations in the field of building materials, it is now possible to use reinforced concrete and structural steel with well-defined strengths, for example, for reinforced concrete, the compressive strength can reach up to 110 MPa, while for structural steel, the yield strength can reach up to 450 MPa. Therefore, through these improvements, it is also possible to use thinner and leaner structural elements, improving the performance and efficiency of materials [7].

3.3 Structural systems

The structural systems used to build tall buildings are many, and over time they have evolved significantly, therefore, the main systems of interest are briefly described and listed below, focusing mainly on the static schemes and functional purposes that characterize them [8]:

1. Cage System: this type of system is characterized by vertical and horizontal structural elements that make the spatial frame of the structure, whose columns are arranged at

3. FUNDAMENTAL PRINCIPLES OF HIGH-RISE BUILDING DESIGN

regular intervals in order to obtain an optimal positioning and size of the spaces, also to facilitate and speed up the design and construction process. In addition, a peculiarity of this type of structural system is that the façade of the building is separated from the external columns.



Figure 6: Havemeyer Building [48]

2. **Oriented System:** this structural system is defined by a "comb-like" composition, as the longitudinal axis of the building is predominant over the transverse one, in fact, the structural elements are positioned transversely to balance the overturning forces acting along the direction of minimum inertia. In addition, due to the type of layout and structural scheme, the interior spaces of the building are divided, in fact, the rooms are arranged along the main facades, while the services are in central positions.
3. **Rigid Frame System with Rigid Nodes:** this type of system is characterized by a structural scheme of beams and columns connected by rigid or semi-rigid joints, which allow the bending of the elements and the distribution of the bending moments generated by external forces, giving the building its characteristic resistance to horizontal forces. However, for buildings that exceed 15 floors in height, lateral displacements become excessive, leading in most cases to an oversizing of the structural elements. Therefore, this structural system is not suitable for the construction of very tall buildings.
4. **Braced Frame System:** this structural system, unlike the previous one, is characterized by reduced lateral displacements, thanks to the presence of a bracing system that accompanies the rigid frame composed of beams and columns, and minimizes the bending moments

applied to it, making the structure efficient even for buildings of more than 30 floors. Thus, these systems function as a truss, in which beams and columns mainly support vertical loads, while bracing elements of various configurations (X, V, K-shaped, concentric or eccentric) absorb horizontal forces.

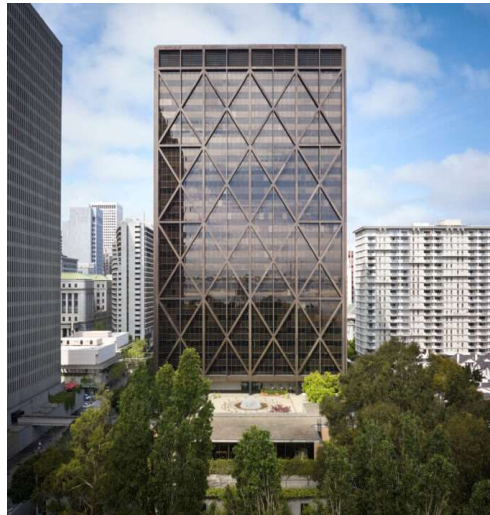


Figure 7: One Maritime Plaza [49]

5. Outrigger system: this structural system is characterized by a central core reinforced either with bracing or by means of horizontal, simple, or lattice beams (outriggers), which also perform the function of connection with the external columns of the building, which are in turn connected to each other by an external tie beam. Furthermore, unlike the traditional braced frame, this type of structural system works well with both steel structures and composite structures, ensuring the possibility of being able to realize buildings that exceed 100 floors, thanks to the presence of the outrigger system, which limit the rotation of the core and improve lateral strength significantly if extended for at least two floors.



Figure 8: Shanghai Tower [51]

3. FUNDAMENTAL PRINCIPLES OF HIGH-RISE BUILDING DESIGN

6. Core system: this system relies on a central service core with high stiffness, which primarily provides the building's bracing resistance, while the rest of the structure is designed to support only vertical loads reducing the weight of the structural elements on the exterior facades, and enhancing symmetry to ensure an uniform response to stresses from various directions.



Figure 9: Dewitt Chestnut Apartments [50]



Figure 10: World Trade Center [52]

7. Outer tube system: the behavior of this type of structural system can be approximated to that of a cantilever beam, as the structure is characterized by very deep foundations and rigid nodes that connect the closely spaced perimeter beams, which create a tubular structure that simulates this behavior. In fact, most of the rigidity of the building falls on the façade, while the internal structural elements only perform the function of resisting the vertical loads generated by the self-weight of the structure, thus improving the response to lateral forces and the general behavior of the structure, which depends mainly on the height/width ratio, the size of the plan, the spacing of the columns and the quality of the connections.

8. Braced tube system: This structural system is characterized by a tubular system incorporated by diagonal braces on the façade, which increase the overall stiffness of the building and absorb the shear forces produced by lateral loads, thus eliminating the "shear lag" effect, allowing the construction of very tall buildings that work mainly by bending as if they were a large cantilever beam. Furthermore, in this type of structural system, the bracing elements can be made either by means of diagonal steel elements, or by concrete walls if the building is made of reinforced concrete.



Figure 11: John Hancock Center in Chicago, Illinois [53]

9. Double-tube system: this system improves the stability of the structure through the rigid connection of the outer shell to the central core. This connection can be achieved either discontinuously at certain points or continuously in every direction. The system essentially consists of two coaxial tubes, which share a proportional tensile and compressive load, and allows for greater cooperation and load sharing between structural elements. This system has several efficiencies built into new high-rise building designs, as the total amount of material can be minimized and the central core can be taller than standard structural systems. The applicability of the tube system also makes it an excellent option for a tall building, particularly as the height approaches the 100 stories and lateral sway becomes a prominent part of the design process.
10. Tube bundle system: it increases resistance to overturning by linking together (ideally) several tube elements, which act in total independence of all other tubes without following the historical annular pattern of a floor plan. The service systems become easier to arrange, as they do not have to conform to rigid positional limitations and still use the least amount of interior space needed. Each modular independence of the tube allows for complete

3. FUNDAMENTAL PRINCIPLES OF HIGH-RISE BUILDING DESIGN

flexibility in the placement and number of tubes, relative to the overall form and height of the entire assembly can vary as needed.



Figure 12: Sears Tower [54]

11. Diagrid system: the name of the system is a combination of two words, “diagonal” and “grid”. The term refers to a structural system of diagonal grids. The system consists of beams, either of steel or reinforced concrete, connected diagonally. This system requires significantly less structural steel than frame systems have traditionally used. The diagrid system is now commonly used for high-rise buildings of the third millennium and is characterized by phenomenal efficiency in the elastic range. Due to the triangulation of the grid, global stresses that develop due to vertical and horizontal loading largely convert to axial forces and deformations in the grid beams. The result of this triangulation, when subjected to horizontal loads, drastically reduces both the shear lag effect and shear deformability of the overall system performance.



Figure 13: Hearst Tower [55]

3.4 Characteristics of the structural system and the effect of external forces

Strength and functionality are fundamental requirements for an effective design, which is why particular attention must be given to the perceived effect of external actions on the occupants. The design process is therefore influenced by the building's intended function, as well as the stiffness, mass, and damping characteristics of the structural system. Modern tall buildings are typically designed to limit elastic displacement under wind loads to a maximum of $h/500$, where h is the building's height, for wind events with a return period of 50 years. This criterion allows the stiffness of the structural system to be determined as a function of its mass and damping properties [4].

Excessive lateral displacements can result in significant $P-\Delta$ (second-order) effects, which may amplify displacements and stresses in the vertical load-bearing elements. Additionally, attention must be given to the vertical structural elements, as they are prone to shortening under the substantial loads they carry. This shortening begins during construction and can persist over time due to viscous effects. Such displacements must remain within the limits prescribed by regulations, as they can impact non-structural elements and systems. Nevertheless, these phenomena can be anticipated, and their effects are carefully accounted for during the construction sequence to ensure proper performance [4].

4. DIAGRID STRUCTURES

4.1 History of diagrid structures

The structural system of diagrids was introduced thanks to the work done by the Russian engineer Vladimir Shukhov, who was the first to use a structural system consisting of a single-layer network of diagonal elements arranged in a triangular configuration, giving the structure stability, aesthetics and structural efficiency. This innovative structural system was developed by Shukhov to solve the problem of creating a structure capable of withstanding vertical loads and lateral forces without relying on a central core. His first experiments were characterized by utilitarian simplicity and the use of innovative materials, in fact, among these we have the Shabolovka Radio Tower, which summarizes the principles behind this structural system, as it was built by optimizing the use of the material thanks to the reticular configuration, and without a conventional central core, thus introducing the innovative approach to structural stability [9].



Figure 14: Shabolovka Radio Tower [56]

Though Shukhov's work was largely a pragmatic approach, it inspired architects. In fact, architects, like Norman Foster, considered Shukhov's towers a baseline change to the diagrid in that it made the diagrid a vehicle not only for architectural expression but also a method for performing structural function. Foster revisited the diagrid as a structural system that supports the floor loads of the tower through a cladding system that is erected. The other significant works show this point of progression with involvement through other projects like

the Swiss Re Tower and Hearst Magazine Tower. As a system, the diagrid has evolved from an idea of a "hollow" tower to looking more like a scaffolding structural system.



Figure 15: 30St Mary Axe [57]

This transformation involved a remarkable improvement in detailing and construction process and truly represents a new mindset regarding how diagrid structures could be conceived and constructed in a modern architectural sense. In addition to all the new construction of buildings with diagrids, diagrids have been used in comprehensive upgrading and renovation projects. A diagrid that incorporates both load adjacent items (depending on the structural arrangement of the building), along with energy-saving systems and building elements, allows for the renovation of buildings with minimal negative impacts. Diagrids have historically addressed common issues that occur in rehabilitation projects like permanently relocating occupants, high costs and prolonged periods of inactivity. Additionally, diagrid structures are traditionally exoskeletons, as they are built up from the outside, meaning the work claim consumption can be minimized, and prefabricated solutions can be used, expediting the construction process [10]. The evolution of diagrid exoskeletons also extended to alternative mesh patterns that have different shapes like hexagonal and irregular mesh patterns, all of which enhance structural performance. Some buildings with these mesh arrangements include the National Stadium in Beijing (commonly known as the Bird's Nest) which has a unique and organic configuration driven by the bird's nest shapes. Another building is the National Aquatic Center (also referred to as the Water Cube) also in Beijing, but with a diagrid mesh configuration that used the Weaire-Phelan foam configuration pattern. There is also the Voronoi patterned mesh, which is an enhancement of the hexagonal patterns, that offers improved performance and appearance [11].

4. DIAGRID STRUCTURES

The examples mentioned here showcase the potential for the use of diagrid structures in modern architecture and can lead to the design and construction of complicated contextual and high-performance buildings that push the boundaries of design.



Figure 16: Beijing National Stadium, "Birds Nest" [58]



Figure 17: Beijing National Aquatic Center, "Water Cube" [59]

4.2 Structural behavior of a diagrid structure

This paragraph provides a concise description of diagrid structures, emphasizing their modular façade configuration and the role of triangular units in their structural behavior. It highlights the importance of geometry, particularly the inclination angle of the diagonal elements, in determining the structural response of each module. The triangular unit consisting of two inclined diagonals and a ring beam represents a basic diagrid façade unit. The diagonals mainly resist vertical and lateral loads by means of an axial force, either compression or tension. To achieve this action, the diagonals are usually pinned at the panel nodes, as shown in Figure 18 [12].

The inclination of the diagrid structure and its load distribution often results in the inclined diagonals extending several stories and, as a result, the diagrid diagonals support the external floor beams of intermediate stories. The extent of support from the diagonal to the external

4.2 Structural behavior of a diagrid structure

floor beam generates minimal shear and bending stresses within the diagonals. Preliminary design considerations generally dismiss these stresses as very little, relative to the large axial stresses built up from applied vertical and lateral loads on the building.

A three-dimensional view of the tubular diagrid structure is shown in Figure 19. A tubular, diagrid building typically manifests as a tube-in-tube structure. Most often, the exterior diagrid tube has an interior core that is concrete or steel braced, with the desire to secure additional structural performance [13].

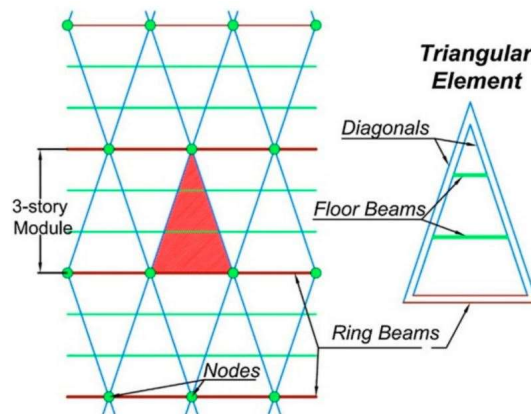


Figure 18: 3-story diagrid modules and a sample triangular element [12]

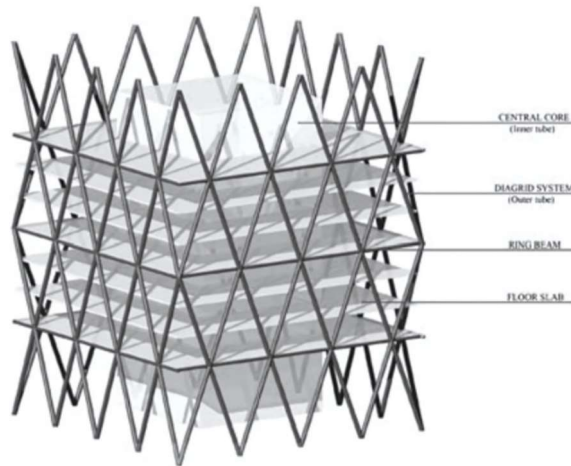


Figure 19: Diagrid tubular configuration [13]

Understanding the structural performance of diagrid nodes is important, as nodes act as key locations for loading transfer and redistribution. Looking at their performance in a more thorough way, emphasis is given to specific behaviors including loading distributions across the members and strength characteristics, which are all majorly imposed by axial forces [14]. Axial forces are critical to how diagrid node connections perform, particularly because the axial load capacity of the node is impacted not only by axial load, but also by bending

4. DIAGRID STRUCTURES

moments, lateral deflection, and more. Consequently, the ultimate limit state of these connections can be quite complex due to the variable-section characteristics of the nodes. Axial forces under gravity, wind, or earthquake loading are critical in the inclined columns of diagrid structures. Under vertical loading, the slabs transfer the load to the connecting beams or shear walls, and ring-beams, which further distribute in the case of ring beams. Under lateral load conditions, the external tube of the diagrid performs the majority of the resisting load, supported by quasi-static loading testing with triangular distributed loads [15].

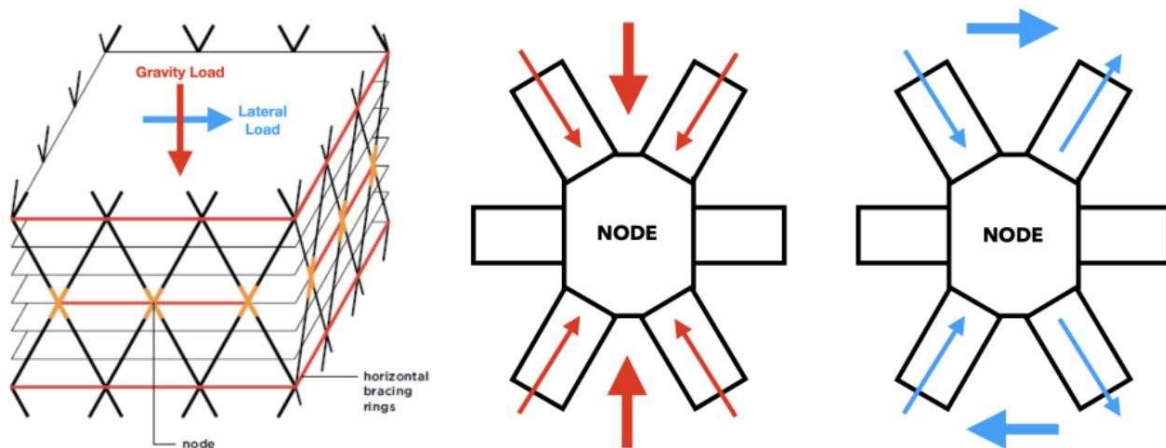


Figure 20: Diagrid module and force distribution [14]

The geometry of the nodes is an important consideration with diagrid structures. The node geometry will often contain gusset plates, stiffeners, and other inductive detailing to account for potentially complex states of stress, and relative to these effects, the fabrication and assembly of nodes needs to be precise, as any errors, including misaligned or fabricated components, will reduce the node's ability to transfer these loads as intended [16].

The geometry of the nodes and load path continuity are closely connected, as the complexity of the node geometry can impact load transfer capacity, while preserving structural performance across the entire structure. In load path continuity, load takes the form of axial forces via the steel web and bending moments via the side stiffener (or secondary element). The structural performance of the node is critical when under cyclic loads. The axial forces induced by the steel web, with relation to their magnitude and internal node design, also affect the capacity of the side stiffener to resist deformation, influence the side stiffness, strength and ductility. The node will have failure mechanisms governed by the axial forces and the additional moments combined, leading to crack initiation, local buckling, and ductility conditions based on whether this compression, tension, or pattern of these can change.

Likewise, the node module size and its effect on load distribution, small modules lend the ability to develop straight diagrid members and a more efficient load transfer throughout the structure [17].

4.3 Geometry-driven performance optimization of diagrid structures

The geometry of the diagrid is a fundamental aspect for the performance, and parameters such as the angle of the diagonal members, the size of the module, and the design of the node can have important influences on load distribution, stiffness, and overall stability [18].

This chapter will discuss several research papers that put forward optimization methods for diagrid structures, to help replicate the best possible solutions from a potentially infinite number of options. These papers will help explain how geometric parameters could be adjusted to achieve optimal structural performance, while considering practicality in terms of efficiency of material choices, and construction.

The first to demonstrate that a specific diagonal angle that can satisfy stiffness requirements while minimizing material usage exists were Moon et al. [19]. Their findings reveal that the optimal angle increases as the aspect ratio of the building rises. They studied a 60-story diagrid structure with an aspect ratio of approximately 7, finding that the optimal angle falls within the range of 65° - 75° . However, for buildings with aspect ratios closer to 5, the optimal angle decreases significantly to around 10° [19].

Under lateral loads, the distribution of shear forces and bending moments varies linearly and quadratically respectively along the height of a building. This variation implies that the structural requirements to resist shear and bending forces differ across the building's height. Shear forces dominate the upper portion of the structure, whereas bending moments govern the design of the lower portion. Based on this observation, Moon [20] investigates diagrid buildings with different diagonal angle configurations. Figure 21(a) illustrates a varying-angle diagrid with steeper angles at the base, Figure 21(b) shows a uniform-angle diagrid, and Figure 21(c) depicts a varying-angle diagrid with steeper angles at the top. More steeply inclined diagonals are more effective at resisting bending moments, while more shallowly inclined diagonals are more effective at shear forces. Thus, the case in Figure 21(a), where the diagonals are inclined more steeply at the base, is expected to overall provide better

4. DIAGRID STRUCTURES

structural performance for the diagrid than the case in Figure 21(c), where more steeply inclined diagonals exist particularly at the top, which conflicts with structural logic and only included for completeness that it will not provide any structural advantage.

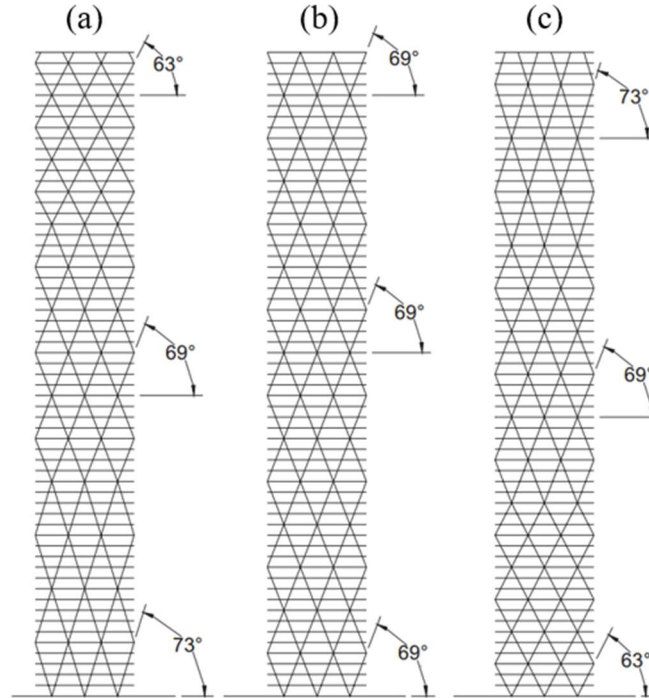


Figure 21: Different diagonal angle patterns diagrids: (a) varying-angle with steeper diagonals at the base; (b) uniform-angle; (c) varying-angle with steeper angle at the top [20]

For shorter buildings with aspect ratios below 7, the uniform-angle configuration proves to be the most efficient in terms of material consumption. This is because shorter buildings behave like shear beams, while steeper diagonals at the base improve bending stiffness. Conversely, high-rise buildings that have greater than 7 aspect ratios primarily deform in bending.

The results indicate that although the steeper diagonals in varying angle configurations decrease the shear stiffness at the base, the increase in bending stiffness more than compensated so that this configuration was still the best solution [20].

Moon [21] presents similar findings, further exploring the "speed" of variation in diagonal angles along the building's height, considering both gradual and abrupt transitions. However, in the proposed variable-angle solutions, the diagonals are not straight throughout their length due to directional changes at the interfaces between modules, which can complicate design and construction.

4.3 Geometry-driven performance optimization of diagrid structures

To address this issue, Zhang et al. [22] propose an alternative approach for generating varying-angle diagrid tubes. As illustrated in Figure 22(a), they introduce a graphical method to create a varying-angle pattern with straight diagonals that extend continuously over the full height of the building. This approach is governed by two key parameters: the top angle (θ_1) and the bottom angle (θ_2). Using stiffness- and strength-based design criteria, Zhang et al. analyse a range of varying-angle diagrids with straight diagonals, applied to buildings between 30 and 75 stories tall, with aspect ratios ranging from 3.6 to 9.

By considering various $\theta_1 - \theta_2$ combinations, the study identifies optimal solutions under gravity and wind loads. Based on their findings, Zhang et al. propose empirical formulas for determining the optimal values of θ_1 and θ_2 as a function of the building's aspect ratio (H/B). These formulas provide a practical framework for designing efficient varying-angle diagrid structures with straight diagonals.

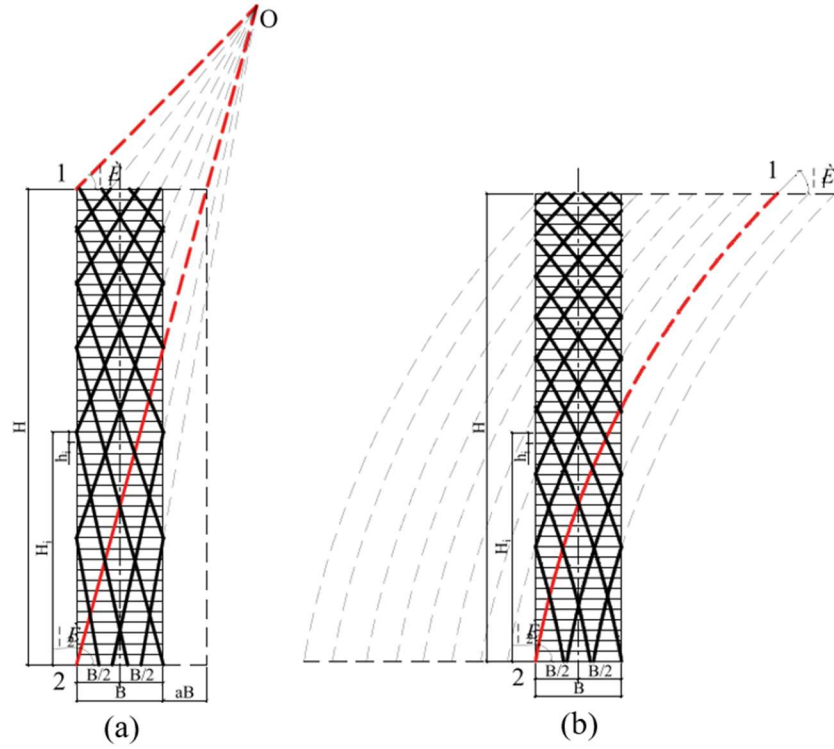


Figure 22: Different diagonal angle patterns diagrids: (a) varying-angle with straight diagonals; (b) varying-angle with curved diagonals [22]

$$\theta_{1,opt} = \begin{cases} \theta_{2,opt} & H/B \leq 3.5 \quad (1) \\ \frac{1}{\left(1 + \ln \frac{H/B}{3.5}\right)^{\frac{H/B}{2}}} \left(\theta_{2,opt} - \arcsin \frac{1}{\sqrt{3}} \right) + \arcsin \frac{1}{\sqrt{3}} & H/B > 3.5 \quad (2) \end{cases}$$

4. DIAGRID STRUCTURES

A critical aspect ratio, $(H/B)_{crit}$, is identified as the threshold distinguishing the efficiency of uniform- and varying-angle diagrids. For aspect ratios below $(H/B)_{crit}$, uniform-angle diagrids are more efficient, while for ratios above this value, varying-angle configurations offer the most economical solutions. In this study, $(H/B)_{crit}$ is found to range between 4.5 and 5, which is lower than the value of 7 previously suggested by Moon [20, 21]. This discrepancy arises primarily from differences in the definition of the diagonal pattern. For aspect ratios below $(H/B)_{crit}$, the bottom angle governs the design, whereas for higher aspect ratios, the top angle becomes a key factor [22].

In their study, Zhao and Zhang [23] introduce an innovative diagrid configuration that incorporates curved diagonals to achieve a varying-angle solution as illustrated in Figure 22(b). This study builds on the current state of the art for diagrid design in considering structural performance with varying loading conditions.

The authors concluded that the optimal lower angle, $\theta_{2,opt}$, for diagrids, with straight diagonal members at varying angles, was independent of loading type. Therefore, generally, Equation (2) can be considered regardless of what load acts on the structure.

However, the optimal top angle, $\theta_{1,opt}$, exhibits a distinct behavior under seismic loads. Specifically, $\theta_{1,opt}$ consistently approaches its lower limit, which is expressed as $\theta_{1,opt} = \arcsin \frac{1}{\sqrt{3}}$. This observation necessitates a correction to Equation (1) to account for seismic load conditions:

$$\theta_{1,opt} = 0.8 \left(\frac{H/B}{8} \right)^{\frac{1}{8}} \theta_{2,opt} \quad (3)$$

$$\theta_{2,opt} = \arctan (H/B) \quad (4)$$

Equations (3) and (4) are valid within the height-to-base ratio (H/B) range of 3.6 to 9. Within this range, the optimal top angle, $\theta_{1,opt}$, is found to lie between 50° and 70° . This range is notably higher than the top angles observed in diagrids with straight diagonals, which typically fall between 35° and 45° . The reduced difference between $\theta_{1,opt}$ and $\theta_{2,opt}$ in the case of curved diagonals results in a smaller curvature of the diagonal members [23].

The analyses in the previous paragraph exclusively assess diagrid performance using square and rectangular configurations for buildings. In order to broaden the analyses to alternative plan shapes, Mirniazmandan et al. [24] recently examined the combined effects of diagonal

4.3 Geometry-driven performance optimization of diagrid structures

inclination and plan geometry on top lateral displacement and the weight of diagrids. The authors' study simulated tall buildings of 180 m in height, with planar geometries using a variety of polygons with 3, 4, 5, 6, 8, 10, and 12 sides, along with circles. They achieved eight plan shapes for the base and eight corresponding plan shapes for the structure's top.

This yielded a total of 64 distinct models, which are shown in their pictorial modelling in Figure 23. In addition to the variety in the plan shapes, the authors also evaluated five diagonal angles (33° to 81°). They concluded that a diagonal angle of 63° achieves both reduced top lateral deflection and minimized structural material necessary.

The authors also concluded that increasing the number of base and top sides provided improved efficiency of the diagrid systems in lateral displacement, however, the improved performance was not related to changes in plan shape and geometry as compared to changing the diagonal inclination.

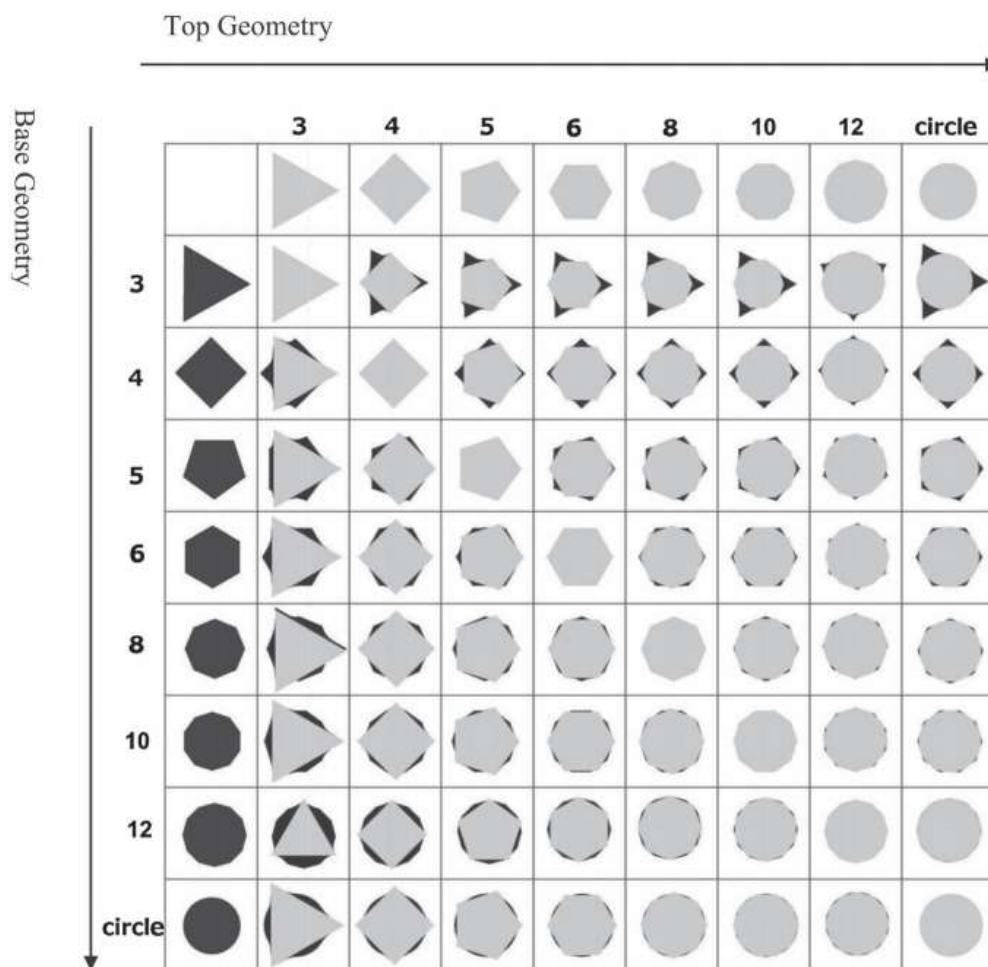


Figure 23: Combinations of base and top geometries [24]

4. DIAGRID STRUCTURES

Lacidogna et al. [25] recently conducted a detailed analysis to investigate the combined effects of diagonal inclination and plan shape on the structural behavior of diagrid tube systems. Their study considered four building heights: 126 m, 168 m, 210 m, and 252 m, corresponding to 36, 48, 60, and 72 floors, respectively. For each height, four distinct floor plan shapes were analyzed: square, hexagonal, octagonal, and circular. To account for variations in diagonal inclination, six different configurations were adopted by varying the number of floors included within each diagonal module: 1, 2, 3, 4, 6, and 12 intra-module floors. This approach resulted in the investigation of 24 diagrid models for each building height, amounting to a total of 96 structures. Each diagrid module consisted of 24 diagonals distributed uniformly along the building's exterior. The details of these geometrical configurations are illustrated in Figure 24 [25].

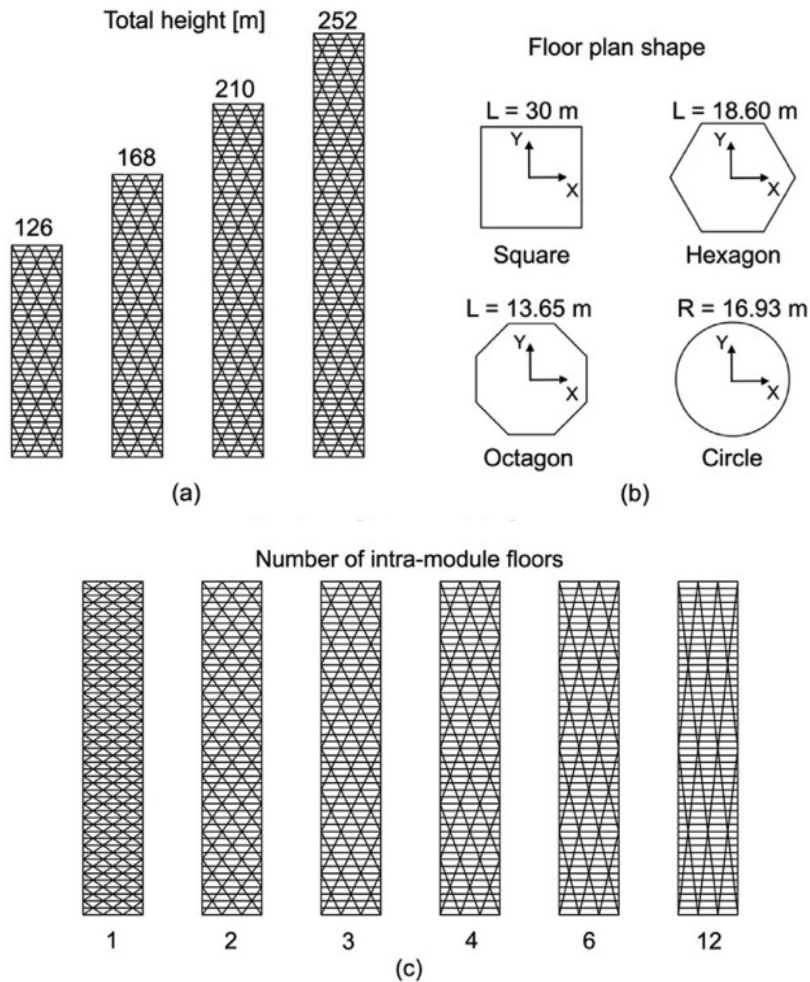


Figure 24: Geometry of the generated diagrid buildings: (a) four different total heights; (b) four different floor plan shapes; (c) six different diagonal inclinations [25]

4.3 Geometry-driven performance optimization of diagrid structures

Unlike earlier studies, this research evaluated structural performance not only in terms of lateral deflection but also by analyzing torsional rotations. To achieve this, each structure was subjected to a horizontal load of 30 kN/m along the horizontal axis and a torque load of 70 kNm/m, both uniformly distributed along the building's height, as depicted in Figure 25. These distributed loads were converted into concentrated forces and moments applied at the floor levels. The resulting lateral displacements and torsional rotations of the floors were then calculated using the Matrix-Based Method (MBM) [25].

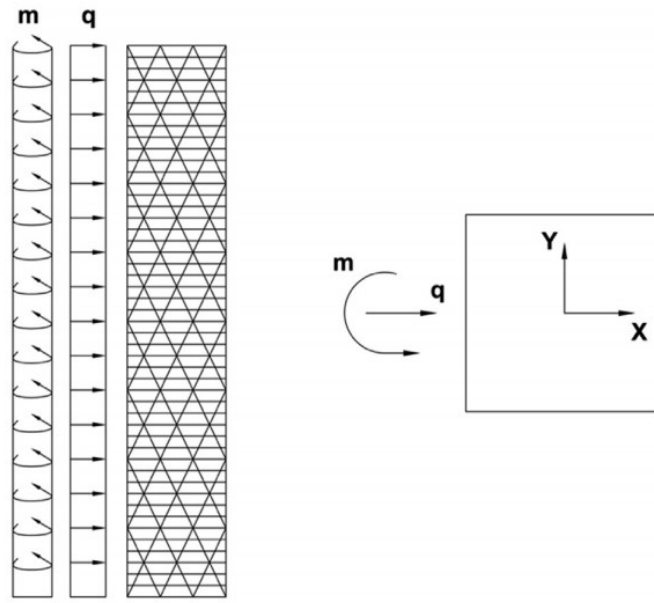


Figure 25: Uniform load pattern: q refers to the distributed horizontal load, m to the distributed torque moments [25]

This research examined how the variation of important geometric parameters like external diagonal inclination, floor plan shape and aspect ratio influenced the diagrids' structural responses. Of these parameters, the authors identified the diagonal's inclination angle as the most influential parameter for structural behavior.

For each of the diagrid structures reported in the research, it was found that the most effective diagonal inclination angle to minimize lateral displacement was within the range of 64° - 72° . This diagonal inclination range will increase with an increasing aspect ratio of the building, since an increase in aspect ratio also influences the interaction of shear and bending rigidity of the built structure. Conversely, the angles associated with the most torsional stiffness were consistently within the 35° - 38° range. Further, and in contrast to lateral displacements, torsional stiffness was not influenced by the overall height of the building, torsional stiffness only depended upon the shear rigidity of the diagrid modules used.

4. DIAGRID STRUCTURES

It was further concluded that the geometric shape of the floor plan influenced but had a limited effect on overall diagrid structural response, given that the diagonal inclination was in the optimal range to minimize lateral displacements. When inclination was within the optimal range to minimize the lateral displacements of all buildings subjected to the testing conditions, the differences, irrespective of floor plan shape, geometric performance measure were less than 5%. However, when diagonal inclination was outside the mentioned optimal range, the influence of plan geometry on structural response became much clearer. In the cases discussed where lateral displacements differ by 25% or greater as a result of changing plan geometry, the influence of plan shape is evident. With regards to torsional behavior when diagonal inclination is optimally set to minimize torsional rotations, circular plan groups were also proven to minimize torque actions, generally, for all tall buildings considered.

The results, illustrated in Figure 26 for the four building heights, highlight a key finding: the structural configurations that minimize lateral displacements are not the same as those that minimize torsional rotations. This underscores the need to balance these competing requirements when designing diagrid structures. Additionally, the study emphasized the importance of sustainability by advocating for structural solutions that not only limit deformability but also minimize the amount of material used [25].

4.3 Geometry-driven performance optimization of diagrid structures

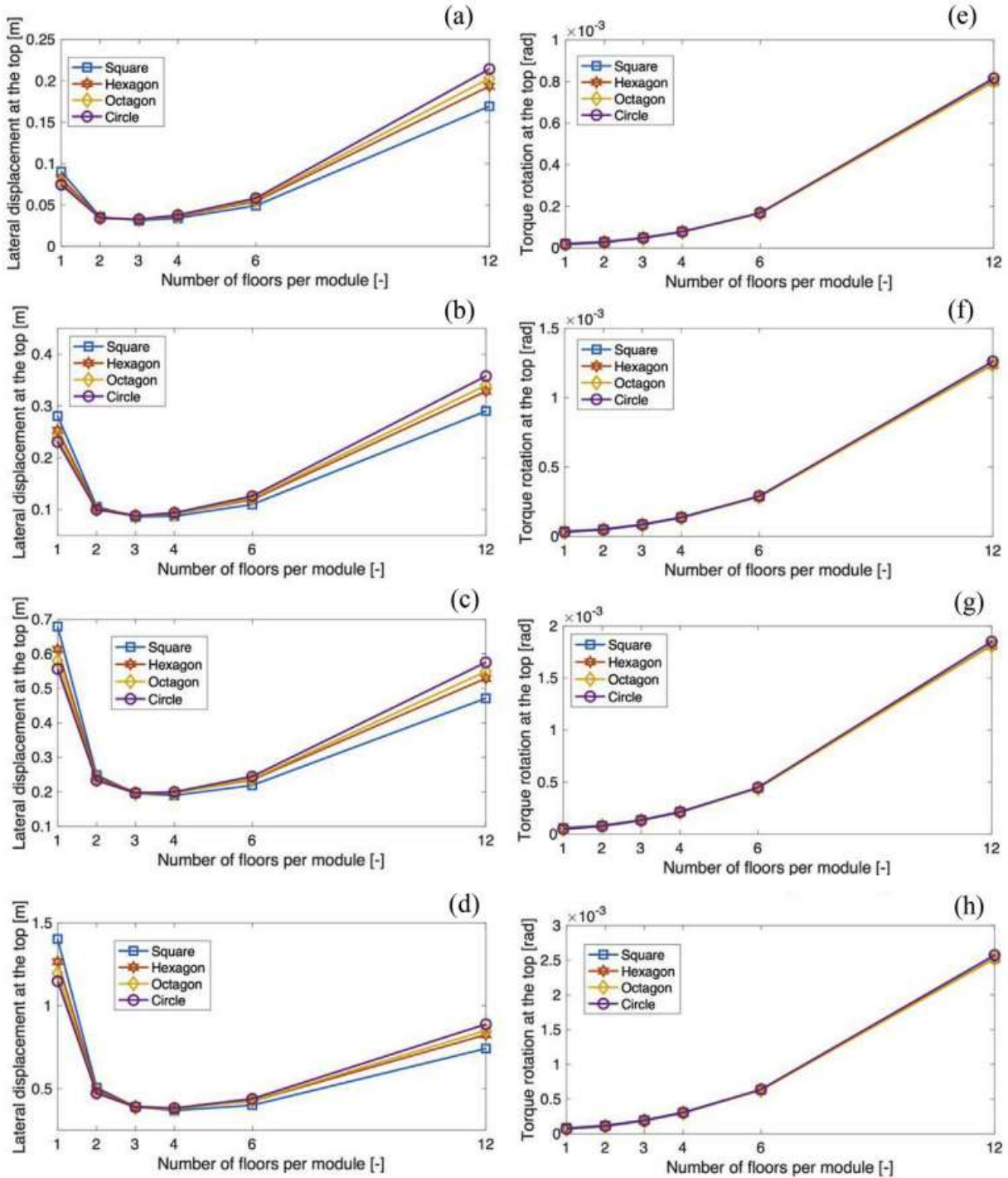


Figure 26: Displacements (a-d) and torsional rotations (e-h) for the four buildings – Variable cross-sectional area [25]

Further research by Scaramozzino et al. [26] employed the desirability function approach in conjunction with the matrix-based method (MBM) to determine the optimal diagonal pattern for diagrid tall buildings within a multi-response framework. Initially, the method was applied to the same set of uniform-angle patterns analyzed in the previous study, as depicted in Figure 24(a). This was then expanded to a larger set of geometries with varying angles. All of the geometries were created by wrapping the building with diagrid modules that consisted of a

4. DIAGRID STRUCTURES

varying number of intra-module stories, which were represented as j . For the purposes of this analysis, the j considered were 1, 2, 3, 4, 5, and 6.

By employing combinatorial calculus, each unique possible combination of the diagrid modules was resolved.

However, only configurations that exactly covered the total number of floors N in the building were considered feasible. This condition was expressed mathematically as:

$$N = \sum_{j=1}^6 (jM_j) \quad (5)$$

where M_j represents the total number of modules in the diagrid pattern with j intra-module floors.

The total number of feasible patterns for buildings with $N = 36$, $N = 48$, $N = 60$, and $N = 72$ floors were calculated as 9,728, 31,040, 79,432, and 175,008, respectively. Four examples of these varying-angle geometries for buildings with 48 floors and a square plan shape are illustrated in Figure 27 [26].

The study examined only steep diagonals at the bottom and shallower diagonals at the top. This style of the diagrid follows more closely the structural logic, as the diagrid can effectively resist lateral loads with those configurations. The shallow diagonal at the bottom and steep diagonal at the top are not structurally logical and perform poorly [20].

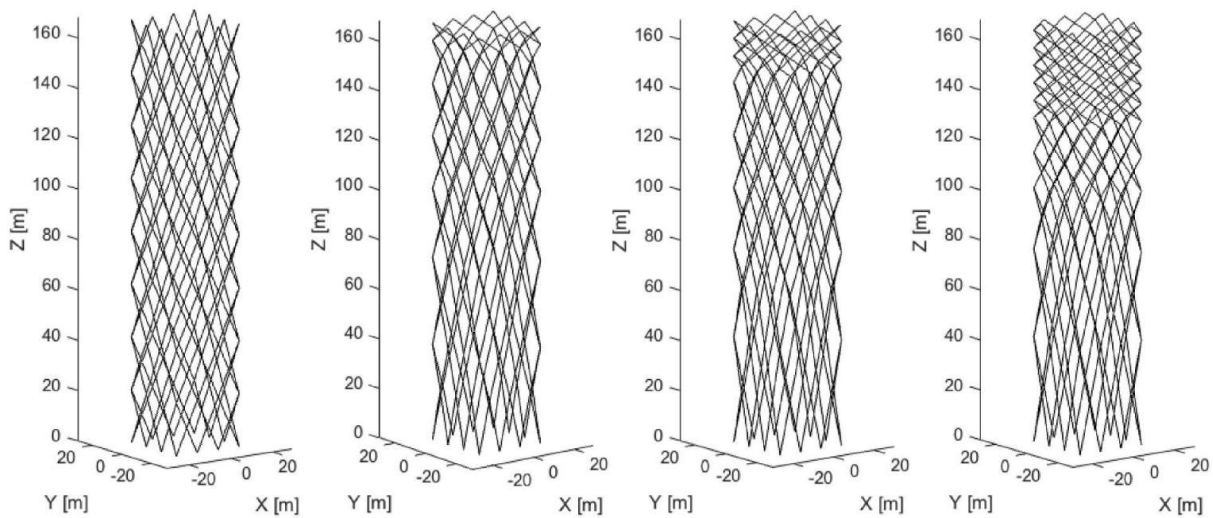


Figure 27: Four examples, out of the 7760, of varying-angle diagrid patterns for the square 48-floor building [26]

4.3 Geometry-driven performance optimization of diagrid structures

The preferred diagonal layout was chosen using overall desirability (OD) in that the optimal preference minimized four attributes: (I) wind lateral displacement, (II) torsional rotation, (III) diagrid structural weight, and (IV) construction complexity. This provided a simple way to show all four attributes of desirability in terms of the best possible diagrid pattern.

The article [26] also detailed uniform-angle diagrids, including several key points on the diagrid members' cross-sectional area consideration, based on conventional strength- and stiffness-based preliminary design of diagrids subjected to vertical, lateral, and torsional loads.

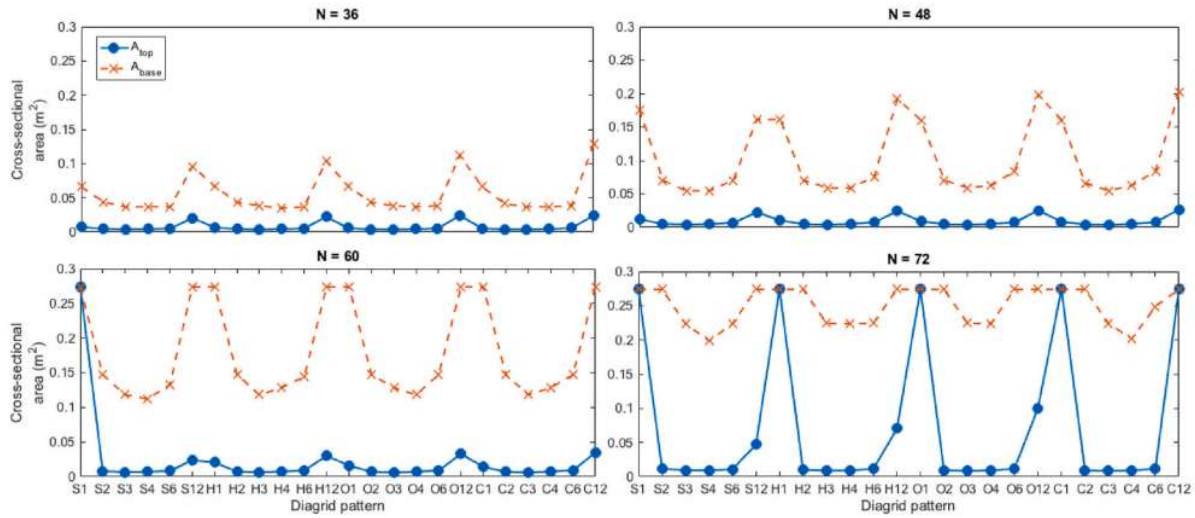


Figure 28: Cross-sectional areas (in m^2) for the top (continuous blue line) and base (dashed orange line) modules of the twenty-four uniform-angle diagrid patterns, for the building with 36, 48, 60, and 72 floors [26]

Figure 28 illustrates the maximum and minimum cross-sectional areas assigned to diagrid patterns across varying building heights, with the maximum areas corresponding to the ground modules and the minimum areas to the top modules. Insights from Scaramozzino et al. [26] analysis of the data were summarized in two key points. First, that height is an important contributor to the cross-sectional areas. Taller buildings require much bigger cross-sections, because the external and internal loads both increase quickly in proportion to height. More structure is required to keep things stable and allow for performance at the new height and associated loads.

Second, the effect of the building shape is relatively small with respect to cross-sectional areas. Given a building height and diagonal inclination, the areas would be the same for all planar shapes. This indicated that the individual shape of plan geometry is not the most

4. DIAGRID STRUCTURES

important factor for the conceptual design, since other parametric influences (height, diagonal inclination, etc.) would outweigh the importance of shape.

Additionally, the number of intra-module floors (n) has a noticeable effect on cross-sectional areas. For a given building height and plan shape, configurations with either the minimum or maximum number of intra-module floors result in larger cross-sectional areas. This indicated the existence of an optimal range of diagonal inclinations that minimizes the cross-sectional areas, leading to a lighter structural weight (W_i) and a more efficient design.

Finally, certain diagrid configurations are found to be inherently too flexible. In these cases, no circular hollow section (CHS) members available in the referenced database [27] were sufficiently large to satisfy the stiffness and strength requirements. This highlighted the limitations of some diagrid patterns, particularly for taller or more complex structures, where achieving the necessary stiffness and strength becomes increasingly challenging.

Figure 29 illustrates the lateral displacement values at the top of the building under lateral wind pressure for various building heights and diagonal patterns. For the shortest building, with $N = 36$ and an aspect ratio of 4.2, the analysis done in [26] revealed that the preliminary design is primarily governed by strength conditions rather than stiffness. This becomes evident from the overall results, in which almost all of the diagrid patterns do not specifically fit the target displacement limit ($\delta_{lim} = 0.25\text{m}$). Several of the patterns get close to δ_{lim} , but all have the top lateral displacements ($\delta_{i,top}$) below the allowable lateral target, which indicates that for this height, stiffness is not the governing design constraint.

Among the various diagonal patterns, pattern S3 stands out for achieving the minimum top lateral displacement, with $\delta_{i,top} = 0.15\text{m}$. This value is more than 40% lower than the maximum allowable displacement defined by the stiffness design criteria, demonstrating that S3 provides superior lateral stiffness compared to other configurations. This highlights the effectiveness of pattern S3 in minimizing lateral displacements, even in a design scenario where strength requirements dominate.

4.3 Geometry-driven performance optimization of diagrid structures

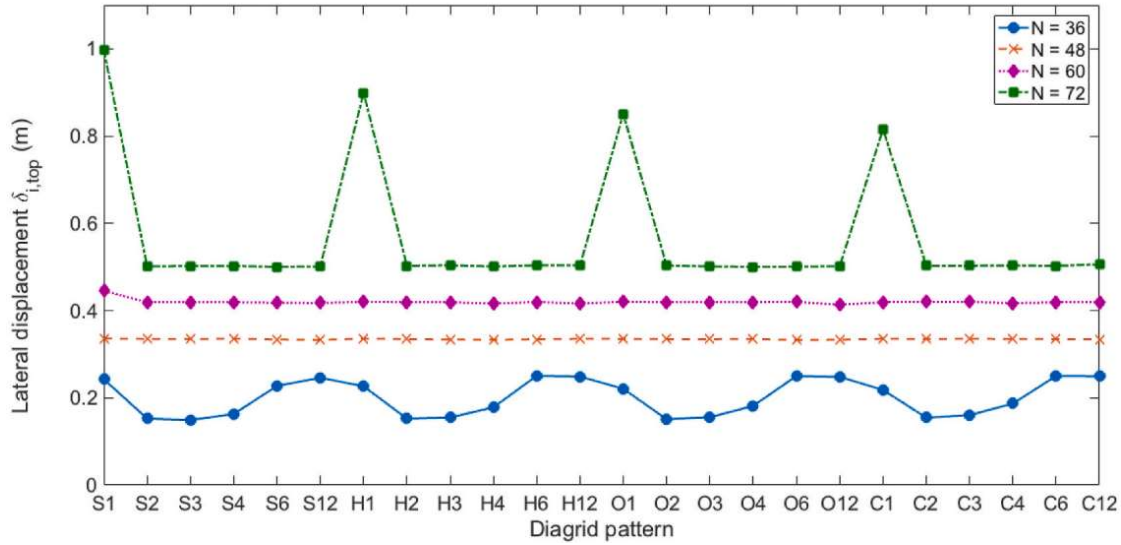


Figure 29: Lateral displacement at the top of the building $\delta_{i,top}$ for the twenty-four uniform-angle diagrid patterns, for the building with 36 (continuous blue line), 48 (dashed orange line), 60 (dotted purple line), and 72 (dashed-dotted green line) floors [26]

For the 48-floor building, with an aspect ratio of 5.6, the analysis done in [26] shows that all diagrid patterns successfully meet the target displacement limit ($\delta_{lim} = 0.34$ m). This indicates that stiffness requirements govern the preliminary design for these configurations, as lateral displacement becomes the critical factor in determining structural performance. The ability of all patterns to satisfy the displacement criteria highlights the adequacy of the diagrid designs for this height in terms of stiffness.

For taller buildings, such as those with 60 floors (aspect ratio of 7.0) and 72 floors (aspect ratio of 8.4), the maximum displacement requirements also dominate the preliminary design process. However, in these cases, certain diagrid patterns fail to meet the stiffness criteria, resulting in unfeasible solutions where the top lateral displacement ($\delta_{i,top}$) exceeds the allowable limit (δ_{lim}).

In the 60 - floor building, pattern S1 was identified as unfeasible, as it produces a top displacement exceeding the target limit. For the 72 - floor building, the issue is more pronounced, with multiple patterns, S1, H1, O1, C1, and C12, failing to satisfy the stiffness requirements. These patterns result in top displacements that surpass the allowable limit, highlighting their inadequacy for taller structures.

Figure 30 presents the maximum demand-to-capacity ratio (DCR) values for the top and base diagrid modules obtained in [26], offering insights into the structural behavior and design priorities. The results indicated that the DCR values follow a consistent trend across different plan floor shapes, confirming that the specific plan geometry has only a minor impact on the

4. DIAGRID STRUCTURES

structural behavior and preliminary design. This observation aligns with earlier findings, emphasizing that factors such as building height and diagonal inclination play a more significant role in determining structural performance.

For shorter buildings, such as the one with $N = 36$, the design is primarily governed by strength requirements. This is evident from the maximum DCR values for both the top and base modules, which are very close to 1 for most diagrid patterns. These values indicated that the structural members are utilized to their full strength capacity, confirming that strength criteria dominate over stiffness considerations in the preliminary design of shorter buildings. In contrast, for taller buildings, the design is predominantly driven by stiffness requirements [28]. This shift reflects the increasing importance of controlling lateral displacements and ensuring overall structural stability as building height increases. The transition from strength- to stiffness-driven design highlights the evolving priorities in diagrid systems as the structural demands change with height.

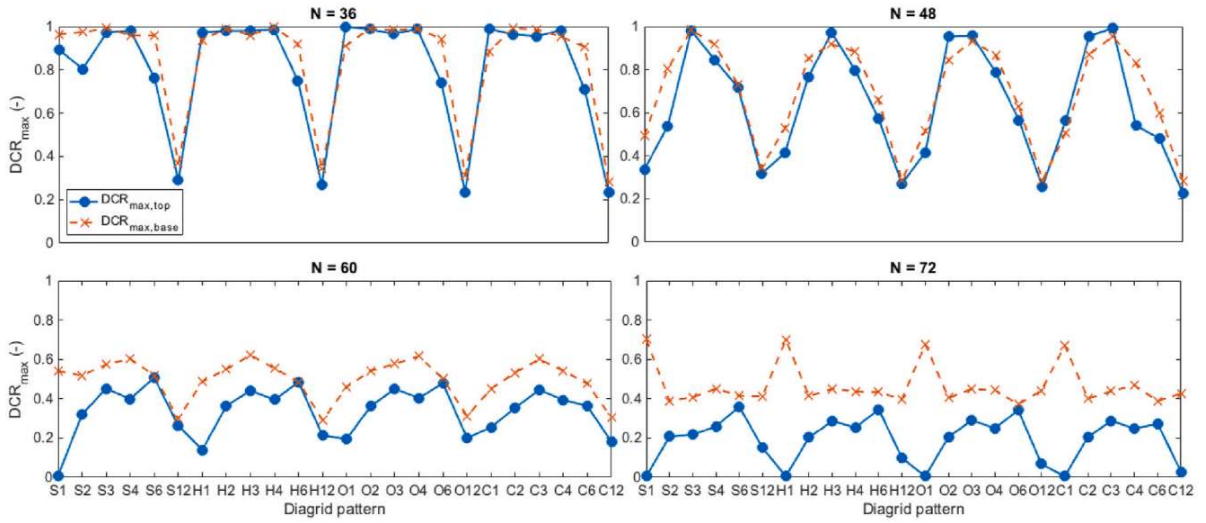


Figure 30: Maximum demand-to-capacity ratio (DCR) for the top (continuous blue line), and base (dashed orange line) diagrid modules of the twenty-four uniform-angle patterns, for the building with 36, 48, 60, and 72 floors [26]

For the building that has $N = 48$ (with an aspect ratio of (5.6), maximum demand-to-capacity ratio (DCR) analysis found that suitable diagrid patterns, with diagonal inclinations in the intermediate range (i.e., $\sim 60^\circ - 70^\circ$), achieve maximum DCR values approaching or equal to 1, as indicated in Figure 29, and also satisfy the lateral deflection limit (δ_{lim}) in the preliminary design. This implied that these suitable diagrid patterns, with intermediate inclinations, provided a good compromise, in the preliminary stages, for a layout that is both strong and stiff enough to use the structural members as fully as necessary.

4.3 Geometry-driven performance optimization of diagrid structures

For diagrid patterns with a very narrow or steep diagonal inclination, their maximum DCR values are lower due to their additional lateral flexibility, which results in being governed by stiffness and not strength in their preliminary design. This means these are poor configurations from a material use perspective, as structural designs that rely on controlling lateral displacements had to be adopted.

For taller buildings, such as those with $N = 60$ (aspect ratio of 7.0) and $N = 72$ (aspect ratio of 8.4), the preliminary design is entirely dominated by stiffness criteria across all diagrid patterns. The maximum DCR values for these buildings are generally low, often below 0.6, indicating that the structural members are underutilized in terms of their strength capacity. At the same time, the top lateral displacement ($\delta_{i,top}$) consistently reaches, and in some cases exceeds, the target limit (δ_{lim}), as shown in Figure 29. This highlighted the increasing challenge of achieving adequate lateral stiffness in taller buildings, where controlling deflections becomes the primary design driver.

Figure 31 illustrates the relationship between the torsional flexibility of diagrid structures and the number of intra-module floors ($n_{f,m}$), as well as the influence of diagonal inclination and plan shape on torsional behavior. The research results presented in [26] showed that torsional flexibility increased with the increase of interior floor module floors ($n_{f,m}$), which also resulted in values of diagonal inclination that were steeper; however, this was true for torsional rigidity as well and ultimately demonstrated the variability of torsional response of the building based upon diagonal geometry and increasing torsional flexibility corresponding to an increased diagonal inclination. The specific plan shape has little effect on torsional rigidity.

Rounder plan shapes exhibit slightly stiffer torsional behavior compared to other geometries, suggesting that while plan shape plays a secondary role, it can still contribute marginally to the overall torsional performance.

In [26] the dramatic variation in torsional rotations was observed, with maximum values being up to forty times higher than the minimum. This underscored the critical influence of diagonal inclination on torsional behavior. The choice of diagonal pattern and inclination is therefore essential for controlling torsional flexibility and ensuring the building performs adequately under torsional loads.

4. DIAGRID STRUCTURES

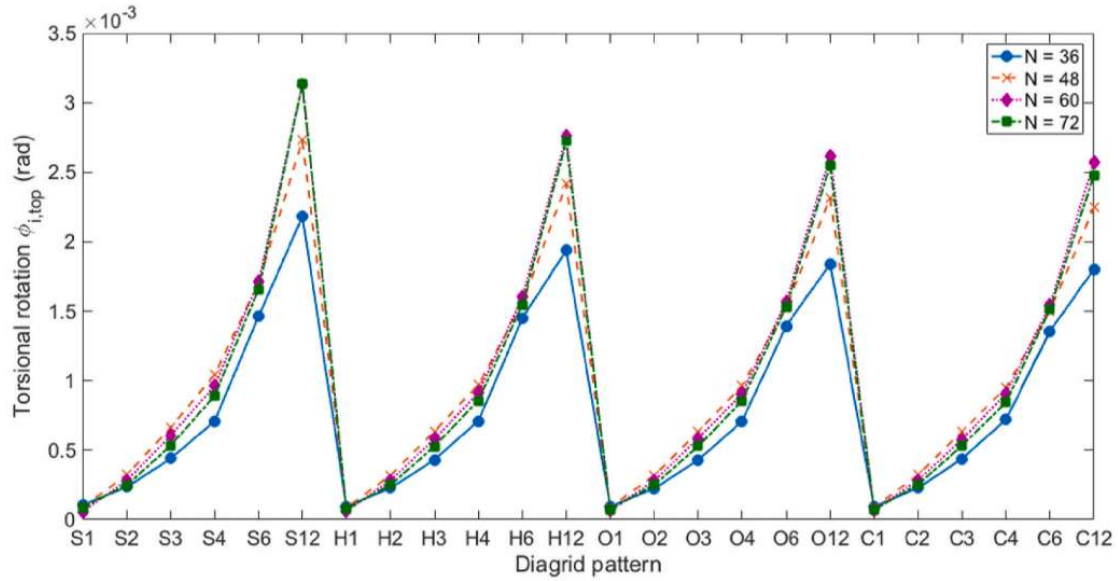


Figure 31: Torsional rotation at the top of the building $\phi_{i,top}$ for the twenty-four uniform-angle diagrid patterns, for the building with 36 (continuous blue line), 48 (dashed orange line), 60 (dotted purple line), and 72 (dashed-dotted green line) floors [26]

Figure 32 presents the total amount of steel and gives perspective on the relationship between the diagonal inclination and material efficiency. The work in [26] identified a useful range of diagonal inclinations, approximately $65^\circ - 70^\circ$ (equivalent to $n_{f,m} = 3$ and 4), where the usage of steel is minimized. The range of $65^\circ - 70^\circ$ is more material efficient because it represents the best balance between the structural requirements of strength and stiffness.

In terms of material usage, the impact of plan shape was small, which further supports diagonal inclination being the single most important factor impacting structural weight. Shape is secondary to providing efficient material usage, and the diagonal inclination is much more significant in terms of material efficiency.

There is a huge variation in material usage among configurations, and even the maximum weight of the diagrid was 4 times the minimum. This variation illustrated the importance of selecting the correct diagonal inclinations. Poorly selected inclinations that are very shallow or very steep will yield poorly optimized, structurally inefficient designs, which require far more material.

4.3 Geometry-driven performance optimization of diagrid structures

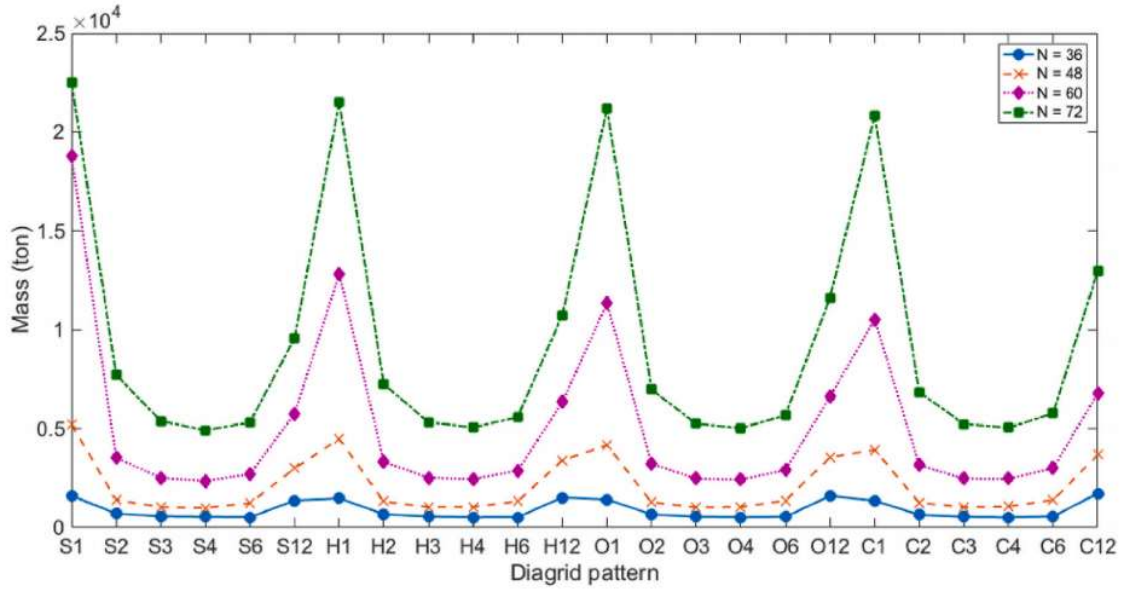


Figure 32: Diagrid weight W_i for the twenty-four uniform-angle diagrid patterns, for the building with 36 (continuous blue line), 48 (dashed orange line), 60 (dotted purple line), and 72 (dashed-dotted green line) floors [26]

Figure 33 presents the construction complexity index (CI) for a variety of diagrid patterns and building heights considering [26] and explained in this article based on five key construction parameters: (N_1) Number of nodes, (N_4) Number of diagonals, (N_2) Number of cross-sectional profiles, (N_3) Number of slices for transportation, (N_5) Length of the diagonals. These five parameters, when combined, define the complexity in constructing a diagrid system.

The analysis explored in [26] also showed that the CI values cover a small variation across different shapes of the floor plan. The reason for this is that the most important contributing parameters to the construction complexity (N_1 , N_3 , N_4 , N_5), are independent of the actual plan geometry. The only parameter that varies as a result of the shape of the plan is N_2 , which represents the variation in the number of profiles. Thus, the construction complexity index does not depend on the geometry of the floor plan and establishing that plan shape is of minor importance in establishing construction complexity.

In summary, the CI values included a degree of significance based on the contributing factors that are directly related to the diagrid pattern and the height of the building. The elements contributing the most to the construction complexity were the total number of nodes, the number and length of diagonals, and the number of segments that had to be built for transportation to ensure the diagonal members would not exceed the maximum allowable length of 12 m.

4. DIAGRID STRUCTURES

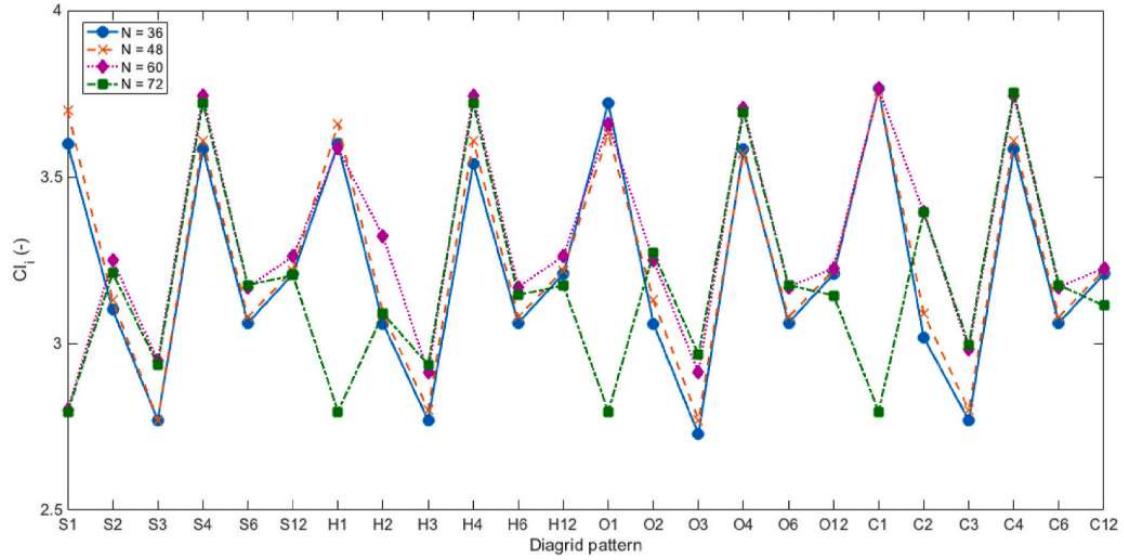


Figure 33: Complexity index CI_i for the twenty-four uniform-angle patterns, for the building with 36 (continuous blue line), 48 (dashed orange line), 60 (dotted purple line), and 72 (dashed-dotted green line) floors [26]

Figure 34 illustrates the overall desirability (OD) scores for various diagrid configurations, combining individual desirability metrics into a comprehensive evaluation. The results obtained in [26] were presented as three-dimensional plots, where the vertical axis represents the OD value, ranging from 0 to 1, while the two horizontal axes correspond to the plan shape (square, hexagon, octagon, circle) and the number of intra-module floors ($n_{f,m}$).

The analysis conducted in [26] showed that across all building heights, the most desirable diagrid solution relates to three intra-module floors ($n_{f,m} = 3$). The analysis revealed that this configuration achieved a reasonable balance in terms of structural performance, material efficiency, and complexity of construction, thus it was reasonable to support a three-intra-module floor solution. Concerning plan shapes, the octagonal plan shape (O3) was the most desirable for buildings with 36, 48, and 60 floors, as it achieved OD values of 0.54, 0.64, and 0.74, respectively. The OD values suggested that there may be an overall performance benefit for mid-rise buildings by using the octagonal shape, as it offered a favourable balance of structural and construction elements.

The hexagonal plan shape (H3) was elicited as the most desirable form for the 72-floor building, confirming hexagonal shapes perform best for taller buildings, as evidenced with an OD of 0.72. Additionally, while the most desirable plan shape for the 72-floor building was hexagonal, it is worth noting that the circular plan shape (C3) also elicited a highly desirable plan shape, further confirming some advantages of curved shapes for taller buildings. Overall,

4.3 Geometry-driven performance optimization of diagrid structures

the findings showed that the number of intra-module floors and plan shapes strongly influence the overall desirability of diagrid solutions. We expect to find $n_{f,m} = 3$ still achieving the overall best OD results, while we find that each plan shape is height-dependent. As building height increases, various structural and design elements demand changes to priority levels. The OD surfaces in Figure 34 were cylindrical along the plan shape axis, although subtle, which confirms that there are not significant differences among plan shapes and justifies that an individual plan shape to have a small impact on the diagrid's efficiency; Relative to the number of intra-module floors which directly impacts diagonal inclination, individual plan shapes have a negligible impact on structural response and therefore the overall desirability of the diagrid pattern.

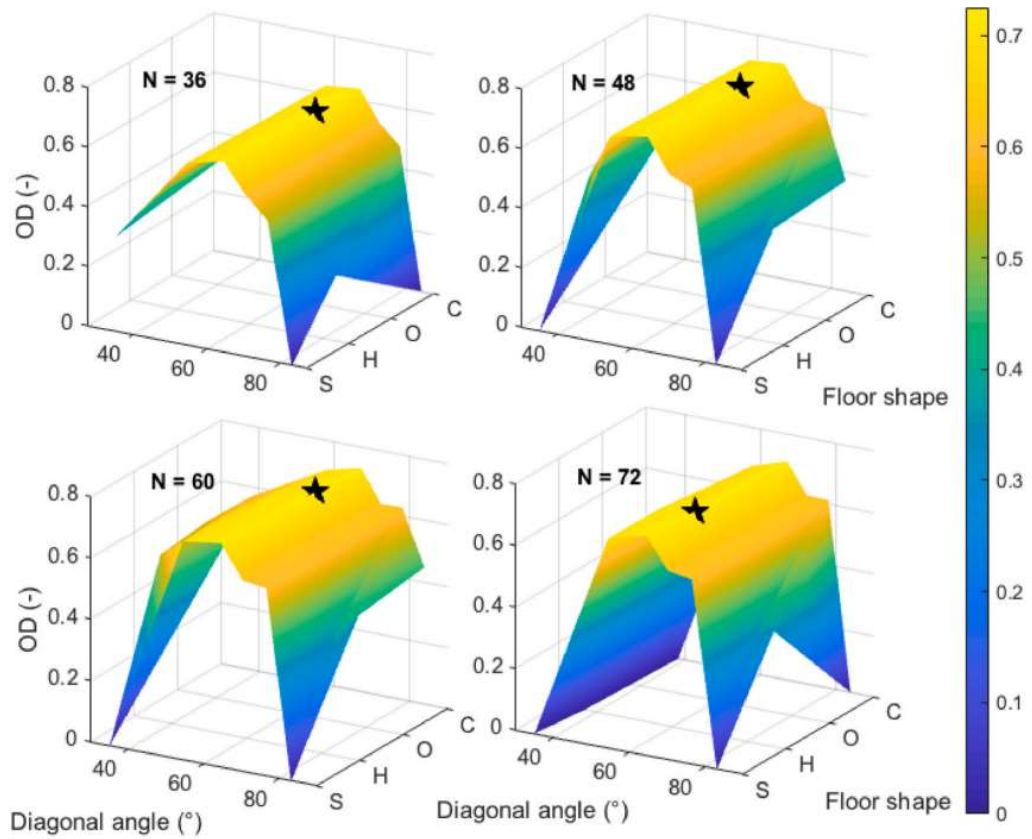


Figure 34: Overall desirability values OD_i for each diagrid pattern i , for the building with 36, 48, 60, and 72 floors. The OD values are reported here as an interpolated surface in the 3D space. The vertical axis represents the value of the OD while the horizontal axes are associated with the two geometrical features of each diagrid pattern, i.e., plan shape and number of intra-module floors $n_{f,m}$. Colors are drawn according to the OD values ranging from dark blue (minimum OD) to bright yellow (maximum OD). Black stars identify the solutions with the highest overall desirability (O3 for $N = 36$, O3 for $N = 48$, O3 for $N = 60$, and H3 for $N = 72$). [26]

In conclusion, for the uniform-angle population analysis done in [26], diagrid patterns with modules containing three intra-module floors (corresponding to a diagonal inclination of approximately 65°) were identified as the most desirable when all four responses were taken

4. DIAGRID STRUCTURES

into account. Patterns with two intra-module floors (diagonal inclination of about 55°) were also found to be competitive. While patterns with 2 intra-module floors performed worse with respect to structural weight and construction complexity, their relative torsional performance made their OD values competitive with those of the 3-floor modules. Notably, the study found that the optimal diagonal inclination remains unchanged as the overall height of the building rises. This is in contrast to many studies that have claimed that taller buildings are associated with steeper diagonals providing better performance. This inconsistency can result from the necessity to balance a range of responses. While balancing lateral displacement and structural weight in taller buildings may drive the use of steeper diagonals, the need to limit torsional flexibility and construction complexity does not. A steeper diagonal inclination would reduce the torsional performance of the diagrid and often incur greater construction complexity. Therefore, the optimal inclination is a result of a compromise between these needs.

Always regarding the study done by Scaramozzino et al. [26], Figure 34 presents the maximum and minimum cross-sectional areas for the base and top diagonal modules, respectively, after member sizing for the broader population of varying-angle diagrid patterns. The diagrid patterns were organized into four groups, with the first quarter representing the square diagrids, the second quarter corresponding to the hexagonal shapes, the third quarter to octagonal configurations, and the final quarter to circular buildings.

The graphs in Figure 35 demonstrate that the cross-sectional area values are trending similarly across different plan floor shapes, reinforcing the observation that specific plan geometry has a minimal impact on the preliminary sizing of members. On the other hand, the diagonal pattern within the same plan shape population appears to exert a noticeably greater influence on the cross-sectional areas. While many of the solutions have similar maximum and minimum cross-sectional area values across the height of the building, how the areas are distributed over the height of the building appears to be more diverse.

Figure 35 indicates that some diagrid patterns produce exaggerated peaks in cross-sectional area values, which represents wastefulness. This means that those patterns required a significant material quantity to meet the strength and stiffness requirements, which are less than optimal for construction purposes. Accordingly, it is of little surprise that these wasteful solutions are characterized by diagrid patterns that have very shallow diagonals spaced throughout the height of the building.

4.3 Geometry-driven performance optimization of diagrid structures

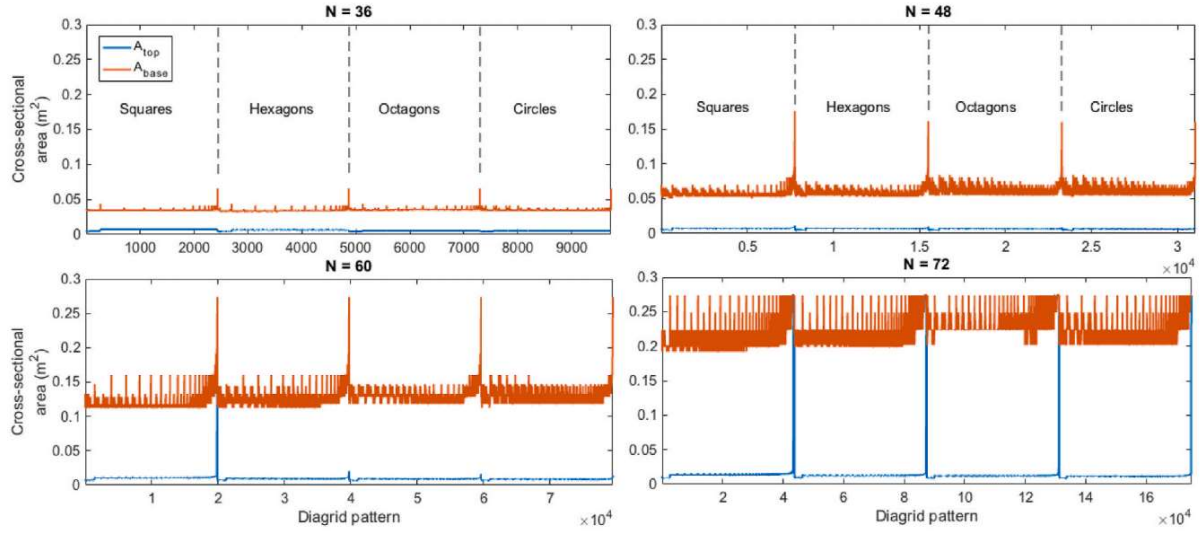


Figure 35: Cross-sectional areas (in m^2) for the top (blue line) and base (orange line) modules of all varying-angle diagrid patterns, for the building with 36, 48, 60, and 72 floors. Diagrid pattern numbers are defined according to the specific combination of different diagrid modules with different diagonal combinations. The first quarter of the pattern numbers refer to the square diagrids, the second quarter to the hexagons, the third quarter to the octagons, and the last quarter to the circles [26]

Figure 36 presents the lateral displacements under wind load for each diagrid pattern and building height. Similar to the observations made in [26] for the uniform-angle diagrid population in Figure 28, for buildings with $N = 60$ and $N = 72$, certain diagrid solutions exceeded the displacement limit δ_{lim} . This is particularly noticeable in the spikes shown in the lower panels of Figure 36, which highlight these non-compliant solutions.

The comparison between uniform-angle and varying-angle diagrid patterns revealed that there is not much difference in their performance regarding lateral displacements. Both populations exhibit similar trends, with some patterns failing to meet the displacement criteria for taller buildings.

4. DIAGRID STRUCTURES

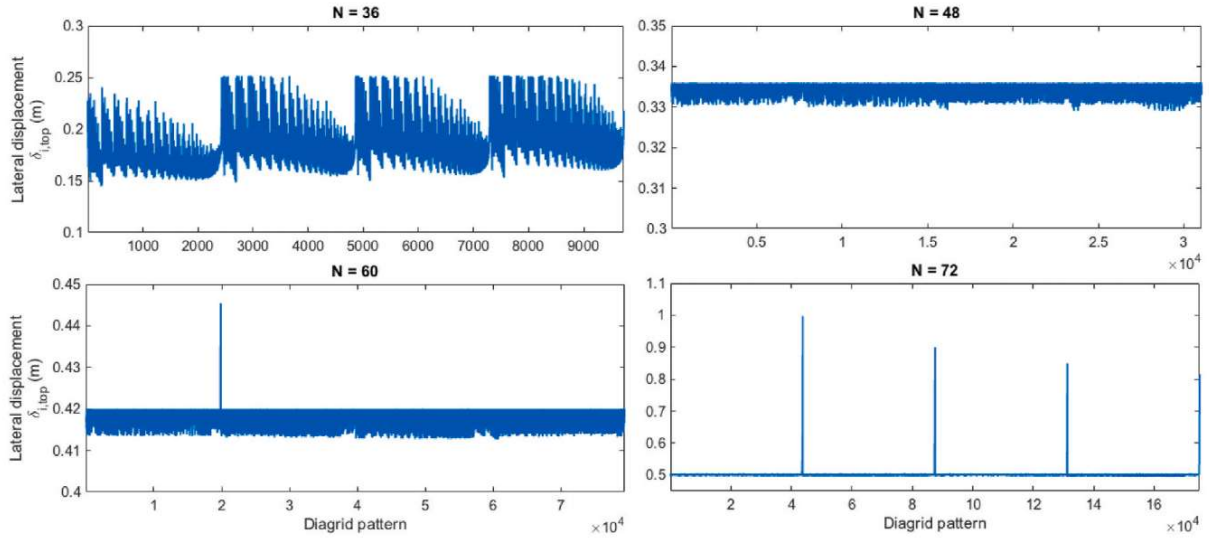


Figure 36: Lateral displacement at the top of the building $\delta_{i,top}$ for all varying-angle diagrid patterns, for the building with 36, 48, 60, and 72 floors [26]

Figure 37 illustrates the maximum demand-to-capacity ratio (DCR) values for the top and base diagrid modules across all varying-angle diagrid patterns and building heights. The results obtained in [26] reaffirmed that as the building height increases, stiffness criteria become increasingly dominant in the preliminary design process.

With the case for $N = 36$, the top and base modules exhibited a DCR close to 1 for most diagrid patterns, indicating that for a low building, the design is primarily governed by strength requirements and structural members are used to their full capacity. As the height of the building increases, the effect of stiffness criteria increases until it becomes the most dominant design constraint to limit lateral displacements ($\delta_{i,top} < \delta_{lim}$) as seen in in Figure 36. The lower DCR values for taller buildings demonstrate the extent to which design constraints change regarding the use of strength, particularly in lateral elements. For example, maximum DCR values occurred between 0.6 and 0.9 for $N = 48$, between 0.4 and 0.6 for $N = 60$, and between 0.2 and 0.5 for $N = 72$.

4.3 Geometry-driven performance optimization of diagrid structures

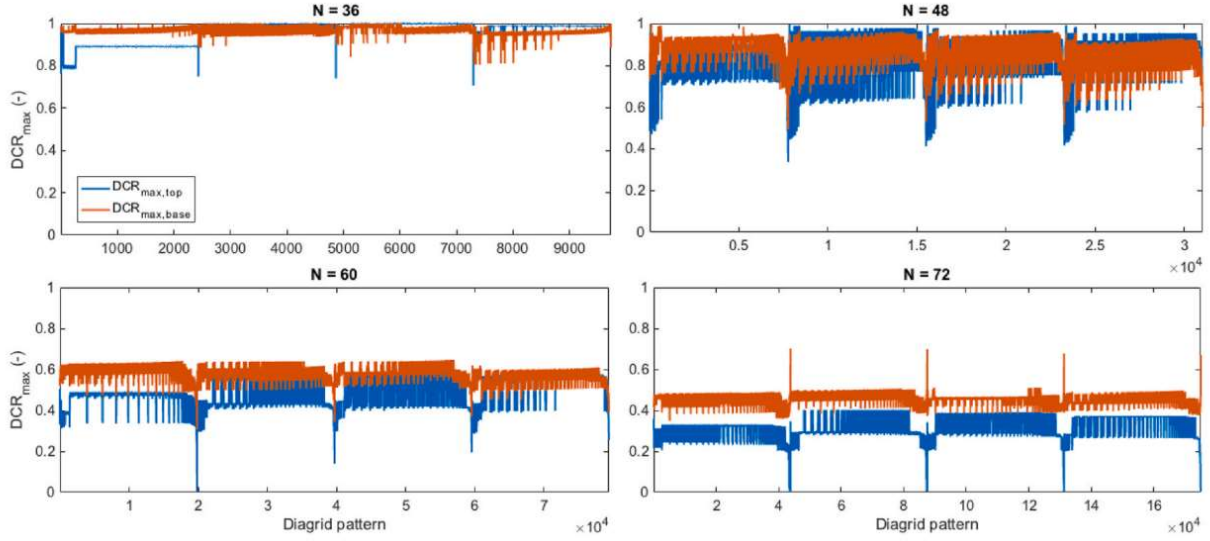


Figure 37: Maximum demand-to-capacity ratio (DCR) for the top (blue line) and base (orange line) diagrid modules of all varying-angle diagrid patterns, for the building with 36, 48, 60, and 72 floors [26]

In the reviewed study [26], the structural and geometrical characteristics of the differing-angle diagrid patterns, along with additional responses included in the multi-response method, such as torsional rotations, total weight, and the complexity index were used to compute, the desirability and overall desirability (OD) score for each of the diagrid patterns. The OD scores are presented in Figure 38 and provide a complete evaluation into the performance of each diagrid pattern. Through the evaluation of the OD values for the various diagrid patterns, the preferred designs will be identified.

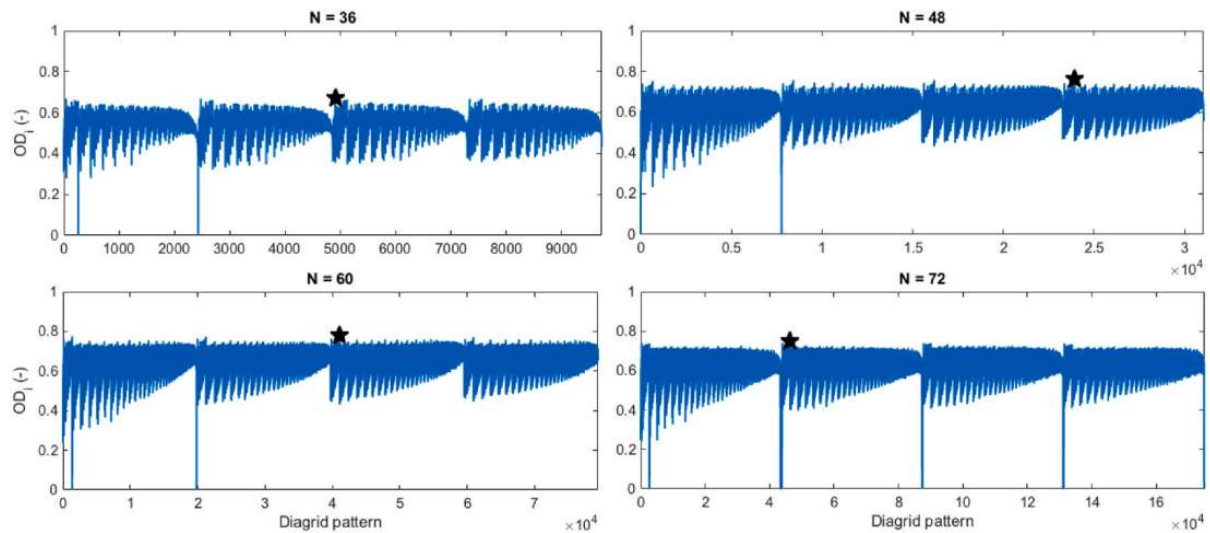


Figure 38: Overall desirability values OD_i for each diagrid pattern i , for the building with 36, 48, 60 and 72 floors. Black stars identify the solutions with the highest overall desirability, i.e., pattern #4908 for the 36-floor building, pattern #23936 for the 48-floor building, pattern #41107 for the 60-floor building, and pattern #46370 for the 72-floor building [26]

4. DIAGRID STRUCTURES

Figure 39 illustrates the distribution of OD values across the diagrid populations for the four buildings. The most desirable pattern, marked with a black star in both Figures 37 and 38, represents the configuration with the highest OD score. The distribution of OD values, as shown in Figure 39, follows a normal-like pattern: the majority of diagrid patterns exhibit OD scores near the average, while only a small subset of the population achieves very low or very high OD values. This distribution highlighted the rarity of exceptionally desirable patterns within the population.

The detailed characteristics of the fifteen most desirable diagrid geometries defined in [26], those with the highest OD scores, are presented in Tables 1 – 4 for the 36-, 48-, 60-, and 72-floor buildings, respectively.

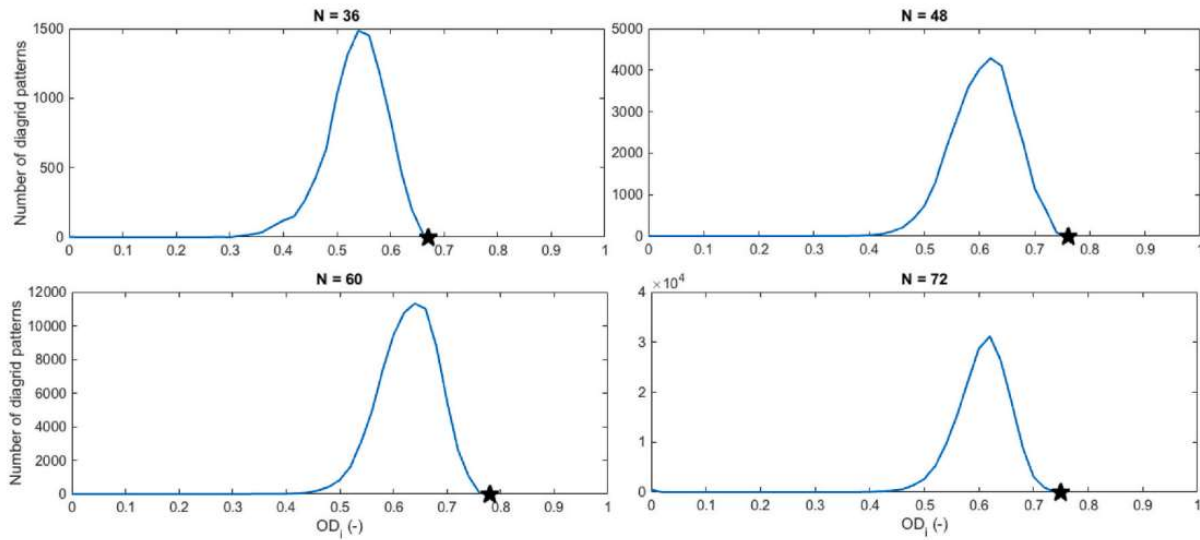


Figure 39: Distribution of overall desirability values OD_i , for the building with 36, 48, 60 and 72 floors. Black stars identify the solutions with the highest overall desirability, i.e., pattern #4908 for the 36-floor building, pattern #23936 for the 48-floor building, pattern #41107 for the 60-floor building, and pattern #46370 for the 72-floor building [26]

For the 36-floor building, diagrid pattern #4908 was identified as the most preferable pattern having the overall desirability (OD) value of 0.67. This pattern corresponds to the octagonal uniform-angle with twelve modules each made of three intra-module floors, designated O3. The individual desirability scores for this pattern are clearly strong across all considered responses in Table 1, so the high overall desirability score can be attributed to strong performance across factors.

Table 1 also indicates that other diagrid geometries have similarly desirable OD values, with the fifteen most preferable patterns showing a very narrow range of 0.66 - 0.67. Among them, a large percentage (7 out of 15) are uniform-angle geometries like H3 (the second most

4.3 Geometry-driven performance optimization of diagrid structures

desirable with an OD of 0.667), C2 (the third most desirable with an OD of 0.667), and S3 (the fourth most desirable with an OD of 0.667). Overall, the uniform-angle geometries scored consistently well to emphasize that uniform-angle configurations have desirable structural and geometric attributes.

The remaining eight geometries among the top fifteen range from varying-angle patterns. The varying-angle patterns consistently came out of modules that contain two or three intra-module floors.

#	Diagrid patter no.	Floor shape	M_1	M_2	M_3	M_4	M_5	M_6	$d_{i,\delta}$	$d_{i,\psi}$	$d_{i,w}$	$d_{i,cl}$	OD
1	4908 (O3)	O	0	0	12	0	0	0	0.691	0.719	0.658	0.617	0.670
2	2476 (H3)	H	0	0	12	0	0	0	0.692	0.718	0.655	0.609	0.667
3	7556 (C2)	C	0	18	0	0	0	0	0.693	0.851	0.601	0.559	0.667
4	44 (S3)	S	0	0	12	0	0	0	0.704	0.713	0.647	0.609	0.667
5	7340 (C3)	C	0	0	12	0	0	0	0.682	0.713	0.665	0.609	0.666
6	7554	C	0	15	2	0	0	0	0.696	0.823	0.621	0.547	0.664
7	7547	C	0	12	4	0	0	0	0.692	0.793	0.641	0.551	0.664
8	5124 (O2)	O	0	18	0	0	0	0	0.700	0.853	0.588	0.551	0.663
9	5115	O	0	12	4	0	0	0	0.701	0.798	0.633	0.542	0.662
10	7530	C	0	9	6	0	0	0	0.685	0.764	0.657	0.555	0.661
11	2666	H	0	9	6	0	0	0	0.693	0.766	0.647	0.555	0.661
12	200	S	0	6	8	0	0	0	0.696	0.732	0.650	0.576	0.661
13	2692 (H2)	H	0	18	0	0	0	0	0.698	0.851	0.580	0.551	0.660
14	5098	O	0	9	6	0	0	0	0.696	0.769	0.649	0.546	0.660
15	2683	H	0	12	4	0	0	0	0.699	0.795	0.630	0.542	0.660

Table 1: The fifteen most desirable diagrid patterns for the 36-floor building, ordered for decreasing value of OD [26]

Tables 2 – 4 extend the analysis presented in Table 1 to the taller buildings, specifically those with 48, 60, and 72 floors. For the 48-floor building, the most desirable diagrid pattern was identified as the circular uniform-angle configuration with two intra-module floors (C2), achieving an OD value of 0.76. Similarly, for the 60-floor building, the octagonal uniform-angle diagrid with two intra-module floors (O2) emerges as the most desirable, with an OD value of 0.78. For the 72-floor building, the hexagonal uniform-angle diagrid with two intra-module floors (H2) was found to be the most desirable, with an OD value of 0.75.

These results obtained in [26] highlighted a consistent trend: despite the inclusion of a wide variety of varying-angle geometries in the analysis, uniform-angle diagrids consistently outperformed their varying-angle counterparts in terms of overall desirability. This finding underscored the efficiency and robustness of uniform-angle configurations, which represent a specific subset of the broader diagrid population. Furthermore, as observed in the case of the 36-floor building, many uniform-angle patterns with two or three intra-module floors are consistently ranked among the fifteen most desirable patterns for all building heights.

4. DIAGRID STRUCTURES

#	Diagrid patter no.	Floor shape	M_1	M_2	M_3	M_4	M_5	M_6	$d_{i,\delta}$	$d_{i,\varphi}$	$d_{i,w}$	$d_{i,CI}$	OD
1	23936 (C2)	C	0	24	0	0	0	0	1.000	0.810	0.760	0.544	0.761
2	8416 (H2)	H	0	24	0	0	0	0	1.000	0.812	0.748	0.544	0.758
3	16176 (O2)	O	0	24	0	0	0	0	1.000	0.812	0.756	0.537	0.758
4	23934	C	0	21	2	0	0	0	1.000	0.782	0.776	0.534	0.754
5	16174	O	0	21	2	0	0	0	1.000	0.781	0.774	0.534	0.754
6	654	S	0	21	2	0	0	0	1.000	0.777	0.756	0.547	0.753
7	8414	H	0	21	2	0	0	0	1.000	0.783	0.766	0.534	0.752
8	656 (S2)	S	0	24	0	0	0	0	1.000	0.810	0.733	0.537	0.751
9	23927	C	0	18	4	0	0	0	1.000	0.753	0.788	0.530	0.749
10	16150	O	0	15	6	0	0	0	1.000	0.726	0.795	0.540	0.747
11	630	S	0	15	6	0	0	0	1.000	0.716	0.785	0.553	0.747
12	16167	O	0	18	4	0	0	0	1.000	0.755	0.786	0.524	0.747
13	8390	H	0	15	6	0	0	0	1.000	0.728	0.790	0.540	0.747
14	9578	H	2	23	0	0	0	0	1.000	0.805	0.750	0.514	0.746
15	23910	C	0	15	6	0	0	0	1.000	0.726	0.796	0.533	0.745

Table 2: The fifteen most desirable diagrid patterns for the 48-floor building, ordered for decreasing value of OD [26]

#	Diagrid patter no.	Floor shape	M_1	M_2	M_3	M_4	M_5	M_6	$d_{i,\delta}$	$d_{i,\varphi}$	$d_{i,w}$	$d_{i,CI}$	OD
1	41107 (O2)	O	0	30	0	0	0	0	1.000	0.837	0.829	0.534	0.780
2	1391 (S2)	S	0	30	0	0	0	0	1.000	0.836	0.812	0.534	0.776
3	21249 (H2)	H	0	30	0	0	0	0	1.000	0.837	0.823	0.522	0.774
4	60965 (C2)	C	0	30	0	0	0	0	1.000	0.835	0.832	0.509	0.771
5	41098	O	0	24	4	0	0	0	1.000	0.800	0.848	0.518	0.770
6	21189	H	0	18	8	0	0	0	1.000	0.757	0.858	0.536	0.768
7	41047	O	0	18	8	0	0	0	1.000	0.758	0.861	0.529	0.767
8	21240	H	0	24	4	0	0	0	1.000	0.800	0.843	0.512	0.767
9	41105	O	0	27	2	0	0	0	1.000	0.816	0.840	0.503	0.767
10	21247	H	0	27	2	0	0	0	1.000	0.817	0.835	0.503	0.766
11	1389	S	0	27	2	0	0	0	1.000	0.813	0.827	0.509	0.765
12	20013 (H3)	H	0	0	20	0	0	0	1.000	0.663	0.866	0.596	0.765
13	39871 (O3)	O	0	0	20	0	0	0	1.000	0.660	0.869	0.596	0.765
14	60963	C	0	27	2	0	0	0	1.000	0.814	0.843	0.497	0.764
15	21223	H	0	21	6	0	0	0	1.000	0.778	0.852	0.514	0.764

Table 3: The fifteen most desirable diagrid patterns for the 60-floor building, ordered for decreasing value of OD [26]

#	Diagrid patter no.	Floor shape	M_1	M_2	M_3	M_4	M_5	M_6	$d_{i,\delta}$	$d_{i,\varphi}$	$d_{i,w}$	$d_{i,CI}$	OD
1	46370 (H2)	H	0	36	0	0	0	0	1.000	0.850	0.678	0.549	0.750
2	46361	H	0	30	4	0	0	0	1.000	0.821	0.713	0.531	0.747
3	46310	H	0	24	8	0	0	0	1.000	0.791	0.738	0.530	0.746
4	46344	H	0	27	6	0	0	0	1.000	0.809	0.725	0.522	0.744
5	46154	H	0	18	12	0	0	0	1.000	0.761	0.752	0.534	0.743
6	46250	H	0	21	10	0	0	0	1.000	0.776	0.747	0.526	0.743
7	44001 (H3)	H	0	0	24	0	0	0	1.000	0.684	0.764	0.579	0.742
8	90122 (O2)	O	0	36	0	0	0	0	1.000	0.849	0.691	0.513	0.741
9	87753 (O3)	O	0	0	24	0	0	0	1.000	0.684	0.767	0.573	0.741
10	249 (S3)	S	0	0	24	0	0	0	1.000	0.681	0.761	0.579	0.740
11	46009	H	0	15	14	0	0	0	1.000	0.745	0.757	0.530	0.739
12	89761	O	0	15	14	0	0	0	1.000	0.742	0.763	0.524	0.738
13	131505 (C3)	C	0	0	24	0	0	0	1.000	0.681	0.768	0.568	0.738
14	2592	S	0	27	6	0	0	0	1.000	0.803	0.716	0.516	0.738
15	90002	O	0	21	10	0	0	0	1.000	0.775	0.753	0.508	0.738

Table 4: The fifteen most desirable diagrid patterns for the 72-floor building, ordered for decreasing value of OD [26]

In conclusion, for the wider population of varying-angle diagrid patterns, it was again observed that the floor plan shape has only a minor influence on the building's overall performance. Interestingly, a specific subset of varying-angle patterns, namely, uniform-angle geometries, consistently emerged as some of the most desirable solutions across all the investigated buildings. This finding is in disagreement with previous studies that indicated that uniform-angle diagrids were more efficient for short buildings, while truly varying-angle

diagrids would be superior for tall buildings. However, the difference in findings came from the criteria that we used to define the "optimal" geometry. The previous studies determined the optimal geometric condition with respect to minimizing structural mass while satisfying strength and lateral displacement constraints.

When additional responses, such as construction complexity and torsional flexibility, are considered, the outcomes shift. In this case, the analysis revealed that uniform-angle diagrids are the most desirable configurations for both shorter and taller buildings. This is because they offer advantages in terms of torsional performance and construction simplicity, which outweigh the potential benefits of varying-angle patterns in other aspects.

Furthermore, the study confirmed that diagrid patterns with diagonals spanning two or three floors (corresponding to diagonal inclinations of approximately 55° - 65°) are the most desirable in this multi-response framework. These patterns strike a balance between structural efficiency, torsional stiffness, and construction feasibility, making them optimal solutions for a wide range of building heights [26].

4.4 Preliminary design of diagrid structures

The preliminary design of diagrid structures has been extensively studied in the literature, with numerous researchers proposing methodologies to optimize their structural performance and efficiency. In this section, the key contributions from existing studies will be reviewed and analyzed to provide a comprehensive and clear understanding of this topic.

Among these contributions, particular attention is given to the work of Moon et al. [19] where the authors addressed the specific structural response of diagrids and their pivotal role in the lateral stiffness of tall buildings, emphasizing that, in well-designed diagrid structures, braced cores contribute only 15 - 20 % of the total lateral stiffness.

Typically, these methodologies begin by distributing the bending and shear deformation contributions to the total lateral displacement of the structure, taking into account critical factors such as the height-to-width ratio of tall buildings. The bending and shear deformation demands are then converted into the required cross-sectional areas of diagrid members using simplified equations, facilitating a straightforward and effective design process.

4. DIAGRID STRUCTURES

The model for the preliminary design of the building is a beam, subdivided longitudinally into modules according to the repetitive diagrid pattern. Each module is defined by a single level of diagrids that extend over n -stories. Figure 40 illustrates the case of a 6-story module.

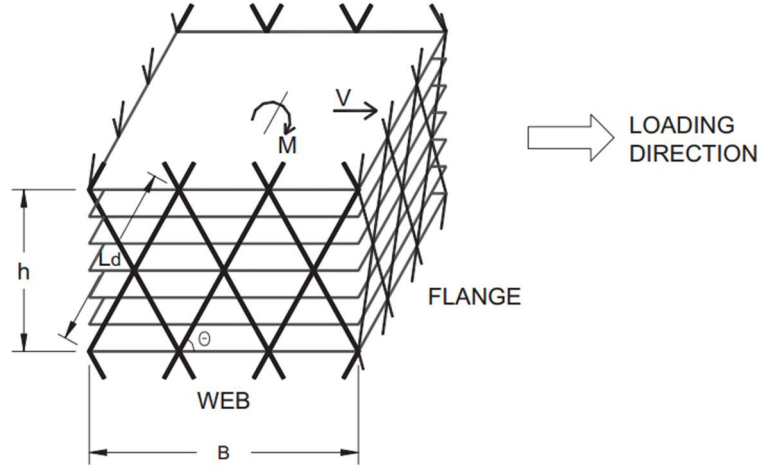


Figure 40: Six-story diagrid structure module and load distribution [19]

Depending upon the direction of loading, the faces act as either web or flange elements. The diagonal members are assumed to be pin-ended, and therefore to resist the transverse shear and moment through only axial action. With this schematization, a stiffness-based approach has been used to determine the cross-sectional area of typical web and flange members for each module.

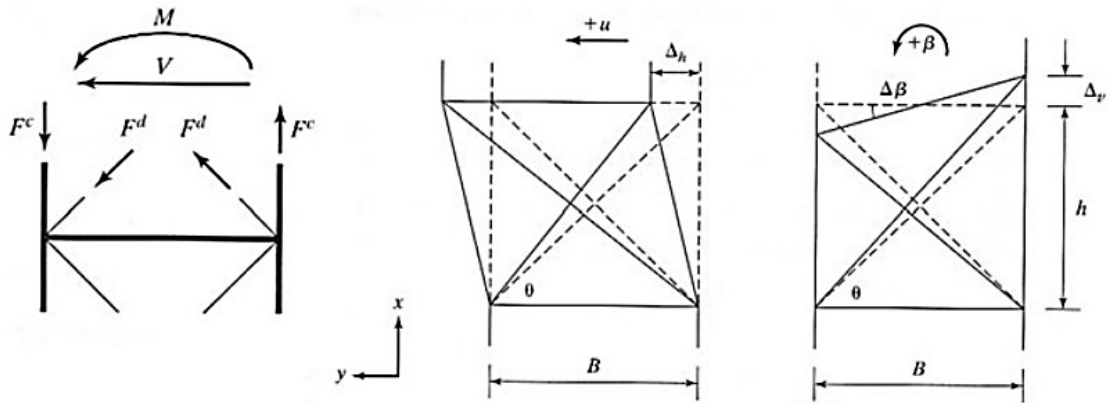


Figure 41: Brace frame model [19]

Referring to Figure 41, both shear force and bending moment for the module are expressed in terms of the relative displacement and rotation measures given by the product of module height and transverse shear γ and bending deformation χ , respectively:

$$V = K_T \Delta u = \gamma \cdot h \quad (6)$$

$$M = K_B \Delta\beta = \chi \cdot h \quad (7)$$

Considering N_w as the number of diagonals extending over the full height in one web plane, and N_f as a similar count for one flange plane, for the compatibility, constitutive and equilibrium equations, it is possible to evaluate the bending and shear stiffnesses as:

$$K_T = 2N_w \left(\frac{A_{d,w} E}{L_d} \cos^2 \theta \right) \quad (8)$$

$$K_B = N_f \left(\frac{B^2 A_{d,w} E}{2L_d} \right) \sin^2 \theta \quad (9)$$

Where $A_{d,w}$ and $A_{d,f}$ represent the cross-sectional areas of the web and flange members, respectively, E is the elastic modulus, B is the web dimension, L_d is the diagonal length, and θ denotes the contribution of the web diagonals to bending rigidity. At this stage, by setting the desired transverse shear and bending deformations, γ^* and χ^* , and for given values of V (shear force) and M (bending moment), the preliminary expressions for the cross-sectional areas of the web and flange members can be derived:

$$A_{d,w} = \frac{VL_d}{2N_w E_d \chi h \cos^2 \theta} \quad (10)$$

$$A_{d,f} = \frac{2ML_d}{N_f B^2 E_d \chi h \sin^2 \theta} \quad (11)$$

Since the diagonal members are assumed to remain uniform within a plane, it is necessary to account for loading in both directions to determine an upper bound for the cross-sectional areas.

Furthermore, the same study proposes an optimal design approach from a motion perspective, corresponding to a state of uniform shear and bending deformation under the design loading. Uniform deformation states can only be achieved in statically determinate structures. Assuming the diagrid structure is modelled as a cantilever beam, the total deflection at the top can be expressed as the sum of contributions from shear and bending deformations. Specifically, the deflection at the top is given by:

$$u(H) = \gamma \cdot H + \frac{\chi \cdot H^2}{2} \quad (12)$$

4. DIAGRID STRUCTURES

where γ^*H and $\chi^*H^2/2$ represent the contribution from shear deformation and the contribution from bending deformation, respectively. In order to evaluate the relative contributions of bending and shear deformation, Moon et al. [19] introduce a non-dimensional parameter, s , which is defined as the ratio of the bending contribution to the shear contribution. This parameter is expressed as:

$$s = \frac{\chi \cdot H^2}{2\gamma \cdot H} \quad (13)$$

By combining Equations (12) and (13) and considering that the top lateral displacement is typically specified as a fraction of the total building height, expressed as $u(H) = H/\alpha$ (where α is usually 500), the following relationships between γ^* , χ^* , and s are obtained:

$$\gamma^* = \frac{1}{(1+s)\alpha} \quad (14)$$

$$\chi^* = \frac{2\gamma \cdot s}{H} = \frac{2s}{(1+s)\alpha H} \quad (15)$$

By substituting Equations (14) and (15) into Equations (10) and (11), the cross-sectional areas of the web and flange members can be determined for different values of the parameters α , s , and H .

If a unique s value is adopted, the initial sizing of the external diagonal members will vary. If a very small s is used, the axial deformation mode is preferred over the bending deformation mode which can lead to overuse of material in the flange members and thus excess members were sized to limit bending deflection. Conversely, if a very high s is used the axial deformation can be ignored and deformation due to bending will prevail, thus much of the cross-sectional area will be determined by the web façades that limit shear deformability. Therefore, there is an optimal s , called s_{opt} , that gives balanced control to limit shear and bending deformations. In this case the member sizes along the higher stories are governed by shear deformation modes, while the member sizes in the lower stories are governed by bending deformation modes.

The value of s_{opt} depends on the building's aspect ratio (H/B) and provides the most efficient design solution, meeting the target maximum displacement while minimizing material usage.

4.4 Preliminary design of diagrid structures

For diagrid structures taller than 40 stories, with an aspect ratio (H/B) greater than 5 and diagonal angles between 60° and 70° , the following empirical equation is proposed for s_{opt} :

$$s_{opt} = \frac{H}{B} - 3 \quad (16)$$

Another important variable that significantly impacts the initial design of diagrids is the angle of diagonal inclination. Moon et al. [19] researched 20 - to 60 - story buildings and found the optimal diagonal angle depended on the aspect ratio for the building. For diagrids near an aspect ratio of about 7, optimal diagonal angles fell between 65° and 75° . For diagrids with a lower aspect ratio (approximately 5), the optimal diagonal angle was exceedingly lower (around 10°). The difference is the best diagonal angle depends on how shear and bending stiffness influence the deformation mode, and how they depend on the diagonal angle. Shear stiffness, for this case, is maximized when diagonal inclination is about 35° . Bending stiffness is maximized when the elements are vertical ($\theta = 90^\circ$). An optimal angle must exist between the two extremes that can balance and maximize shear and bending stiffness yielding an effective response to design loading conditions.

Moon committed to using the same stiffness-based method to braced tube structures described in the previous paragraphs in [20]. In these systems, the external mega-diagonals see shear force only, while the exterior vertical columns carry the bending moment. Moon's analyses conducted on braced tubes approximately 40 - to 100 - stories, showed an optimal diagonal angle of 45° which is less dependent on aspect ratio of the building. This is a lower dependence because the external diagonals do not have much influence on resisting bending moments and they mainly provide shear stiffness.

In the cases investigated by Moon [19, 20], it is observed that stiffness requirements primarily govern the preliminary design, with strength criteria generally being satisfied. Only a limited number of members, particularly in the leeward façade, are found to fail when the maximum allowable displacement is relaxed, i.e., when $\alpha < 500$. However, due to the high rigidity provided by the diagonalized façades, which make diagrid structures exceptionally efficient, strength requirements can become critical. In certain scenarios, they may even dictate the design criteria, as highlighted by Montuori et al. in [28] who proposed a simplified strength-based methodology for the preliminary design of diagrid tubes. This approach considers both gravity and lateral loads applied to the building, ensuring that strength requirements are

4. DIAGRID STRUCTURES

adequately addressed. Figure 42 illustrates the adopted scheme used to develop this strength-based design methodology, providing a practical framework for integrating strength considerations into the early stages of diagrid design.

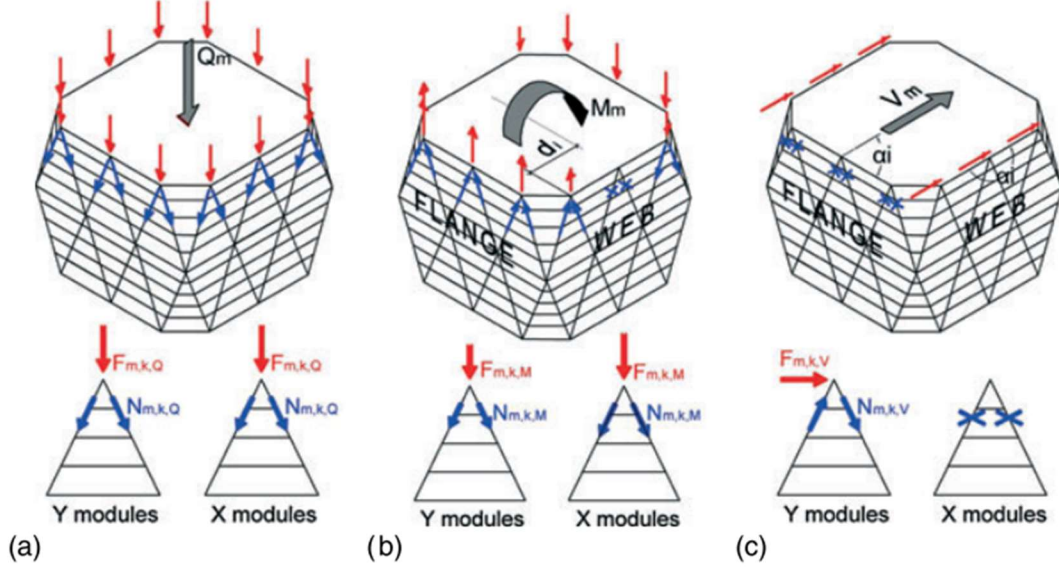


Figure 42: Axial forces in diagonals of the k -th triangular scheme of the m -th module for: (a) gravity loads, Q_m ; (b) overturning moment, M_m ; (c) global shear, V_m [28]

Assuming that the internal core occupies 25% of the total floor area, the diagrid system is responsible for carrying 37.5% of the gravity load at the level of the m^{th} module, denoted as Q_m (Figure 42(a)). Under this vertical loading condition, a uniform compression state is induced in all the n_k diagonal members of the module. The axial force in each diagonal member due to the gravity load is given by:

$$N_{m,k,Q} = 0.375 \cdot Q_m \sin \theta / 2n_k \quad (17)$$

Lateral loads acting on the structure generate a bending moment, M_m , and a shear force, V_m , at the level of the m^{th} module. The bending moment, M_m , induces a uniform compression state in the diagonals of the leeward flange and a uniform tension state in the diagonals of the windward flange. Additionally, it creates a linear distribution of axial forces (tension and compression) in the web diagonals, depending on the distance d_i of the i^{th} diagonal from the center of the floor (Figure 42(b)). The axial force in the diagonals due to the bending moment is expressed as:

$$N_{m,k,M} = \pm M_m d_k \sin \theta / 2 \sum d_i \quad (18)$$

Conversely, the shear force, V_m , induces only tension and compression stresses in the web diagonals. The axial force in the web diagonals due to the shear force is given by:

$$N_{m,k,M} = \pm V_m \cos \alpha_k \cos \theta / 2 \sum \cos \alpha_i \quad (19)$$

where α is the angle between the direction of the horizontal force and the orientation of the diagrid module, and α_k is the angle for the k^{th} diagonal, (Figure 42).

Considering all loading conditions (gravity, bending, and shear), the total axial force in a generic diagonal is obtained as:

$$N_{m,k} = N_{m,k,Q} + N_{m,k,M} + N_{m,k,V} \quad (20)$$

The total axial force, $N_{m,k}$, is used to size the members. The design of the members is based on both the tensile strength and the buckling compressive resistance of the diagonal members and will achieve both strength and stability based on the combination of loading scenarios that may be present.

After structural analyses were performed on the designed buildings, it was evident that slightly more balanced structures were being created with the stiffness-based approach, as it resulted in very efficient structures in terms of top lateral deflection that were very close to the target deflection input values. However, it was also evident that there were performance issues related to the inter-story drift of the upper modules, as well as the demand-capacity ratio (DCR) of the strength demand associated with the members that were driven by buckling. Thus, all of the stiffness-based methodologies cannot provide reasonable performance-based satisfaction to strength requirements, as the strength-based methodologies cannot provide reasonable satisfaction to stiffness requirements, therefore, there were a variety of means to balance performance expectations of the individual building in question. In both methods, excessive inter-story drifts of the upper modules were observed, which could have serious repercussions for the performance of the structure. This issue has been studied by Montuori et al. [29], who proposed solutions such as incorporating special internal systems, like the secondary bracing system (SBS), to address these challenges effectively. More recently, the simultaneous effects of slenderness and diagonal angle have been incorporated into the preliminary design process [30]. Diagrid structures ranging between aspect ratios of 2 and 8 were studied with diagonal angles from 50° to 80° .

4. DIAGRID STRUCTURES

The assessment of the structures indicated that for aspect ratios between 2 and 4 the design is primarily based on strength for the different diagonal angles. On the other hand, when the aspect ratio is greater than 6, stiffness is the dominant designer, and the structural weight increases greater than linearly with slenderness. An aspect ratio of approximately 5 appeared to be a boundary condition, where the stiffness and strength design produced similar design solutions.

These results highlight that, due to the exceptional rigidity of the diagrid tubular system, it is not always possible to determine in advance whether stiffness- or strength-based criteria will govern the preliminary design. This underscores the importance of considering both factors simultaneously to achieve an optimal and efficient design solution tailored to the specific characteristics of the structure.

4.5 Structural Analysis Methodologies for Diagrid Tall Buildings

The methods for the structural analysis of diagrid structures have been widely explored in academic literature, with various researchers proposing innovative approaches to enhance the accuracy and efficiency of computations and the reliability of the results. In this section, the most significant contributions from existing studies will be reviewed and critically analyzed to offer a thorough and clear understanding of the methodologies developed for the structural analysis of diagrid systems.

4.5.1 Finite Element Method (FEM)

In academic literature, the Finite Element Method (FEM) is the most widely used approach for the structural analysis of diagrid systems. However, simplified methodologies have also been developed to enable a quicker evaluation of the overall structural behavior of diagrids. Mele et al. [31] introduced a hand-based method for estimating the axial stresses in diagrid members. This method focuses on analyzing the internal forces within the basic triangular element caused by gravity and vertical loads, while also accounting for the effects of the horizontal and vertical curvatures of the diagrid façade. Although this approach does not directly calculate the displacements of the structure, it has proven to be effective in

determining the axial forces in the diagonal members. The methodology has been applied to three real-world case studies: the Swiss Re Building in London, the Hearst Headquarters in New York, and the West Tower in Guangzhou. The axial stresses obtained through hand calculations show excellent agreement with FEM results.

4.5.2 Modular Method (MM)

More recently, Liu and Ma introduced a simplified methodology, known as the Modular Method (MM), for the structural analysis of diagrid tubes with arbitrary polygonal shapes [32]. While most existing research has focused on rectangular diagrids with vertical façades functioning as webs or flanges, limited attention has been given to diagrids with polygonal geometries.

The Modular Method is based on the modularization of the diagrid structure and the calculation of the lateral stiffness of individual diagrid modules to determine the total lateral deflection. The lateral displacement, u_i , of the i^{th} module is obtained by superimposing the contributions of shear displacement, $u_{V,i}$, and bending displacement, $u_{M,i}$. These contributions are calculated based on the shear and bending rigidity of the i^{th} module, $K_{V,i}$ and $K_{M,i}$, respectively, as follows:

$$u_{V,i} = \frac{V_1}{K_{V,1}} + \frac{V_2}{K_{V,2}} + \dots + \frac{V_i}{K_{V,i}} \quad (21)$$

$$u_{M,i} = \frac{M_1}{K_{M,1}} h i + \frac{M_2}{K_{M,2}} h (i - 1) + \dots + \frac{M_i}{K_{M,i}} h [i - (i - 1)] \quad (22)$$

where V_i and M_i are the shear force and bending moment at the level of the i^{th} module, and h is the height of the module.

The core of the Modular Method (MM) lies in the calculation of the shear and bending rigidities, $K_{V,i}$ and $K_{M,i}$, which is based on standard assumptions for diagrid tubes. These assumptions include: (I) the diagonals are subjected only to axial stress and remain within the linear elastic regime; (II) the building floors act as rigid bodies, with no internal deformation; and (III) intra-module floors are neglected in the calculation of the modular rigidities.

Shear rigidity, $K_{V,i}$, is defined as the total shear force, F_V , required to produce a unitary horizontal displacement, Δ_V , of the module (Figure 43(a)). Similarly, bending rigidity, $K_{M,i}$,

4. DIAGRID STRUCTURES

is defined as the bending moment, M , required to induce a unitary floor rotation, $\Delta\beta$, of the module (Figure 43(b)).

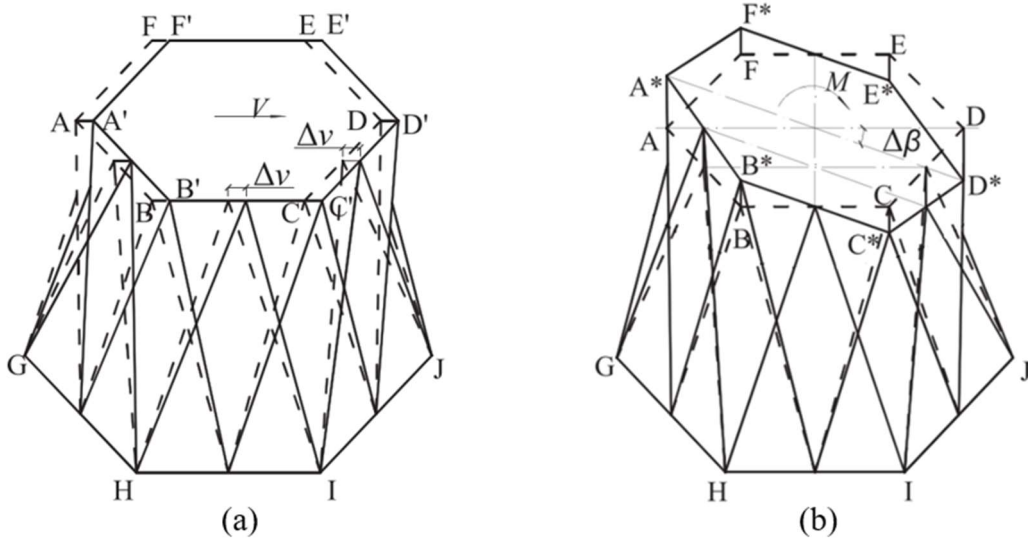


Figure 43: Diagrid tube structure module: (a) schematic diagram of shear deformation; (b) schematic diagram of bending deformation [32]

By independently applying unitary horizontal displacements and rotations to the module and calculating the resulting total shear force and bending moment, the values of $K_{V,i}$ and $K_{M,i}$ can be directly evaluated. The calculation of the shear force and bending moment in the Modular Method (MM) is derived using geometrical compatibility equations, the constitutive relations of the diagonals, and the equilibrium equations at the floor level. These steps lead to the following formulations for the shear rigidity, K_V , and bending rigidity, K_M :

$$K_V = \frac{EA \cos^2 \theta \sin \theta \sin \gamma}{h} \sum_{d=1}^N \cos^2 \alpha_d + \frac{EA \cos^3 \theta \cos^2 \gamma \sin \gamma}{h} \sum_{d=1}^N \sin^2 \alpha_d \quad (23)$$

$$K_M = \frac{EA \sin^3 \theta \sin^3 \gamma}{h} \sum_{d=1}^N B_d^2 \quad (24)$$

where E and A are the Young's modulus and cross-sectional area of the diagonals, θ is the angle between the diagonal and the main ring beam in the façade, γ is the angle between the ring beam plane and the façade, N is the total number of diagonals in the module, α is the angle between the ring beam and the shear direction, and B_d is the distance of diagonal d from the neutral axis in the main ring beam plane [32].

By applying these equations for each module, along with the expressions for the shear and bending displacements (Equations (23) and (24)), the lateral deformation of the diagrid building under horizontal loads can be evaluated.

The MM has been validated against Finite Element Method (FEM) calculations by analysing square, hexagonal, and octagonal diagrid tubes with both vertical and inclined façades under various horizontal loading conditions. The differences in top displacement between the MM and FEM results are consistently within 10%, confirming the accuracy and reliability of the proposed methodology.

4.5.3 Matrix-Based Method (MBM)

Lacidogna et al. [30] proposed a new way to understand the structural behavior of diagrids, called the matrix-based method (MBM). MBM is a procedure that relies on matrix calculus and is similar to the finite element method (FEM). The significant difference is that FEM first formulates stiffness matrices for each element (in the case of a diagrid; the diagonal member, the horizontal member or the vertical member) which are then enlarged and assembled together to form a large global stiffness matrix of the total structure (including any constraint conditions like supports of the structure). Instead, MBM will formulate the structural problem directly in terms of a matrix relation that connects the vector of external forces acting on the structure to the vector of displacements on the floors, using global stiffness matrix.

In the MBM, the inputs consist of the forces and moments applied to the structure's floors, while the outputs are the unknown displacements and rotations of these floors. The method operates under specific assumptions, consistent with those adopted by other researchers in the field (as detailed in references [19 – 32]). These assumptions include: (I) the diagonals exhibit linear elastic behavior and are subjected only to axial forces; (II) the floors remain planar after deformation, behaving as rigid bodies with a limited number of degrees of freedom; and (III) the floors within the diagonal modules are neglected in the analysis.

The stiffness matrix of the structure is determined based on the following principle: each coefficient k_{ij} in the matrix represents the total reaction force (or moment) on the i -th floor caused by a unitary displacement (or rotation) imposed on the j -th floor. By following the same process for every element and making all of the assumptions in the previous sections along the way, the entire global stiffness matrix has been formulated. At this stage, the

4. DIAGRID STRUCTURES

structural problem can be solved, including determining the floor displacements and rotations, as well as the axial forces in the diagonals. The MBM is applicable for both two-dimensional or three-dimensional systems. It offers a computable stiffness matrix for the diagrid and solves the structural problem by providing a comprehensive solution for structural analysis.

This method holds particular importance as it forms the foundation of the analysis conducted in this thesis, which will be detailed in the following chapters. For this reason, and as outlined in the research by Lacidogna et al. [30], the analysis of two-dimensional diagrid structural systems is first presented, primarily to illustrate the fundamental concepts of the matrix-based method (MBM). Subsequently, the focus will shift to a generic three-dimensional diagrid structural system to further explore and apply the method.

As illustrated in Figure 44, the analysis considers a diagrid structure composed of M floors and N modules of diagonals, with $M \geq N$. Both floors and modules are conventionally numbered from the top to the bottom of the system, within a two-dimensional space defined by an XY reference system.

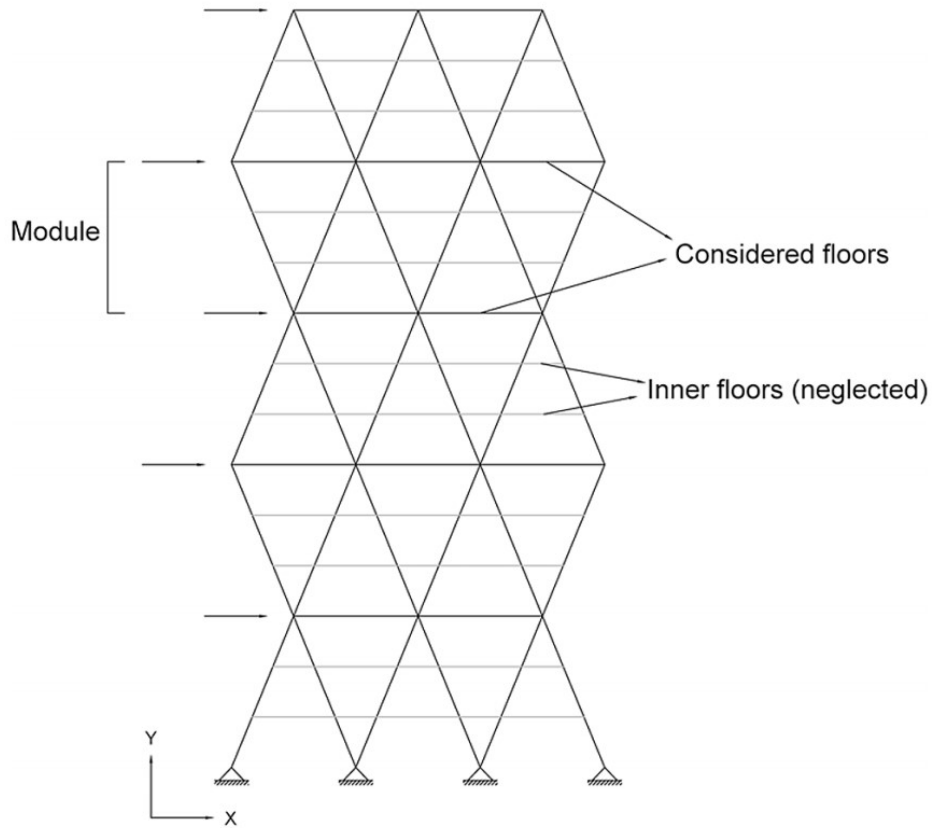


Figure 44: Two-dimensional diagrid structural system [30]

The floors located within the diagonal modules are neglected, focusing only on the N floors at the ends of the diagonals. These floors are assumed to be continuous and infinitely rigid in-plane, while the diagonals are modeled as simply hinged.

The structure is subjected to horizontal forces, and the hypothesis of two degrees of freedom per floor is adopted: horizontal displacement and out-of-plane rotation. The structural problem is then formulated through a matrix relation, which can be expressed as follows:

$$\begin{Bmatrix} \{F\} \\ \{M\} \end{Bmatrix} = \begin{bmatrix} [K_{F\delta}] & [K_{F\varphi}] \\ [K_{M\delta}] & [K_{M\varphi}] \end{bmatrix} \begin{Bmatrix} \{\delta\} \\ \{\varphi\} \end{Bmatrix} \quad (25)$$

Here:

- $\{F\}$ and $\{M\}$ are N -vectors containing the floor forces and moments, respectively;
- $\{\delta\}$ and $\{\varphi\}$ are N -vectors containing the unknown floor displacements and rotations, respectively;
- $[K_{F\delta}]$ is the $N \times N$ stiffness matrix relating floor forces to floor displacements;
- $[K_{M\phi}]$ is the $N \times N$ stiffness matrix relating floor moments to floor rotations;
- $[K_{F\phi}]$ is the $N \times N$ stiffness matrix relating floor forces to floor rotations;
- $[K_{M\delta}]$ is the $N \times N$ stiffness matrix relating floor moments to floor displacements.

Equation (25) can be reformulated by explicitly defining the components of the force and displacement vectors, as well as the terms within the structure's stiffness matrix:

$$\begin{Bmatrix} F_1 \\ \dots \\ F_i \\ \dots \\ F_N \\ M_1 \\ \dots \\ M_i \\ \dots \\ M_N \end{Bmatrix} = \begin{bmatrix} k_{11}^{F\delta} & \dots & k_{1i}^{F\delta} & \dots & k_{1N}^{F\delta} & k_{11}^{F\varphi} & \dots & k_{1i}^{F\varphi} & \dots & k_{1N}^{F\varphi} \\ \dots & \dots & \dots & \dots & \dots & \dots & \dots & \dots & \dots & \dots \\ k_{i1}^{F\delta} & \dots & k_{ii}^{F\delta} & \dots & k_{iN}^{F\delta} & k_{i1}^{F\varphi} & \dots & k_{ii}^{F\varphi} & \dots & k_{iN}^{F\varphi} \\ \dots & \dots & \dots & \dots & \dots & \dots & \dots & \dots & \dots & \dots \\ k_{N1}^{F\delta} & \dots & k_{Ni}^{F\delta} & \dots & k_{NN}^{F\delta} & k_{N1}^{F\varphi} & \dots & k_{Ni}^{F\varphi} & \dots & k_{NN}^{F\varphi} \\ k_{11}^{M\delta} & \dots & k_{1i}^{M\delta} & \dots & k_{1N}^{M\delta} & k_{11}^{M\varphi} & \dots & k_{1i}^{M\varphi} & \dots & k_{1N}^{M\varphi} \\ \dots & \dots & \dots & \dots & \dots & \dots & \dots & \dots & \dots & \dots \\ k_{i1}^{M\delta} & \dots & k_{ii}^{M\delta} & \dots & k_{iN}^{M\delta} & k_{i1}^{M\varphi} & \dots & k_{ii}^{M\varphi} & \dots & k_{iN}^{M\varphi} \\ \dots & \dots & \dots & \dots & \dots & \dots & \dots & \dots & \dots & \dots \\ k_{N1}^{M\delta} & \dots & k_{Ni}^{M\delta} & \dots & k_{NN}^{M\delta} & k_{N1}^{M\varphi} & \dots & k_{Ni}^{M\varphi} & \dots & k_{NN}^{M\varphi} \end{bmatrix} \begin{Bmatrix} \delta_1 \\ \dots \\ \delta_i \\ \dots \\ \delta_N \\ \varphi_1 \\ \dots \\ \varphi_i \\ \dots \\ \varphi_N \end{Bmatrix} \quad (26)$$

In the linear system expressed in Equation (26), the generic term k_{ij} represents the total horizontal force (F_i) or moment (M_i) acting on the i -th floor when a unitary horizontal displacement (δ_j) or rotation (φ_j) is applied to the j -th floor, while all other floor displacements

4. DIAGRID STRUCTURES

and rotations are kept null. This analytical definition allows for the complete computation of the stiffness matrix in Equation (26) through the following steps:

1. A unitary horizontal displacement (δ_j) or rotation (ϕ_j) is applied to the j -th floor, while all other floors remain fixed (as illustrated in Figure 45).
2. The deformations of the diagonals within the deformed modules are determined using geometric considerations.
3. The axial forces in the diagonals are calculated, assuming a linear elastic behavior for the diagonals.
4. The total reaction force (F_i) or moment (M_i) acting on the i -th floor, resulting from the axial forces in the diagonals, is computed.

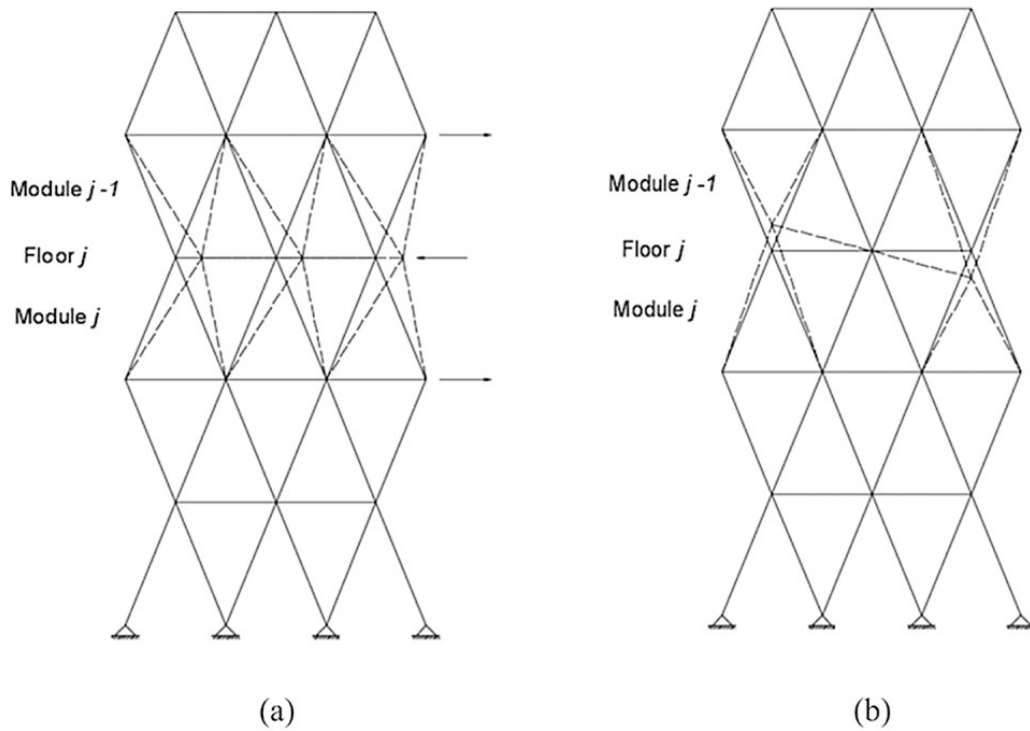


Figure 45: Computation method of the stiffness coefficients: (a) unitary horizontal displacement applied to the j th floor; (b) unitary rotation applied to the j th floor [30]

To calculate the reaction floor moments or imposed floor rotations, these are evaluated with respect to the stiffness centroid of the j -th floor. The x -coordinate of this stiffness centroid is given by the following expression:

$$x_{c,j} = \frac{\sum_{d=1}^{n_i} \frac{E_{d,j} A_{d,j}}{L_{d,j}} x_{d,j}}{\sum_{d=1}^{n_i} \frac{E_{d,j} A_{d,j}}{L_{d,j}}} \quad (27)$$

Next, considering a generic diagonal within the j-th module, subjected to a unitary horizontal displacement imposed on the j-th floor, and referring to the parameters illustrated in Figure 45(a), the elongation of the diagonal can be expressed as:

$$\delta_{diag}^{\delta_h} = \delta_h \cos \vartheta = \delta_h \frac{\Delta x}{L} \quad (28)$$

Here:

- δ_h is the imposed horizontal displacement on the j-th floor;
- θ is the angle of the diagonal with respect to the horizontal direction;
- L is the diagonal length;
- Δx and Δy are the projections of the diagonal length along the reference axes.

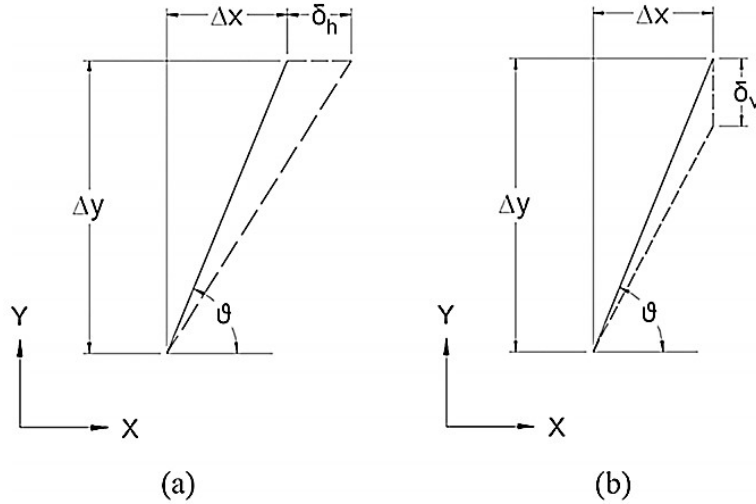


Figure 46: Deformation of the diagonal for (a) horizontal displacements and (b) vertical displacements [30]

Assuming a unitary imposed displacement δ_h and a linear elastic behavior for the diagonal, the axial force in the diagonal can be written as:

$$F_{diag}^{\delta_h} = \frac{EA}{L} \delta_{diag}^{\delta_h} = \frac{EA}{L^2} \Delta x \quad (29)$$

where:

- E is the Young's modulus of the diagonal;
- A is the cross-sectional area of the diagonal.

4. DIAGRID STRUCTURES

Now, considering the diagonal subjected to the vertical displacement caused by the unitary imposed rotation of the j -th floor (as shown in Figure 46(b)), the elongation of the diagonal can be expressed as:

$$\delta_{diag}^{\delta_h} = -\delta_v \sin \vartheta = -\delta_v \frac{\Delta y}{L} \quad (30)$$

In this case, δ_v is the vertical displacement generated by the imposed rotation and depends on the position of the diagonal relative to the centroid of the floor, as follows:

$$\delta_v = \varphi(x - x_c) \quad (31)$$

Thus, the axial force in the diagonal resulting from the unitary rotation of the j -th floor can be expressed as:

$$F_{diag}^{\delta_h} = \frac{EA}{L} \delta_{diag}^{\delta_v} = -\frac{EA}{L^2} (x - x_c) \Delta y \quad (32)$$

By decomposing the axial forces obtained in the diagonals into their horizontal and vertical components, and by calculating the total reactive forces in the horizontal direction as well as the reactive moments on each floor, the four stiffness submatrices in Equation (25) can be determined. The complete expressions for these submatrices are provided below. In these expressions, n_i and n_{i-1} represent the number of diagonals in the i -th and $(i-1)$ -th modules, respectively. For each variable, the first subscript refers to the specific diagonal involved in the summation, while the second subscript refers to the module to which the diagonal belongs. Regarding the x -coordinates, $x_{d,i-1,i}$ denotes the x -coordinate of the diagonal d in the $(i-1)$ -th module, referred to the i -th floor, and $x_{C,i}$ represents the x -coordinate of the centroid of the i -th floor.

Matrix $[K_{F\delta}]$:

$$k_{i,i}^{F\delta} = \sum_{d=1}^{n_{i-1}} E_{d,i-1} A_{d,i-1} \frac{\Delta x_{d,i-1}^2}{L_{d,i-1}^3} + \sum_{d=1}^{n_i} E_{d,i} A_{d,i} \frac{\Delta x_{d,i}^2}{L_{d,i}^3} \quad (33)$$

$$k_{i-1,i}^{F\delta} = - \sum_{d=1}^{n_{i-1}} E_{d,i-1} A_{d,i-1} \frac{\Delta x_{d,i-1}^2}{L_{d,i-1}^3} \quad (34)$$

$$k_{i+1,i}^{F\delta} = - \sum_{d=1}^{n_i} E_{d,i} A_{d,i} \frac{\Delta x_{d,i}^2}{L_{d,i}^3} \quad (35)$$

Matrix $[K_{F\varphi}]$:

$$k_{i,i}^{F\varphi} = - \sum_{d=1}^{n_{i-1}} E_{d,i-1} A_{d,i-1} \frac{\Delta x_{d,i-1} \Delta y_{d,i-1}}{L_{d,i-1}^3} (x_{d,i-1,i} - x_{c,i}) - \sum_{d=1}^{n_i} E_{d,i} A_{d,i} \frac{\Delta x_{d,i} \Delta y_{d,i}}{L_{d,i}^3} (x_{d,i,i} - x_{c,i}) \quad (36)$$

$$k_{i-1,i}^{F\varphi} = \sum_{d=1}^{n_{i-1}} E_{d,i-1} A_{d,i-1} \frac{\Delta x_{d,i-1} \Delta y_{d,i-1}}{L_{d,i-1}^3} (x_{d,i-1,i} - x_{c,i}) \quad (37)$$

$$k_{i+1,i}^{F\varphi} = \sum_{d=1}^{n_i} E_{d,i} A_{d,i} \frac{\Delta x_{d,i} \Delta y_{d,i}}{L_{d,i}^3} (x_{d,i,i} - x_{c,i}) \quad (38)$$

Matrix $[K_{M\delta}]$:

$$k_{i,i}^{M\delta} = - \sum_{d=1}^{n_{i-1}} E_{d,i-1} A_{d,i-1} \frac{\Delta x_{d,i-1} \Delta y_{d,i-1}}{L_{d,i-1}^3} (x_{d,i-1,i} - x_{c,i}) - \sum_{d=1}^{n_i} E_{d,i} A_{d,i} \frac{\Delta x_{d,i} \Delta y_{d,i}}{L_{d,i}^3} (x_{d,i,i} - x_{c,i}) \quad (39)$$

$$k_{i-1,i}^{M\delta} = \sum_{d=1}^{n_{i-1}} E_{d,i-1} A_{d,i-1} \frac{\Delta x_{d,i-1} \Delta y_{d,i-1}}{L_{d,i-1}^3} (x_{d,i-1,i-1} - x_{c,i-1}) \quad (40)$$

$$k_{i+1,i}^{M\delta} = \sum_{d=1}^{n_i} E_{d,i} A_{d,i} \frac{\Delta x_{d,i} \Delta y_{d,i}}{L_{d,i}^3} (x_{d,i,i+1} - x_{c,i+1}) \quad (41)$$

Matrix $[K_{M\varphi}]$:

$$k_{i,i}^{M\delta} = \sum_{d=1}^{n_{i-1}} E_{d,i-1} A_{d,i-1} \frac{\Delta y_{d,i-1}^2}{L_{d,i-1}^3} (x_{d,i-1,i} - x_{c,i})^2 + \sum_{d=1}^{n_i} E_{d,i} A_{d,i} \frac{\Delta y_{d,i}^2}{L_{d,i}^3} (x_{d,i,i} - x_{c,i})^2 \quad (42)$$

$$k_{i-1,i}^{M\delta} = - \sum_{d=1}^{n_{i-1}} E_{d,i-1} A_{d,i-1} \frac{\Delta y_{d,i-1}^2}{L_{d,i-1}^3} (x_{d,i-1,i} - x_{c,i})(x_{d,i-1,i-1} - x_{c,i-1}) \quad (43)$$

$$k_{i+1,i}^{M\delta} = - \sum_{d=1}^{n_i} E_{d,i} A_{d,i} \frac{\Delta y_{d,i}^2}{L_{d,i}^3} (x_{d,i,i} - x_{c,i})(x_{d,i,i+1} - x_{c,i+1}) \quad (44)$$

4. DIAGRID STRUCTURES

With these expressions, the diagrid stiffness matrix in Equation (25) is fully computed, enabling the calculation of the structure's displacements as follows:

$$\begin{Bmatrix} \{\delta\} \\ \{\varphi\} \end{Bmatrix} = \begin{bmatrix} [K_{F\delta}] & [K_{F\varphi}] \\ [K_{M\delta}] & [K_{M\varphi}] \end{bmatrix}^{-1} \begin{Bmatrix} \{F\} \\ \{M\} \end{Bmatrix} \quad (45)$$

Once the displacements of the structure are determined, it is possible to compute the axial force in each diagonal within the i -th module ($F_{diag,i}$) by referring back to Equations (26) and (27):

$$F_{diag,i} = \frac{E_{d,i}A_{d,i}}{L_{d,i}^2} [\Delta x_{d,i}(\delta_i - \delta_{i+1}) - \Delta y_{d,i}\varphi_i(x_{d,i,i} - x_{c,i}) + \Delta y_{d,i}\varphi_{i+1}(x_{d,i,i+1} - x_{c,i+1})] \quad (46)$$

As previously mentioned, Lacidogna et al. [30] also extended their analysis to a generic three-dimensional diagrid structural system to further explore and apply the matrix-based method. In this context, a generic three-dimensional diagrid structure is now considered (Figure 47). This system consists of N floors (neglecting the inner ones) within a three-dimensional space defined by an XYZ reference system, where X and Y are the horizontal axes, and Z is the vertical axis.

The main assumptions remain consistent with those adopted for the two-dimensional diagrid structural systems. Specifically, the structure is assumed to be subjected to horizontal floor forces (along the X and Y axes), vertical floor forces (along the Z axis), and in-plane floor torque moments (around the Z axis).

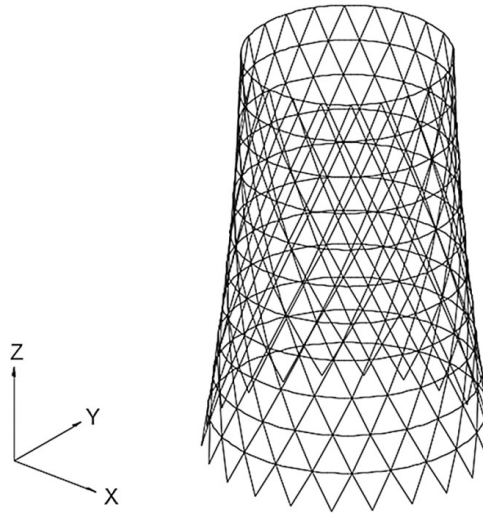


Figure 47: Three-dimensional diagrid structural system [30]

When considering six degrees of freedom per floor, the structural problem in Equation (25) can be reformulated to account for the contributions of the six generalized displacements as follows:

$$\begin{bmatrix} \{F_x\} \\ \{F_y\} \\ \{M_z\} \\ \{M_x\} \\ \{M_y\} \\ \{F_z\} \end{bmatrix} = \begin{bmatrix} [K_{F_x\delta_x}] & [K_{F_x\delta_y}] & [K_{F_x\phi_z}] & [K_{F_x\phi_x}] & [K_{F_x\phi_y}] & [K_{F_x\delta_z}] \\ [K_{F_y\delta_x}] & [K_{F_y\delta_y}] & [K_{F_y\phi_z}] & [K_{F_y\phi_x}] & [K_{F_y\phi_y}] & [K_{F_y\delta_z}] \\ [K_{M_z\delta_x}] & [K_{M_z\delta_y}] & [K_{M_z\phi_z}] & [K_{M_z\phi_x}] & [K_{M_z\phi_y}] & [K_{M_z\delta_z}] \\ [K_{M_x\delta_x}] & [K_{M_x\delta_y}] & [K_{M_x\phi_z}] & [K_{M_x\phi_x}] & [K_{M_x\phi_y}] & [K_{M_x\delta_z}] \\ [K_{M_y\delta_x}] & [K_{M_y\delta_y}] & [K_{M_y\phi_z}] & [K_{M_y\phi_x}] & [K_{M_y\phi_y}] & [K_{M_y\delta_z}] \\ [K_{F_z\delta_x}] & [K_{F_z\delta_y}] & [K_{F_z\phi_z}] & [K_{F_z\phi_x}] & [K_{F_z\phi_y}] & [K_{F_z\delta_z}] \end{bmatrix} \begin{bmatrix} \{\delta_x\} \\ \{\delta_y\} \\ \{\phi_z\} \\ \{\phi_x\} \\ \{\phi_y\} \\ \{\delta_z\} \end{bmatrix} \quad (47)$$

Here:

- $\{F_x\}$, $\{F_y\}$, and $\{F_z\}$ are the N-vectors containing the floor forces along the X, Y, and Z axes, respectively;
- $\{M_z\}$ is the N-vector containing the in-plane floor torque moments (around the Z-axis);
- $\{M_x\}$ and $\{M_y\}$ are the N-vectors containing the out-of-plane floor moments along the X and Y axes, respectively.

For the floor displacements:

- $\{\delta_x\}$, $\{\delta_y\}$, and $\{\delta_z\}$ are the N-vectors containing the displacements along the X, Y, and Z axes, respectively;
- $\{\phi_z\}$ is the N-vector containing the in-plane floor rotations (around the Z-axis);
- $\{\phi_x\}$ and $\{\phi_y\}$ are the N-vectors containing the out-of-plane floor rotations along the X and Y axes, respectively.

The complete stiffness matrix of the structure, which has dimensions $6N \times 6N$, is presented in Equation (47). It is partitioned based on the six degrees of freedom, where each submatrix ($N \times N$) represents the stiffness matrix that relates a specific floor force/moment vector to a corresponding displacement/rotation vector. For clarity, Figure 48(a) illustrates the conventions used for the displacements and rotations.

4. DIAGRID STRUCTURES

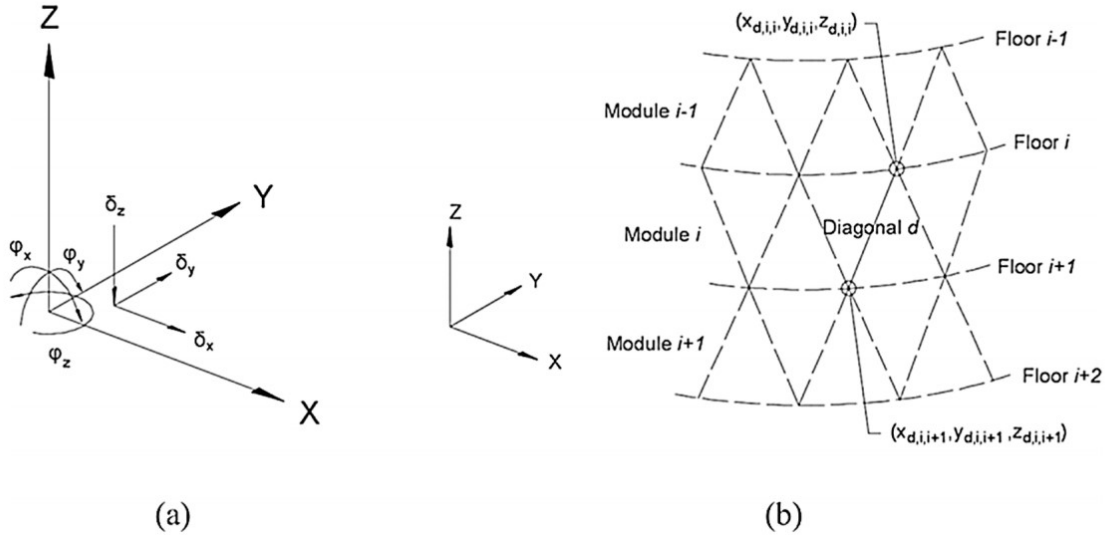


Figure 48: Conventions for three-dimensional diagrid structure: (a) displacements and rotations of the floors; (b) floors and modules numbering and subscripts of diagonal coordinates [30]

Each of the submatrices in the stiffness matrix can be computed using the same procedure applied for the two-dimensional diagrid structure. The stiffness coefficients in the thirty-six submatrices can be determined systematically by applying the conventions shown in Figure 48(b). When the entire stiffness matrix of the three-dimensional diagrid system has been constructed, the structural problem can be automatically solved by inverting the linear system in Equation (47).

Once the displacements and rotations of the rigid floors are known, the axial forces in the generic diagonals can be determined. This is done using an equation similar to Equation (46), but it is far more complicated since it includes the contributions from all six degrees of freedom (DOFs).

The matrix-based method (MBM) described here has been extended beyond structural analysis of diagrids to understand the interaction of diagrid tubes with other structural elements in a building. The MBM has been embedded into the General Algorithm (GA) framework, which is a matrix-based analytical methodology developed for preliminary tall building analysis in 1985 [33].

The GA framework actually makes it easier since it considers only three DOFs for each floor (two lateral displacements and one torsional rotation).

In order for the MBM to be suitable for the GA, Lacidogna et al. [30] used a static condensation process to materially condense the contributions of the vertical displacements and out-of-plane rotations, which produced a less complicated stiffness matrix.

Specifically, Equation (18) is reformulated to separate the horizontal and vertical components:

$$\begin{Bmatrix} \{F_H\} \\ \{F_V\} \end{Bmatrix} = \begin{bmatrix} [K_{HH}] & [K_{HV}] \\ [K_{VH}] & [K_{VV}] \end{bmatrix} \begin{Bmatrix} \{\delta_H\} \\ \{\delta_V\} \end{Bmatrix} \quad (48)$$

Where:

- $\{\delta_H\}$ and $\{F_H\}$ represent horizontal displacements (forces) and torsional rotations (moments);
- $\{\delta_V\}$ and $\{F_V\}$ account for the vertical displacements (forces) and out-of-plane rotations (moments).

Through the condensation process, the vertical DOFs are eliminated, resulting in a reduced stiffness matrix $[K_{HH}]^*$, which is of dimension $3N \times 3N$. This condensed matrix relates only to the horizontal DOFs, enabling the MBM to be seamlessly incorporated into the GA framework:

$$\{F_H\} = ([K_{HH}] - [K_{HV}][K_{VV}]^{-1}[K_{VH}])\{\delta_H\} = [K_{HH}]^*\{\delta_H\} \quad (49)$$

The MBM has been used within the GA framework to investigate the stiffness interaction between an external steel diagrid and an internal concrete core. In particular, a square, 18-story tall building is considered in [30], and the coupled behavior is analyzed under lateral forces and torque moments. Although the torsional behavior is obviously governed by the external diagrid tube, the distribution of shear forces at the various floor levels is not trivial, and gives rise to an oscillating trend along the height of the building, due to the shear-bending coupling of the two structural systems (Figure 49).

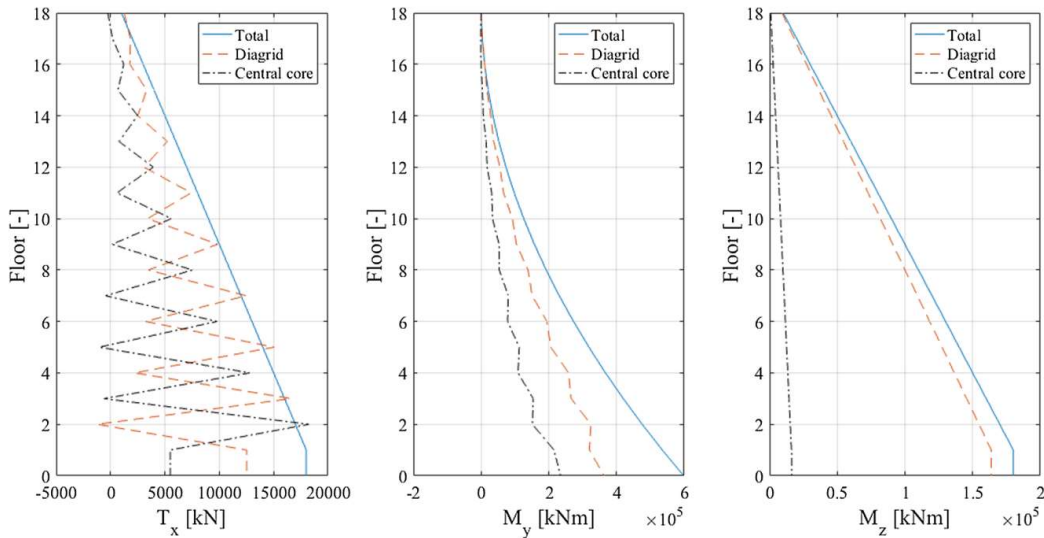


Figure 49: Diagrid system coupled with central core: (a) shear; (b) bending moment; (c) torque moment [30]

4. DIAGRID STRUCTURES

In a more recent study, Lacidogna et al. [34] examine the impact of diagonal inclination on the behavior of the diagrid-core coupled system. As previously highlighted by Moon et al. [19], when the diagrid angle falls within the optimal range, the lateral stiffness of the diagrid dominates over that of the internal core. Lacidogna et al. [34] further examine how the core type, defined by internal closed-section and open-section shear walls, affects their torsional behavior. According to the authors, while the coupling mechanism of lateral deformability is essentially the same, a noticeable difference occurs in torsional behavior, whereby a specific inflection point is evident in the torsional deformation curve for internal, open-section shear walls, in conjunction with the diagrid steep angles, and this was attributed to the warping of the internal shear wall which had a noticeable effect in these conditions.

This finding underscores the importance of considering the type of internal core and its interaction with the diagrid when analyzing and designing diagrid-core systems, particularly for tall buildings subjected to torsional loads.

Analytical methods for diagrid systems, combined with stiffness- and strength-based preliminary design methods, provide a simplified alternative to FE for use during early design stages for rapid assessment of total structural behavior and key performance parameters, and therefore they offer a more straightforward approach to understanding structural behavior. While access to contemporary computing power can be liberating for the generation of detailed FE models with more and more DOFs, it has the potential to cloud the ability to formulate a clear picture of global structural behavior during the preliminary design stage of a project, which is essential for developing and selecting effective resisting elements at a preliminary design stage and emphasizes the need for alternative methods. The optimal choice of a resisting element has a significant effect on the cost and efficiency, especially for tall buildings, because the selection of resisting elements can have a significant effect on overall structural performance. These early design stages simplified methodologies can aid in the ability to understand total behavior and structural response, which might not be intuitively apparent through detailed FE models, so it can be an important capability for designers.

5. REQUIREMENTS AND PRELIMINARY FRAMEWORK FOR DIAGRID MODEL DEVELOPMENT

5.1. Methodological Framework, Geometric and Structural Assumptions

The thesis builds upon the MATLAB code developed by Lacidogna et al. [30] as part of their Matrix-Based Method (MBM) framework, which serves as the foundation for analyzing the diagrid models under consideration. As detailed in Chapter 4.3, the study by Scaramozzino et al. [26] examined a wide range of diagrid configurations, encompassing square, hexagonal, octagonal, and circular floor shapes. The floor dimensions were designed to ensure a gross floor area of 900 m², resulting in an average building footprint of 30 m × 30 m (Figure 24(b)). Four building heights were analyzed, 126 m, 168 m, 210 m, and 252 m (Figure 24(a)), corresponding to total floor counts of 36, 48, 60, and 72, given a fixed inter-story height of 3.5 m. These configurations yielded four building aspect ratios: 4.2, 5.6, 7.0, and 8.4. The diagrid structure is modelled using steel hollow circular sections (CHS) with an elastic modulus of 210 GPa, a steel density of 7.8 tons/m³, and a yielding strength of 275 MPa. These structures are designed to withstand both vertical and horizontal loads. The vertical load is determined by combining a dead load of 7 kN/m² with a live load of 4 kN/m². However, it is important to note that the diagrid structure does not bear the entirety of the vertical load, as the internal central core carries a significant portion of it. Following the approach adopted by Montuori et al. [28], where the core is assumed to occupy 25% of the total area, only 37.5%. The original study considered a total of 175,008 possible diagrid configurations, including both uniform-angle and varying-angle diagrids. However, for the purposes of this thesis, only the configurations reported in Tables 1 - 4 were analyzed. This selection was made to ensure consistency with the methodological approach used in [26] and to focus on the configurations identified as optimal within their framework. These configurations were selected based on a multi-response framework that balances structural efficiency, torsional stiffness, and construction feasibility. By focusing exclusively on these optimal configurations, the thesis avoids the impracticality of evaluating the entire population of 175,008 combinations. This targeted approach allows for a more in-depth and meaningful analysis while ensuring alignment with the established methodology and maintaining a clear and manageable scope.

5.2. Tall Building Strength and Stiffness Requirements

When designing tall buildings, two main requirements must be satisfied: strength and stiffness since it cannot be known beforehand, which will control the design. In determining the global stiffness of the building, the goal is to limit lateral displacement, in particular, lateral displacement at the top of a building to limit the effect of lateral forces. To achieve this, the stiffness requirement is specified by establishing a limit for the top displacement at $H/500$. In terms of strength, an important consideration is compression in diagonals, as provide the buckling strength to avoid any instability phenomena. Strength values for compression are taken from Eurocode 3 [35], which provides design rules for steel structures. For diagonals subjected to tension forces, the strength requirement is based on assessing the tensile strength to ensure the overall system can sustain the force.

5.2.1. Compressive Strength

The verification of a diagonal under compression, subjected to the design axial force N_{Ed} , is deemed satisfactory when its bearing capacity $N_{c,Rd}$ is not exceeded, as expressed by the condition:

$$N_{Ed} \leq N_{c,Rd} \quad (50)$$

The design compression strength $N_{c,Rd}$ is determined based on the classification of the cross-section. For sections classified as class 1, 2, or 3, the compression strength is given by:

$$N_{c,Rd} = \frac{A \cdot f_y}{\gamma_{M0}} \quad (51)$$

For sections of class 4, the compression strength is instead defined as:

$$N_{c,Rd} = \frac{A_{eff} \cdot f_y}{\gamma_{M0}} \quad (52)$$

Here, A represents the gross cross-sectional area, A_{eff} is the effective cross-sectional area, f_y is the yielding strength, and γ_{M0} is a safety factor.

In the case of class 4 sections, local instability reduces the bearing capacity of the compression elements. This reduction occurs because the failure of these elements takes place at an axial force lower than the yielding force calculated with reference to the gross cross-sectional area.

5. REQUIREMENTS AND PRELIMINARY FRAMEWORK FOR DIAGRID MODEL DEVELOPMENT

Consequently, the effective area A_{eff} is used to account for the effects of local instability, ensuring a more accurate evaluation of the compression strength [35].

5.2.2. Buckling Critical Load

The state of stress in a compressed element, particularly in steel members, is inherently linked to buckling phenomena. As a result, strength verification must be accompanied by buckling verification, which often proves to be the most critical aspect of the design, especially for slender structural elements.

In the absence of geometrical imperfections and assuming linear-elastic material behavior, referred to as the ideal bar, it can be demonstrated that a critical load value, N_{cr} , exists. Beyond this value, global buckling phenomena are triggered. Buckling can manifest in three forms: flexural, torsional, and flexural-torsional [35]. For circular hollow cross sections (CHS), the typical instability mode is flexural buckling, as the section possesses two symmetrical axes. In the case of flexural instability, the critical load is determined as the minimum of two values, which are functions of the geometrical and mechanical parameters of the element:

$$N_{cr} = \min \left\{ \frac{\pi^2 E I_y}{L_{0,y}^2}, \frac{\pi^2 E I_z}{L_{0,z}^2} \right\} \quad (53)$$

Here, E is the Young's modulus, I_y and I_z are the second moments of inertia about the principal axes, and L_0 is the effective length of the member.

From a design perspective, it is often more practical to express the critical load in terms of stress. This can be achieved using the following formula:

$$\sigma = \frac{N_{cr}}{A} = \min \left\{ \frac{\pi^2 E \rho_y^2}{L_{0,y}^2}, \frac{\pi^2 E \rho_z^2}{L_{0,z}^2} \right\} = \min \left\{ \frac{\pi^2 E}{\lambda_y^2}, \frac{\pi^2 E}{\lambda_z^2} \right\} \quad (54)$$

where A is the cross-sectional area, ρ is the radius of gyration, and λ is the slenderness ratio, defined as $\lambda = L_0/\rho$. In the verification process, the slenderness ratio is taken as the maximum value between the slenderness in the y-direction and the z-direction.

However, in structural design, the ideal bar assumption is rarely used, as it applies only to elements with perfectly linear-elastic behavior and no geometrical imperfections. In reality, structural members used in construction exhibit non-linear behavior, are limited by material

5.2. Tall Building Strength and Stiffness Requirements

strength, and are affected by mechanical and geometrical imperfections arising from manufacturing and assembly processes. For an element with cross-sectional area A and no imperfections, the critical load cannot exceed the value at which the section undergoes complete plasticization, given by $f_y A$, where f_y is the yielding strength.

The stability curve, shown in Figure 50, represents the relationship between stress σ and slenderness λ .

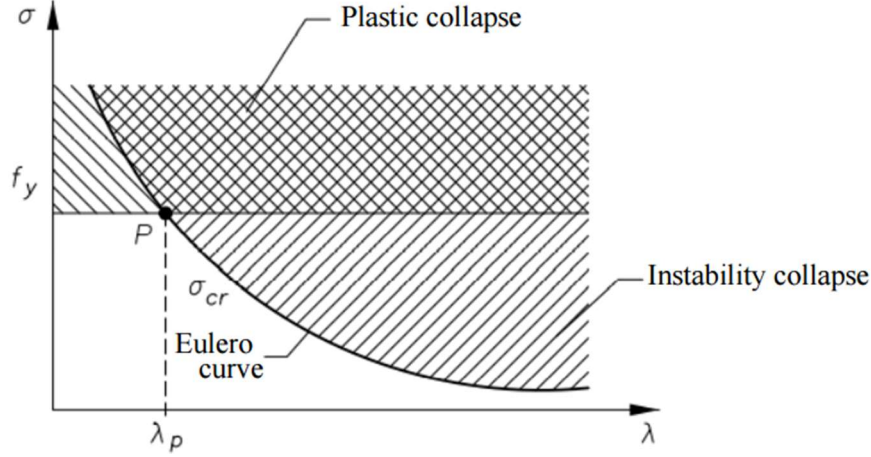


Figure 50: Strength domain tension-slenderness for compressed element [35]

The intersection of the Euler curve with the horizontal line corresponding to f_y defines a point P, whose abscissa is the proportionality slenderness λ_p . This proportionality slenderness is expressed as:

$$\lambda_p = \pi \sqrt{\frac{E}{f_y}} \quad (55)$$

The value of λ_p is critical for determining the type of structural failure. If $\lambda < \lambda_p$, the cross-section reaches full plasticization due to strength failure. If $\lambda > \lambda_p$, elastic instability phenomena dominate. When $\lambda = \lambda_p$, plastic and instability failures occur simultaneously.

Mechanical and geometrical imperfections are inherent in real structural elements and significantly affect their bearing capacity. When an initial imperfection, such as a sinusoidal deformed shape, is considered, the applied load N leads to an increase in deflection δ , which in turn amplifies the bending moment due to the eccentricity. The structural response, in terms of load versus transverse displacement, corresponds to that of an ideal system with initial imperfections. This response curve asymptotically approaches the critical load N_{cr} , as the

5. REQUIREMENTS AND PRELIMINARY FRAMEWORK FOR DIAGRID MODEL DEVELOPMENT

material exhibits elastic behavior, as illustrated in Figure 51(a). The deflection can be approximated as a function of the initial imperfection:

$$\delta = \delta_0 \cdot \frac{1}{1 - \frac{N}{N_{cr}}} \quad (56)$$

At midspan, the section is subjected to combined bending and compression, and the maximum stress σ is calculated as:

$$\sigma = \frac{N}{A} + \frac{N \cdot \delta}{W} = \frac{N}{A} + \frac{N \cdot \delta_0}{W} \cdot \frac{1}{1 - \frac{N}{N_{cr}}} \quad (57)$$

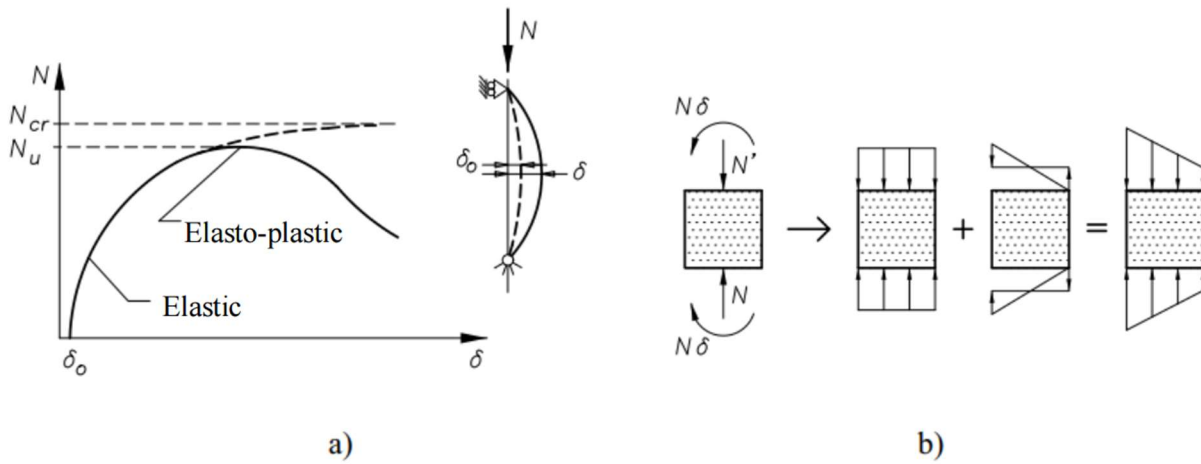


Figure 51: Definition of buckling capacity: (a) Load-transverse displacement behavior with initial imperfection and (b) state of stress in midspan [35]

When the yielding stress is reached, the stiffness of the regions in the post-elastic field decreases. This results in a gradual increase in flexural deformability after surpassing the maximum strength N_u , which is lower than the critical load N_{cr} . A comparison between the stress-slenderness curves of an element without imperfections and one with imperfections reveals that the latter has a reduced bearing capacity. This reduction is attributed to the elasto-plastic behavior and the presence of defects, as shown in Figure 52.

5.2. Tall Building Strength and Stiffness Requirements

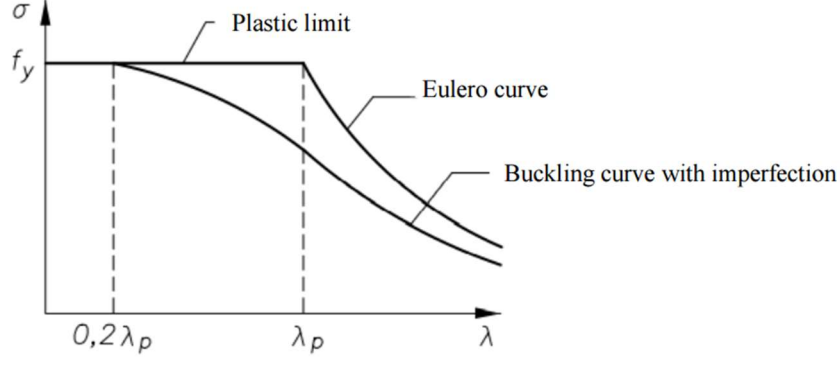


Figure 52: Comparison of tension-slenderness curve with and without imperfection [35]

The plastic collapse to instability driven failure transition is subject to instability phenomena. The transition takes place at $0.2\lambda_p$ (not λ_p), indicating the influence of imperfections and non-linear behavior on the structural performance of the element.

According to Eurocode EC3 [35], the stability verification of a compressed element acting under the axial force N_{Ed} is satisfied, if the applied force does not exceed the bearing capacity $N_{b,Rd}$, given as:

$$N_{Ed} \leq N_{b,Rd} \quad (58)$$

Buckling strength $N_{b,Rd}$ is determined on the basis of the cross-section classification. For sections classified as Class 1, 2 or 3, the buckling strength is given by:

$$N_{b,Rd} = \chi \cdot A \frac{f_y}{\gamma_{M1}} \quad (59)$$

For Class 4 sections, it is expressed as:

$$N_{b,Rd} = \chi \cdot A_{eff} \frac{f_y}{\gamma_{M1}} \quad (60)$$

where A is the nominal cross-sectional area, A_{eff} is the effective cross-sectional area, f_y is the yielding strength, χ is the reduction factor, and γ_{M1} is the safety factor.

The reduction factor χ takes into account the phenomena of instability and is calculated as:

$$\chi = \frac{1}{\phi + \sqrt{\phi^2 - \lambda^2}} \leq 1 \quad (61)$$

where:

$$\phi = 0.5 \cdot [1 + \alpha(\bar{\lambda} - 0.2) + \bar{\lambda}^2] \quad (62)$$

5. REQUIREMENTS AND PRELIMINARY FRAMEWORK FOR DIAGRID MODEL DEVELOPMENT

In this equation, α is the imperfection coefficient, which is determined by the chosen stability curve (see Table 5). The stability curve depends on the type of cross-section, limits, axis of instability, and steel quality.

Buckling curve	a_0	a	b	c	d
Imperfection factor α	0.13	0.21	0.34	0.49	0.76

Table 5: Imperfection factor values in function of stability curve [35]

The relative slenderness $\bar{\lambda}$ also depends on cross-section classification. For Class 1, 2, and 3 sections, it is given as:

$$\bar{\lambda} = \sqrt{\frac{A \cdot f_y}{N_{cr}}} \quad (63)$$

For Class 4 sections, it is expressed as:

$$\bar{\lambda} = \sqrt{\frac{A_{eff} \cdot f_y}{N_{cr}}} \quad (64)$$

where N_{cr} is the critical elastic force.

For the case reviewed, the stability curve for hot-finished circular hollow section (CHS) in Table 6 is appropriate. The buckling curve is a with imperfection coefficient $\alpha = 0.21$. This establishes that the stability check relates to the attributes of the structural member in question.


Transverse section	Limits	Buckling about axis	Buckling curve	
			S 235 S 275 S 355 S 420	S 460
<i>Hollow sections</i> 	Hot finished	Any	a	a_0
	Cold formed	Any	c	c

Table 6: Buckling curve for circular hollow sections CHS [35]

5.2.3. Tensile Strength

The tension verification of a diagonal can be considered satisfactory if you do not exceed its bearing capacity, $N_{t,Rd}$, as specified by the condition:

$$N_{Ed} \leq N_{t,Rd} \quad (65)$$

$N_{t,Rd}$ indicates the design plastic strength of the gross section, which does not take into account any reductions for holes in the members. It is defined as:

$$N_{t,Rd} = \frac{A \cdot f_y}{\gamma_{M0}} \quad (66)$$

where A is the gross cross-sectional area, f_y is the yielding strength and γ_{M0} is a safety factor [35]. In the case currently being examined, we do not incorporate the safety factor γ_{M0} for the sake of simplicity so that the tensile strength check can be more easily evaluated.

5.3. External Actions

In the analysis of structural behavior, the consideration of external actions is a fundamental aspect that has to be taken into account. This thesis focuses on two primary external actions applied to the structures considered: wind action, which will be elaborated upon in the following sections, and a uniform horizontal load, essential for the type of analysis on which this study is based, that The wind action, which will be elaborated upon in the following sections, will be further detailed in the subsequent chapter, where its role in the analytical framework and its implications for structural performance will be thoroughly examined.

5.3.1. Wind Load

In the context of tall buildings, wind load represents a critical factor in structural design, as it induces a dynamic response that can significantly influence the overall behavior of the structure. This is particularly evident in tall buildings with aerodynamic shapes that are highly susceptible to wind action, where the interaction between the wind and the structure becomes so pronounced that it alters the structural response itself, primarily due to substantial lateral displacements. Wind loads generally produce two key effects on structures: aerodynamic and

5. REQUIREMENTS AND PRELIMINARY FRAMEWORK FOR DIAGRID MODEL DEVELOPMENT

aeroelastic actions. As a result, the accurate assessment of wind loads on slender buildings becomes a crucial aspect of the design process. To address this, various methodologies can be employed; however, during the preliminary design phase, engineers often rely on practical codes to estimate wind actions. It is important to note that the use of national regulations for wind load evaluation is generally appropriate only for buildings where higher modes have a negligible influence on the displacement response or when the design is still in its early stages, where the geometry and structural properties of the building remain undefined [36].

5.3.2. ASCE 7-10 Procedure for Evaluating Wind Loads

In this chapter, the procedure for calculating the lateral load induced by wind on tall buildings is presented, following the recommendations outlined in ASCE 7 - 10 [37]. This calculation is essential for conducting the preliminary design of diagrid structures. The basic wind speed, V , is assumed to be 40 m/s, corresponding to the conditions in New York, as previously considered by Mele et al. [31] in their study of the Hearst Tower. The velocity pressure at a given height, z , is determined using the following expression:

$$q_z = 0.613 \cdot K_z \cdot K_{zt} \cdot K_d \cdot V^2 \left[\frac{\text{N}}{\text{m}^2} \right] \text{ for } V \text{ in } \frac{\text{m}}{\text{s}} \quad (67)$$

In this context, K_d represents the wind directionality factor, which depends on the type of structure. For the main wind force-resisting system of enclosed and partially enclosed buildings, ASCE 7 - 10 recommends a value of $K_d = 0.85$. The term K_z is the velocity pressure exposure coefficient, while K_{zt} is the topographic factor, which is assumed to be unitary in this analysis. V denotes the basic wind speed. To determine the velocity pressure exposure coefficient K_z , it is necessary to define the surface roughness and the corresponding exposure categories. Assuming the building is located in an urban area, the exposure category is classified as B, and K_z is calculated using the following expression:

$$K_z = 2.01 \cdot \left(\frac{z}{z_g} \right)^{\frac{2}{\alpha}} \quad [-] \text{ for } 15 \text{ ft.} \leq z \leq z_g \quad (68)$$

Here, z represents the height above ground level, while z_g and α are parameters that depend on the surface roughness and are provided in Table 7.

Exposure	α	z_g [ft]	\hat{a}	\hat{b}	\bar{a}	\bar{b}	c	l [ft]	\bar{e}	z_{min} [ft]*
B	7.0	1200	1/7	0.84	1/4	0.45	0.30	320	1/3.0	30

* z_{min} = minimum height used to ensure that the equivalent height \bar{z} is greater of 0.6h or z_{min} .

Table 7: Terrain exposure constant for definition of wind loads according to ASCE 7-10 [37]

Thus, the design wind pressure for the main wind force-resisting system of enclosed flexible buildings can be expressed as follows:

$$p = q \cdot G_f \cdot C_p - q_i(GC_{pi}) \left[\frac{\text{N}}{\text{m}^2} \right] \quad (69)$$

where q is the velocity pressure at height z , and q_i represents the internal pressure, which is taken as q evaluated at $z = h$ for safety considerations. The term G_f is the gust-effect factor, C_p is the external pressure coefficient, and GC_{pi} is the internal pressure coefficient.

The determination of the design wind pressure for tall buildings is primarily dependent on the definition of the gust-effect factor, as this relates to the interaction between the high-rise building and the imposed wind effects. A crucial step in this process is the determination of the fundamental frequency which is required to evaluate the dynamic response of flexible buildings. For tall buildings (over 400 ft (122 m)), the fundamental frequency, n_1 , can be approximately calculated with the following expression:

$$n_1 = \frac{150}{h} \quad [\text{Hz}] \quad (70)$$

where h is the total building height (in ft.), and 150 is a constant given in the relevant standards.

For flexible buildings, the dimensionless gust-effect factor is determined using the following equation:

$$G_f = 0.925 \left(\frac{1 + 1.7I_{\bar{z}} \sqrt{g_Q^2 Q^2 + g_R^2 R^2}}{1 + 1.7g_v I_{\bar{z}}} \right) \quad (71)$$

where $I_{\bar{z}}$ represents the intensity of turbulence at the equivalent height \bar{z} . The equivalent height \bar{z} is defined as 0.6 h (with h in ft.), but it must not be less than z_{min} for any building height h . The values of z_{min} and the constant c are provided in Table 7.

5. REQUIREMENTS AND PRELIMINARY FRAMEWORK FOR DIAGRID MODEL DEVELOPMENT

$$I_{\bar{z}} = c \left(\frac{33}{\bar{z}} \right)^{\frac{1}{6}} \quad (72)$$

The parameters g_Q and g_v represent the peak factors for the background and wind response, respectively, and are both assigned a value of 3.4. The peak factor for the resonant response, g_R , is determined using the following expression:

$$g_R = \sqrt{2 \ln (3600 n_1)} + \frac{0.577}{\sqrt{2 \ln (3600 n_1)}} \quad (73)$$

The resonant response factor, R , is given by the following expression:

$$R = \sqrt{\frac{1}{\beta} R_n R_h R_B (0.53 + 0.47 R_L)} \quad (74)$$

$$R_n = \frac{7.47 N_1}{(1 + 10.3 N_1)^{\frac{5}{3}}} \quad (75)$$

$$N_1 = \frac{n_1 L_{\bar{z}}}{\bar{V}_{\bar{z}}} \quad (76)$$

$$R_l = \begin{cases} \frac{1}{\eta} - \frac{1}{2\eta^2} (1 - e^{-2\eta}) & \text{for } \eta > 0 \\ 1 & \text{for } \eta = 0 \end{cases} \quad (77)$$

In this context, the subscript l is used to represent h , B , and L , where B and L are the plan dimensions measured perpendicular and parallel to the wind direction, respectively. The fundamental natural frequency is denoted as n_1 , and the resonant response factor R_l is defined as follows:

- $R_l = R_h$ when $\eta = 4.6 n_1 h / \bar{V}_{\bar{z}}$;
- $R_l = R_B$ when $\eta = 4.6 n_1 B / \bar{V}_{\bar{z}}$;
- $R_l = R_L$ when $\eta = 4.6 n_1 L / \bar{V}_{\bar{z}}$.

Here, β represents the damping ratio, which is assumed to be 1%, and $\bar{V}_{\bar{z}}$ is the mean hourly wind speed (in ft/s) at the equivalent height \bar{z} . The constants \bar{b} and $\bar{\alpha}$, which are required for the calculation, are provided in Table 7.

$$\bar{V}_{\bar{z}} = \bar{b} \left(\frac{\bar{z}}{33} \right)^{\bar{\alpha}} \left(\frac{88}{60} \right) V \quad \left[\frac{\text{ft}}{\text{s}} \right] \text{ for } \bar{z} \text{ in ft and } V \text{ in mph} \quad (78)$$

The background response, Q , is given by the following expression:

$$Q = \sqrt{\frac{1}{1 + 0.63 \left(\frac{B + h}{L_{\bar{z}}} \right)^{0.63}}} \quad (79)$$

where the term $L_{\bar{z}}$ represents the integral length scale of turbulence at the equivalent height \bar{z} :

$$L_{\bar{z}} = l \left(\frac{\bar{z}}{33} \right)^{\bar{\epsilon}} \quad (80)$$

Here, l and $\bar{\epsilon}$ are parameters listed in Table 7, which are essential for accurately determining the background response and turbulence effects.

The internal pressure coefficient, GC_{pi} , for enclosed buildings is taken as ± 0.18 . For safety considerations, the sign that increases the wind pressure has been selected to ensure a conservative design approach. Meanwhile, the external pressure coefficients, C_p , are provided in Table 8 for buildings with a square plan.

Surface	L/B	C_p	Use with
Windward Wall	All values	0.8	q_z
Leeward Wall	0-1	-0.5	q_h
Side Wall	All values	-0.7	q_h

Table 8: External Wall Pressure Coefficients for main wind force resisting system [37]

It is important to note that design wind pressure is defined based solely on wind pressure loading on the windward and leeward walls of the structure and disregarding the effect on the side walls. This is a method commonly used in the design stage applying cautionary simplifications around input loading applications for the most severe loading contribution effects. In addition to the just described gravity loading, considering the torsional effects of wind on high-rise buildings is a principle for accurate evaluation. The essential effect of the torsional loading is considered by establishing an eccentricity of 15% of the plan dimension (the perpendicular measurement to the loading direction). For a plan dimension of 30 m, this suggests an eccentricity of $e = 4.5$ m.

For the four varied building heights (126 m, 168 m, 210 m, 252 m), the parameters discussed above ie: wind pressure, turbulence, and structural response are detailed and presented in Table 9.

5. REQUIREMENTS AND PRELIMINARY FRAMEWORK FOR DIAGRID MODEL DEVELOPMENT

Calculation of wind load parameters according to ASCE for different building heights

Height	-	[m]	126	168	210	252
Velocity pressure exposure	K_z	-	1,48	1,61	1,72	1,81
Fundamental natural frequency	n_1	[Hz]	0,36	0,27	0,22	0,18
Intensity of turbulence	I_z	-	0,21	0,20	0,20	0,19
Peak factor for resonant response	g_R	-	3,94	3,87	3,81	3,76
Mean hourly wind speed at height \bar{z}	\bar{V}_z	[ft / s]	97,78	105,07	11,10	116,28
Integral of turbulence	L_z	[ft]	626,83	689,91	743,19	789,75
Reduced frequency	N_1	-	2,33	1,79	1,46	1,23
	η_h	-	7,06	6,57	6,21	5,93
	η_B	-	1,68	1,17	0,89	0,71
	η_L	-	5,62	3,93	2,97	2,36
	R_h	-	0,13	0,14	0,15	0,15
	R_B	-	0,42	0,52	0,60	0,66
	R_L	-	0,16	0,22	0,28	0,33
	R_n	-	0,08	0,10	0,11	0,12
Resonant response factor	R	-	0,53	0,67	0,79	0,91
Background response factor	Q	-	0,80	0,79	0,78	0,77
Gust effect factor for flexible buildings	G_f	-	0,93	0,97	1,01	1,05
Velocity pressure at height h	q_h	[N / m ²]	1235,83	1341,70	1430,03	1506,50

Table 9: Calculation of wind load parameters according to ASCE for different building heights

As can be seen in Table 9, the gust-effect factor is increasing with height since wind forces are more significant to the behavior of the taller building. As mentioned before, wind forces are dynamic in nature, and therefore larger for taller structures.

The lateral load F and the torque moment MT values at each height within the building ranges for the 168-m building can be seen in Table 10, where the height variable was calculated with a step of 3.5 m as it corresponds to the interstorey height. This calculation process was much the same as previous height data for the other structures. In particular, the maximum lateral forces F at the top of the buildings reached the following values - 203 kN, 229 kN, 251 kN and 273 kN for the 126-m, 168-m, 210-m, and 252-m buildings, respectively.

<i>Wind-induced forces along the height of the 168-m tall building</i>					
z [m]	F [kN]	M _T [kNm]	z [m]	F [kN]	M _T [kNm]
3,5	155	700	88	210	946
7	163	735	91	211	950
10,5	169	760	95	212	955
14	173	779	98	213	959
17,5	177	795	102	214	964
21	180	809	105	215	968
24,5	182	821	109	216	972
28	185	832	112	217	976
31,5	187	842	116	218	980
35	189	852	119	219	983
38,5	191	860	123	219	987
42	193	868	126	220	991
45,5	195	876	130	221	994
49	196	883	133	222	998
52,5	198	890	137	223	1001
56	199	897	140	223	1005
59,5	201	903	144	224	1008
63	202	909	147	225	1011
66,5	203	915	151	225	1014
70	205	921	154	226	1018
73,5	206	926	158	227	1021
77	207	931	161	228	1024
80,5	208	936	165	228	1027
84	209	941	168	229	1030

Table 10: Lateral force and torque moment distributions for the 168-m tall building due to wind load

The lateral loads are assumed to be introduced to the structure without regard to the plan shape, thereby providing a consistent analysis approach. The horizontal and torque actions are converted to concentrated horizontal and torque loads in order to run the structural analysis and are introduced at each rigid floor of the diagrid structure. It should be noted that for the top floor of the building, wind force only comes from the wind pressure on the upper half of the top module. Figure 53 demonstrates the distributions of the lateral force and torque moment for the various height buildings. From observation of the figure, the lateral force and torque moments have an increased magnitude with the increased height of the building. This

5. REQUIREMENTS AND PRELIMINARY FRAMEWORK FOR DIAGRID MODEL DEVELOPMENT

increase shown with building height represents the significant effects to the lateral forces and torque moments that wind generates, as they are applicable to the wind pressure and wind dynamic interactions on the structure increase with building height. The trend of increased lateral force and torque moment is an important consideration to assess when accounting for wind loads on high-rise structures. Increased lateral forces and torque moments from wind creates instability and dimensional performance concerns for taller structures when subjected to horizontal loads.

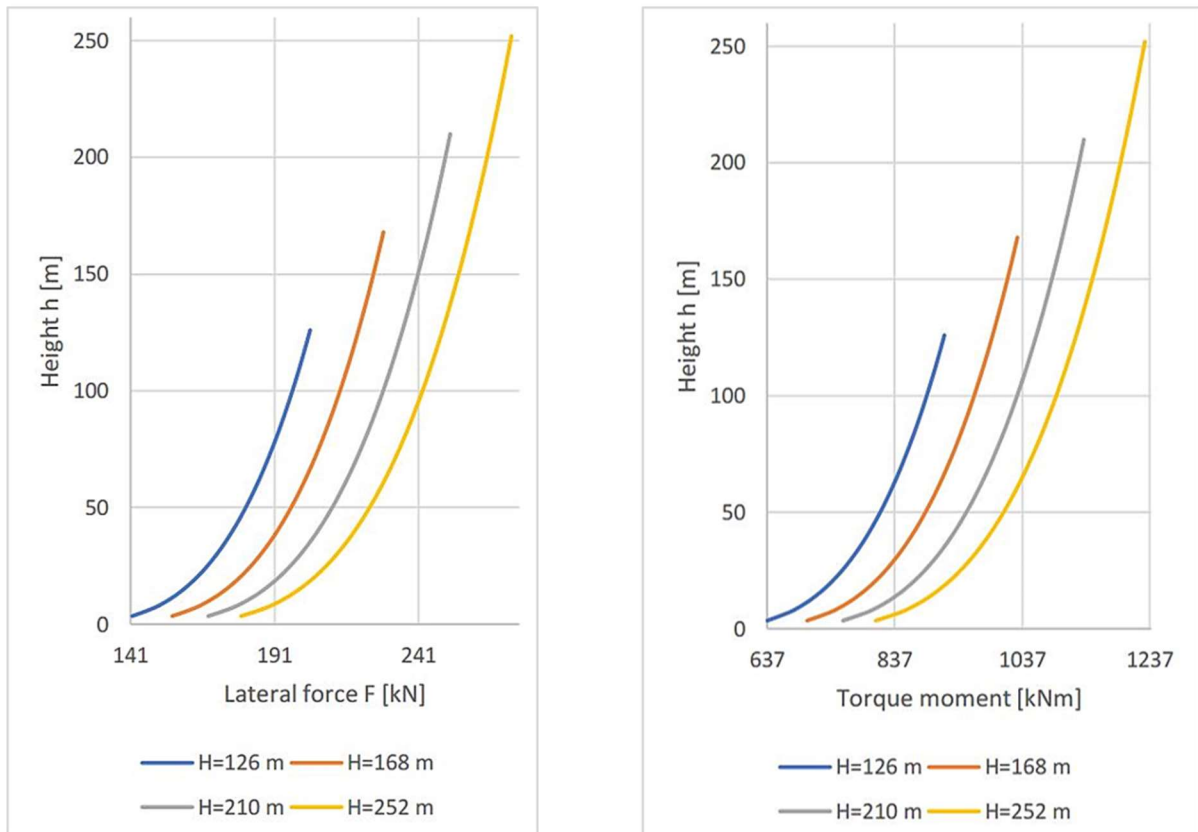


Figure 53: Forces distribution for different building heights due to wind action: (a) Lateral force F (b) Torque moment M

5.4. Strength- and Stiffness-Based Preliminary Design

This chapter presents the strength- and stiffness-based preliminary design developed in the MATLAB environment to establish the geometrical properties defining each model's ability to handle vertical and horizontal loads. The design parameters were able to meet the stiffness and strength requirements and reduce the structural mass.

The structural analysis for the diagrid structures will be conducted using the Matrix-Based Method (MBM) detailed in [30]. In order to conduct the structural analysis, it is necessary to

5.4. Strength- and Stiffness-Based Preliminary Design

define the initial parameter set needed for preliminary design and the MBM codes. The diagrid models assume certain parameters will stay the same regardless of the building height, diagonal angles, or floor plan: moduli of elasticity (E) for the diagonals, density (ρ) of the steel, inter-story height, and total floor area. The values for the parameters are presented in Table 11.

Inter-story height	3,5	m
Total floor area	900	m ²
Diagonals' elastic modulus	210	GPa
Steel density	7,8	ton/m ³

Table 11: Main parameters of the diagrid buildings [38]

In the subsequent step, the geometry of the base module is defined based on the floor plan shape (square, hexagonal, octagonal, or circular) and the number of intra-module floors. It is further assumed that each module consists of diagonals with identical cross-sections. Since the cross-sectional areas of the diagonals are required for the structural analysis, an initial assumption is made during the preliminary stage: the cross-sectional area is set to 0.1 m² for the base module and 0.01 m² for the top module, with linear interpolation applied to determine the areas for the intermediate modules.

The resulting cross-sectional areas are then compared to a predefined vector of commercially available cross-sections, as provided in handbooks of structural profiles. This ensures that the analysis considers realistic cross-sections rather than fictitious ones. Specifically, Table 12 lists the circular hollow sections (CHS) used in this study, characterized by varying outer diameters and thicknesses. These sections belong to classes 1, 2, and 3, as defined by Eurocode 3. Sections classified as class 4, with a diameter-to-thickness ratio exceeding $90 \cdot 235/f_y$, are excluded from consideration due to local instability issues, which cause failure before the yielding resistance is reached, keeping the section in the elastic range. The sections included in the analysis are sorted in ascending order based on their diameters and areas.

5. REQUIREMENTS AND PRELIMINARY FRAMEWORK FOR DIAGRID MODEL DEVELOPMENT

CHS section [mm]	A [cm ²]	CHS section [mm]	A [cm ²]
70 × 16	27	194 × 60	252
70 × 18	29	219 × 50	266
70 × 20	31	219 × 55	284
76 × 18	32	219 × 60	300
76 × 20	35	219 × 65	315
83 × 18	36	219 × 70	328
83 × 20	39	245 × 60	348
83 × 22	42	245 × 65	367
83 × 25	45	245 × 70	384
89 × 22	47	245 × 80	413
89 × 25	50	245 × 90	437
102 × 20	51	267 × 80	470
102 × 22	55	267 × 90	500
102 × 25	60	267 × 100	525
102 × 28	65	273 × 100	543
102 × 30	67	299 × 80	549
108 × 28	70	299 × 90	590
108 × 30	74	299 × 100	624
114 × 28	76	324 × 90	661
114 × 30	79	324 × 100	703
114 × 32	83	356 × 90	751
114 × 36	89	356 × 100	803
127 × 30	91	368 × 100	842
127 × 32	96	406 × 90	895
127 × 36	103	406 × 100	963
127 × 40	109	419 × 100	1002
127 × 45	116	457 × 90	1038
140 × 36	117	457 × 100	1122
140 × 40	125	508 × 90	1182
140 × 45	134	508 × 100	1282
140 × 50	141	559 × 90	1326
152 × 40	141	559 × 100	1442
152 × 45	152	610 × 90	1470
152 × 50	161	610 × 100	1602
159 × 45	161	660 × 90	1612
159 × 50	171	660 × 100	1759
159 × 60	187	711 × 100	1920
168 × 60	204	1620 × 40	1985
178 × 55	212	1820 × 36	2018
178 × 60	222	1820 × 40	2237
194 × 50	226	2020 × 36	2244
194 × 55	240	2020 × 40	2488
		2220 × 40	2739

Table 12: Steel structural circular hollow section (outer diameter × thickness in mm) and area for diagrid structures [38]

Before conducting the analysis, it is essential to define another key input parameter: the load. As established in Chapter 5.1, the vertical load is set at 4.125 kN/m², derived from the

combination of dead and live loads. Additionally, Chapter 5.3 provides the lateral forces (in kN) and torque moments (in kNm) for each rigid floor.

Given the assumption in the MBM framework that intra-module floors are neglected, the lateral actions are carried exclusively by the rigid floors. These actions are evaluated using an isostatic distribution approach. Specifically, the resultant lateral force and torque moment for each module are calculated as the sum of the lateral forces and torque moments acting on the upper half of the lower module and the lower half of the upper module. An exception is made for the top floor, when only half of the top module is considered. This ensures that the MBM process is consistent and straightforward in evaluating lateral actions.

The diagrid design needs to fulfil overall stiffness and strength criteria. The strength of the diagonals can be evaluated through the Demand Capacity Ratio (DCR), which is a measure of the axial force that they can resist, representing their capacity. The DCR is therefore the ratio of the design axial force through the diagonal and its strength. Since a diagonal can be subjected to either compression or tension, the DCR is expressed as follows:

$$DCR = \begin{cases} \frac{|N_{Ed}|}{\min(N_{c,Rd}, N_{b,Rd})} & \text{if } N_{Ed} < 0 \text{ (compression)} \\ \frac{N_{Ed}}{N_{t,Rd}} & \text{if } N_{Ed} > 0 \text{ (tension)} \end{cases} \quad (81)$$

N_{Ed} is the axial load along the diagonal as identified by the MBM which is positive if it is in tension and negative if it is in compression. The tensile and compressive strengths are defined as $N_{t,Rd}$ and $N_{c,Rd}$ respectively, Equations (66) and (51). For compressed diagonals the buckling strength was checked and defined by $N_{b,Rd}$ as in Equation (59) due to the instability, multi-axial loading of the comparison strength approaches. Finally, to present to the user in the DCR, it should be noted that safety factors are extrapolated from the DCR; therefore, the DCR is established across each diagonal in a diagrid module but the early iteration focuses on the maximum DCR value for each module at a stage, which means the diagonals are at a maximum use trend, resulting in reduced structural mass for the diagrid system.

The design method is comprised of three primary steps, providing a specific focus goal, as established in Albitos et al. [38]

Step 1 – Initialization: For an assigned diagonal cross-section distribution, selection by the user has occurred based on the initial cross-sectional areas of the base and top modules, and

5. REQUIREMENTS AND PRELIMINARY FRAMEWORK FOR DIAGRID MODEL DEVELOPMENT

the structured module was analyzed with strength calculations in the MBM framework, establishing the maximum DCR noted amongst the diagonals of the i -th module. The process begins with the top module where each undersized diagonal cross-section area was account for on each module, a refinement of the iterations were adjusted until a $DCR > 1$ was found; this was a relevant application to influenced structural mass to the limit of the diagrid, this could lead ultimately to a diagrid structure in a failure condition (unable to sustain the vertical and horizontal applied loads).

Step 2 – Strength: This step is the opposite of the previous one, as the diagonal cross-sectional area is increased rather than decreased to ensure the resistance of each module. The process begins with the diagonal area distribution along the building height obtained from Step 1. The DCR is then evaluated by performing structural analysis and strength calculations. If the DCR exceeds unity, it indicates that the strength demand is not met, and the diagonal cross-sectional area of the i -th module must be further increased until the DCR is less than or equal to 1. This process is repeated iteratively for all lower modules, step by step.

Additionally, the top lateral displacement is checked at each iteration. If, at the end of Step 2, the top displacement is lower than the target limit value, defined as $H/500$, the structure satisfies both strength and stiffness requirements, and Step 3 does not need to be implemented. However, if the top displacement exceeds the target limit, the preliminary design is incomplete, and Step 3 must be performed to ensure global stiffness, as described in the following section.

In summary, Step 2 defines a diagrid structure capable of withstanding external loads without yielding or buckling issues for all diagonals in each module, while also verifying compliance with stiffness requirements.

Step 3 – Stiffness: This step is executed only if Step 2 results in a structure that is excessively flexible and deformable, as indicated by a top displacement exceeding the allowable limit. Unlike the first two steps, the diagonal cross-sectional area is increased starting from the base module to meet the stiffness requirements. The objective is to iteratively stiffen the structure until the global top lateral displacement is reduced to within the target limit. However, for highly slender and flexible structures, the final geometry may fail to satisfy the stiffness demand due to the maximum allowable diagonal cross-sectional area, $A_{\max} = 0.2739 \text{ m}^2$, as

5.4. Strength- and Stiffness-Based Preliminary Design

specified in Table 8. In such cases, the algorithm produces a structure with constant stiffness along the building height, but this results in a significantly increased structural weight.

The entire iterative process is summarized in Figure 54. The flowchart, developed in [38], is divided into four main parts: the definition of input parameters, the initialization step, the strength step, and the stiffness step.

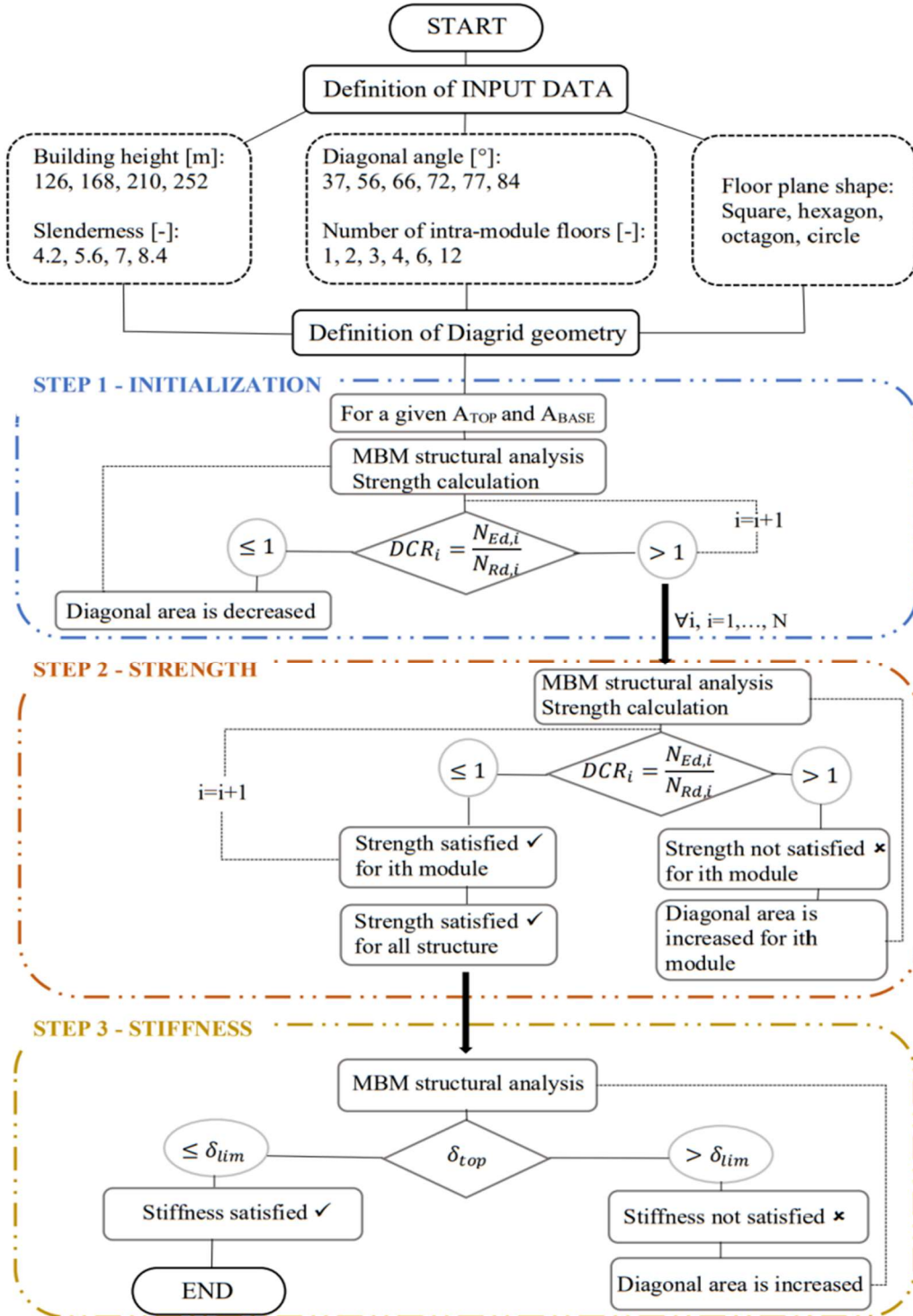


Figure 54: Flow chart of the preliminary design; DCR = Demand to capacity ratio, δ_{top} = top lateral displacement, δ_{lim} = target limit top lateral displacement value [38]

6. CRITICAL LOAD ANALYSIS AND PROGRESSIVE COLLAPSE OF DIAGRID SYSTEMS

This chapter outlines the methodology to determine the critical load factor of a diagrid system and analyze its progressive collapse by removing elements exceeding buckling or tensile strength. In particular, Chapter 6.1 offers an overview of the stability analysis of the diagrid member, giving information about the critical load evaluation based on the elastic equilibrium instability theory. Subsequently, in Chapter 6.2, the general principles of structural stability analysis are explored, with a particular focus on the conditions and verification methods for ensuring the stability of diagrid systems following the removal of multiple members. Chapter 6.3 presents the framework of the analysis developed in the MATLAB environment, based on the preliminary design results obtained through the MBM approach discussed in the previous chapter. Finally, Chapter 6.4 focuses on the validation of the analysis through a Finite Element Method (FEM) simulation.

6.1. Stability Analysis of Diagrid Members

The instability of elastic equilibrium is a fundamental concern in the study of diagrid systems, as these structures often rely on slender, interconnected elements to achieve their distinctive geometric and structural efficiency [39]. In diagrid systems, the instability of elastic equilibrium is not merely a localized issue affecting individual members but can propagate through the entire structural framework due to the high degree of interdependence among the elements. This phenomenon is particularly critical because diagrid systems are designed to optimize material usage and reduce weight, which inherently leads to the use of slender beams and rods that are more susceptible to buckling under compressive loads.

Based on this, the local instability of diagrid members under axial compressive forces can be effectively analyzed using the simplified mechanical model depicted in Figure 55(a). This model consists of two rigid rods connected by an elastic hinge with rotational rigidity k , constrained at one end by a hinge and at the other by a roller support. When subjected to an axial force N , the absolute rotation ϕ of the two arms is taken as the generalized coordinate, and the total potential energy of the system is expressed as:

$$W(\varphi) = \frac{1}{2}k(2\varphi)^2 - 2Nl(1 - \cos\varphi) \quad (82)$$

The conditions of equilibrium are identified by imposing the stationarity of Equation 82:

$$W'(\varphi) = 4k\varphi - 2Nl\sin\varphi = 0 \quad (83)$$

from which we obtain the relation:

$$N = \frac{2k\varphi}{l\sin\varphi} \quad (84)$$

which links loading condition and deformed configuration along the branch of equilibrium presented in Figure 55(b).

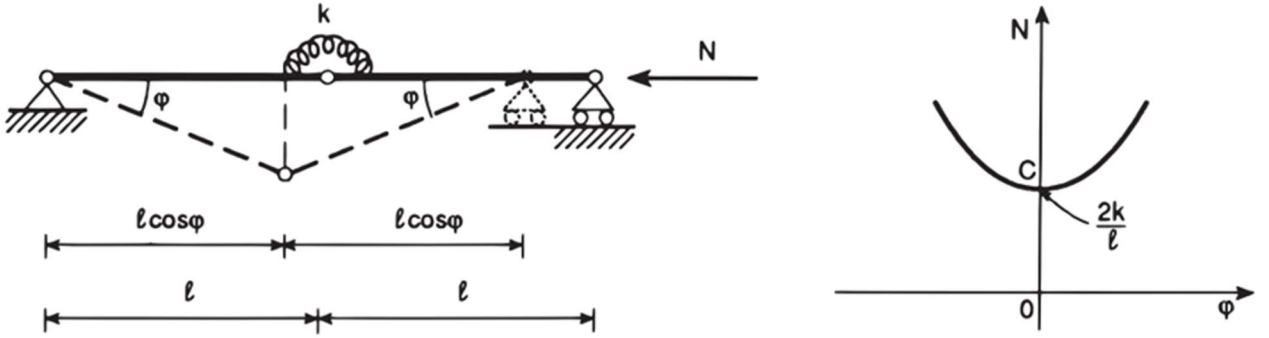


Figure 55: (a) mechanical system consisting of two rigid rods connected by an elastic hinge of rotational rigidity k , and constrained at one end by a hinge and at the other by a roller support, loaded with an axial force N with generalized coordinate of absolute rotation of the two arms φ ; (b) branch of equilibrium where the points of the upper sector represent conditions of instability, while those of the lower sector represent conditions of stability [39]

The plane $N - \varphi$ is thus divided into two sectors by the curve of Equation 84: the points of the upper sector represent conditions of instability of the initial rectilinear form ($\varphi = 0$), while those of the lower sector represent conditions of stability. Starting from the initial condition $\varphi = N = 0$, it will thus be possible to traverse, in a stable manner, the vertical segment of the axis N up to the point C ($\varphi = 0$, $N = N_c = 2k/l$), then to deviate onto one of the two branches of equilibrium of Figure 55(b). Alternatively, it would be possible to proceed along the vertical axis beyond the branching point C , although, in this case, the equilibrium is of an unstable type. The analysis presented above is valid only if the hypothesis of small (negligible) displacements, which assumes that the cardinal equations of statics are evaluated with respect to the undeformed structural configuration, is removed. By removing this hypothesis, it becomes evident that the solution to an elastic problem can represent a condition of stable, neutral, or unstable equilibrium, depending on the magnitude of the applied load. Furthermore, around the condition of neutral equilibrium exists an infinite number of similar

6. CRITICAL LOAD ANALYSIS AND PROGRESSIVE COLLAPSE OF DIAGRID SYSTEMS

equilibrium states, each characterized by distinct static parameters (applied loads) and kinematic parameters (system configurations) [39].

The previous formulation considers finite-amplitude displacements (nonlinear analysis). However, for Eulerian instability problems, a linearized formulation is sufficient for determining the critical buckling load. This implies writing the equilibrium equations with respect to the deformed structural configuration, but assuming small-amplitude displacements so that the equilibrium equations appear in linearized form; this allows investigating the stability of elastic equilibrium.

For the sake of simplicity, in this thesis, the small displacement hypothesis is taken into account, considering that the diagrid member is pinned at both ends and forms part of a diagrid system. Under this framework, the load is increased incrementally until the critical point C is reached, where the critical load factor λ is determined. This marks the transition from stable to unstable behavior, in fact, in Figure 56 is represented that up to point C , the equilibrium curve is considered linear, reflecting the stability of the system, however, above point C , the member is regarded as unstable, so no additional increment of the load is considered, and no further analysis of the behavior of the member will be pursued within the scope of this study.

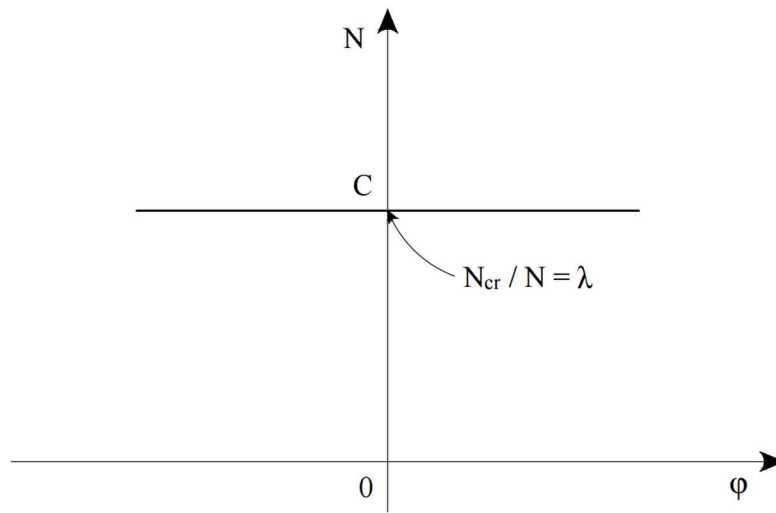


Figure 56: Stability analysis of diagrid members under axial compressive forces, illustrating the division of the N - ϕ plane into stable and unstable regions

Adopting this methodology, the critical load factor is specified, giving an easier threshold for the stability of the axial compressive loads on the diagrid member. This makes it easier to consider such a simplification under real-world usage, as one can evaluate the conditions for stability but still be able to explore the critical elements of the diagrid system in operation.

6.2. Structural Stability Analysis, Conditions, and Verification Methods

From the perspective of Rational Mechanics, a one-dimensional structure can be conceptualized as a system composed of rigid, non-deformable components that are interconnected and anchored to the ground. Such a system may exhibit degrees of freedom, characterizing it as a holonomic system, and its lability is determined by the number of these degrees of freedom. Lability can be classified as external and internal. External lability occurs due to a lack of external constraints given an insufficient number or placement for an arrangement. For flat systems, the minimum number of simple constraints that must be present is three. In spatial structures, the minimum is six. In addition to having a minimum number of constraints, consideration to the organization of these constraints must be made to avoid certain unfavorable arrangements. Internal lability occurs when the structure has a lability of order greater than or equal to four, for flat systems, in the absence of any external constraints, or greater than or equal to seven for spatial structures [40].

The word, isostatic, can be used to refer to a structure that is both non-labile and isostatic to all reactions. A structure can be called isostatic for internal constraints if upon removing external constraints, the body has only three degrees of planar motion associated with rigid systems and isostatic with respect to all internal reactions. A structure can be named isostatic for external constraints if it is non-labile and isostatic with respect to externally applied constraints only. The latter assumes that any internal constraints are also rigid or fixed.

The term hyperstatic is generally used to describe a structure in which at least one reaction is hyperstatic, meaning the structure is not isostatic with respect to all constraining reactions. A structure is classified as hyperstatic due to external constraints when the number of external constraints exceeds what is necessary to fully constrain a rigid body in either the plane or space. In the same way, if there are internal constraints set in a structure, it is considered hyperstatic, if, when the external constraints are removed, at least one reaction still remains hyperstatic.

The order of hyperstaticity relates to the number of simple constraints the structure must endure, which to be rendered isostatic with respect to all reactions, must have those simple constraints removed. The order can be determined most directly according to its definition: progressively remove the constraints until the structure is isostatic with respect to all reactions. The number of simple constraints removed, or equivalent constraints, indicates the

6. CRITICAL LOAD ANALYSIS AND PROGRESSIVE COLLAPSE OF DIAGRID SYSTEMS

order of hyperstaticity. While the approach may sound simple, implementing the approach is not easy, especially distinguishing whether a structure is isostatic. It is relatively easy to identify whether a structure is isostatic for simple structures, however it is much more difficult for more complex structures.

A general method, that can be used for plane systems and may be adapted to other cases, can be applied for the evaluation of hyperstaticity. This method starts by removing all constraints, external or internal, then exposing the structure to cuts along straight sections to break the structure into parts. The parts are set so each component is isostatic because of the internal constraints. In other words, these components are reduced into t single connected beams. This reduction can occur in infinitely different ways, however the best reduction is the one that minimizes t . After reducing the structure, it is made up of t components ($3t$ degrees of freedom) since the t parts can participate in planar motion. Once this is done, the structure is isostatic. Now we need to put the constraints back on the structure to see the number of constraints s of the equivalent simple constraints, which represents the maximum number of degrees of freedom that those constraints can eliminate. This lets us systematically analyze the hyperstaticity of the structure.

A constraint of order r eliminates r degrees of freedom or, equivalently, introduces r degrees of hyperstaticity. Consequently, if we denote the order of lability of the structure by l and the order of hyperstaticity by i , the total order of the constraints s introduced serves two purposes: it eliminates $3t - l$ degrees of freedom and introduces i degrees of hyperstaticity. This relationship can be expressed as:

$$s = 3t - l + i \quad (85)$$

Rearranging this equation, we obtain:

$$3t - s = l - i \quad (86)$$

From this, it follows that:

$$3t - s > 0 \quad (87)$$

It is sufficient for the structure to be labile; since in fact both l and i are positive, the condition $l - i > 0$ imports the other $l > 0$.

This inequality is a sufficient condition for the structure to be labile. Since both l (the order of lability) and i (the order of hyperstaticity) are positive, the condition $l - i > 0$ implies $l > 0$, confirming the structure's lability.

6.2. Structural Stability Analysis, Conditions, and Verification Methods

However, this condition is not necessary. It is possible for $l - i \leq 0$ while $l > 0$, depending on the value of i . In other words, a structure can simultaneously be hyperstatic and labile, with the order of hyperstaticity i equaling or even exceeding the order of lability l .

From Equation (86) we can derive the following relationships:

$$l \geq 3t - s \quad (88)$$

$$i \geq s - 3t \quad (89)$$

From Equation (86) we also derive the condition

$$3t - s < 0 \quad (90)$$

that is sufficient for the structure to be hyperstatic.

Indeed, if $l - i < 0$, it implies $i > 0$, meaning the structure possesses hyperstaticity. However, this condition is not necessary, as it is possible for $l - i \geq 0$ while $i > 0$, depending on the value of l . In such cases, the structure is both hyperstatic and labile, with the order of lability equaling or exceeding the order of hyperstaticity.

The condition

$$3t - s = 0 \quad (91)$$

is necessary for the system to be isostatic.

The structure is labile if $3t - s > 0$, and hyperstatic if $3t - s < 0$. Then applying Equation (91), we find that $l - i = 0$, therefore $l = i = 0$. By definition, such a condition is sufficient for the structure to be isostatic since it is with neither labile nor hyperstatic.

Regarding calculating the degrees of freedom of constraints eliminated, the case of an internal hinge with n beams converging will be examined. Such a hinge will eliminate the relative motion between the beams in a systematic manner. Namely, it will eliminate two degrees of freedom of relative motion between the first and second beams, another two between the first and third beams, and so on. In general, the total number of degrees of freedom eliminated by the hinge is:

$$2(n - 1) \quad (92)$$

This result arises because the hinge constrains the relative motion of each additional beam with respect to the first beam, and there are $n - 1$ such additional beams. Consequently, the

6. CRITICAL LOAD ANALYSIS AND PROGRESSIVE COLLAPSE OF DIAGRID SYSTEMS

hinge effectively reduces the system's overall degrees of freedom by $2(n - 1)$, which must be accounted for in the structural analysis [40].

In the case of lattice structures, including diagrids, all beams are connected by hinges that can be considered spherical. As a result, each beam functions as a hinge. When the loads are concentrated at the nodes (i.e., on the hinges), the beams are subjected exclusively to axial forces. However, for analytical convenience, it is often useful to reverse the roles of nodes and rods. In this perspective, the nodes are treated as point-like bodies, each possessing 2 degrees of freedom in the plane (or 3 in space), while the rods are regarded as simple internal constraints that regulate the relative distance between two nodes. Based on this framework, we can establish the relationship between the number of nodes N_c and the number of rods N_l . If N_e represents the number of simple external constraints, the system will be statically and kinematically determinate (assuming the constraints are properly arranged, which is a sufficient condition) when the total number of constraints $N_l + N_e$ equals the total degrees of freedom of the system [41].

This condition leads to the following relationships:

In the plane:

$$N_l - N_e = 2N_c \quad (93)$$

In space:

$$N_l - N_e = 3N_c \quad (94)$$

As discussed in Chapter 6.1, when a member reaches its critical load and enters the buckling condition, it is no longer considered in the structural analysis. To account for this, the member is effectively removed from the geometry of the structure. This removal leads to a reduction in the total number of members, which in turn alters the structural system's degree of hyperstaticity or stability.

By combining Equation (94) with Equation (89), the degree of hyperstaticity i of the diagrid structure can be expressed as:

$$i = N_l + N_e - 3N_c \quad (95)$$

This equation provides a direct measure of the hyperstaticity of the structure.

When rods are removed from the geometry of the structure, the number of internal constraints N_i decreases, leading to a reduction in i . If the removal of rods continues to the point where the condition:

$$i < 0 \quad (96)$$

is satisfied, so the system becomes labile.

In this case, Equation (87) now represents both a necessary and sufficient condition, since the inequality $l - i \leq 0$ holds only if $l > 0$; that is, the system has positive lability and, therefore, is no longer stable.

On the other hand, the system is defined as non-labile as long as the condition $i < 0$ is not satisfied, assuming the constraints are well placed (a sufficient condition), and thus the structure has maintained enough constraints to be stable even as rods are removed.

However, the condition of well-placed constraints cannot always be guaranteed. Additionally, certain load conditions or structural geometries may still render the system globally unstable, even if the constraints appear sufficient. To address these challenges and ensure structural stability and safety, two key verifications are typically employed:

- Limit State Verifications on Maximum Lateral Displacement;
- Demand Capacity Ratio (DCR).

Both of these methods are powerful options when controlling global instability and ensuring the structural performance of systems.

The first verification method involving the limit state of maximum lateral displacement is based on the NTC 2018 [6], which provides standard (regulation) provisions to limit the maximum allowable displacements and therefore cease structural instability. More specifically, for tall buildings, the ratio defined as the maximum allowable horizontal displacement is defined as the maximum absolute horizontal displacement over the total height of the building where this ratio must not be greater than $1/500$ based on the NTC 2018. By limiting lateral displacements, the deformation of the structure remains within an accepted limit, such as preventing global instability events like the development of a progressive collapse mechanism, etc. When maximum lateral displacement is limited, the applied lateral loads, such as wind or seismic loads, are within the structure's resistance capacity limits, ensuring structural integrity and usability while maintaining global stability.

6. CRITICAL LOAD ANALYSIS AND PROGRESSIVE COLLAPSE OF DIAGRIDS SYSTEMS

The second verification method is the Demand Capacity Ratio (DCR) method which falls under guidelines of standards such as the GSA UFC [42]. The DCR is a tool to evaluate the structural performance of various structural elements under extreme events, such as the instant removal of a column in a specific scenario. The DCR is defined as the ratio of the acting force (bending moment, axial force, shear force, or combined) in the structural element and the element's resistance to that acting force.

A structural element is considered to have failed if its DCR exceeds the following thresholds:

- 2.0 for typical structural configurations.
- 1.5 for atypical structural configurations.

The DCR for structural components is calculated using the formula:

$$DCR = \frac{Q_{UD}}{Q_{CE}} \quad (97)$$

where:

- Q_{UD} is the acting force in the component or connection/joint, determined after the instantaneous removal of a column. This force can include bending moments, axial forces, shear forces, or a combination of these.
- Q_{CE} is the expected ultimate, unfactored capacity of the component or connection/joint, considering the same forces (moment, axial force, shear, or combined forces).

If the DCR remains within these limits, the stability of the building is guaranteed. The reason for this is that the DCR is the actual and direct measure of the structure's capacity to resist extreme loading conditions, such as the abrupt removal of a load-bearing member. Complying the DCR limit ensures that structural members have adequate reserve capacity, to prevent local failure which would lead to progressive collapse. Additionally, ensured compliance with DCR limit ensures stresses, during extreme conditions, remain low enough to preserve structural capacity and system function.

Achieving stability for the removal of one or more members requires that all the verification conditions achieved are verified at the same time. Each verification like complying to the systems non-labile condition, controlling the maximum lateral displacement, and complying with the DCR all address specific aspects of the structure's behavior, but separately and in a

way that is complementary to the other verification conditions to arrive at a total stability assessment.

These verification conditions are neither interchangeable or substitutes of each other, as each answer focuses on a different dimension of structural behavior. In the case of structural behavior, the non-labile condition ensures a stability exist for the system, control of lateral displacements ensure that the maximum deformations do not lead to states of instability, and DCR verification ensures that each member has adequate capacity preserved to counter a local failure or limit progressive collapse.

If any one of these conditions is not verified, safety and structural stability have been compromised; an aspect of the structure's behavior would have been unaccounted for. Therefore, only when all conditions are satisfied concurrently can the structure be said to be safe and stable under worst-case scenarios such as abrupt removal of load bearing elements.

6.3. Methodology

The methodology consists in the evaluation of the critical load factor of the diagrid system and the subsequent analysis of progressive collapse scenarios. This involves determining the critical member most at risk of failure, simulating its removal, and iteratively reanalyzing the structure to assess its stability and performance under reduced hyperstaticity.

The proposed procedure is implemented within the MATLAB environment and employs the matrix-based method (MBM) described in detail in [30] to perform the structural analysis of diagrid structures. The matrix-based method (MBM) allows for identifying axial forces, displacements, and demand-capacity ratio (DCR) for each member throughout the analysis, as well as updating both the stiffness matrix and the geometry for progressive collapse analyses.

Chapter 5.4 explores the process of Strength- and Stiffness-Based Preliminary Design, and the output of the structure provided will meet the characteristic constraints of strength and stiffness while also maximizing the overall efficient use of the diagrid system's diagonal members and minimizing the total weight of the structure. The result is the input for the analysis of the critical load to reach structural instability, as well as to identify the most critical member or stressed member. In the preliminary design stage, the consistent loading is at vertical and lateral load factors. The vertical load (see Chapter 5.1) was defined as 4.125

6. CRITICAL LOAD ANALYSIS AND PROGRESSIVE COLLAPSE OF DIAGRID SYSTEMS

kN/m² and an equally distributed arbitrary weight over each rigid floor of the structure in this study, while the lateral wind loads applied as concentrated loads are spread over the vertical members of the diagrid structures considered. For all the models in Tables 1 - 4, the initial lateral loads applied were for uniform concentrated loads spanning the height of the structure. More specifically, all lateral forces in this study will consist of a constant uniform lateral load of 1 kN lateral load for all models, and it will be combined with the respective preliminary design vertical loads, and will provide the base loading for all systems analyzed in this study. Once the input lateral force is established, the axial forces for each member in the diagrid structural system are developed using Equation (46). The axial loads are calculated for the diagrid member cross-sectional area compiled from the preliminary design. The axial loads from this calculation will either be in compression (negative forces) and tension (positive forces) and then be compared with their respective resistance values based on the strength criteria established in Chapter 5.2. At this point, the demand-capacity ratio (DCR) will also be calculated based on the loads examined in this study. The DCR is a key metric for assessing structural performance under extraordinary events, and it is a key parameter for the progressive collapse analysis, which will be discussed in detail in the second step.

To conclude the first part of the procedure, the primary task of this work is to find the critical load factor that causes the structure to be unstable due to buckling. In comparing the axial compression forces with the compressive strength, only the buckling instability for members in compression is considered, as given in Equation (59). For members subjected to tension, the tensile strength of the member is used to note that before reaching the critical buckling compression value, the member still does not exceed its tensile strength. This condition is rare, as the buckling compression value was determined with respect to a factor that reduces the resistance of the members due to instability found in compression, therefore resulting in a lower resistance value. However, due to some load and geometry configurations, it is still possible that the tensile strength will be exceeded first. In these situations, this analysis has become unreasonable, and different assumptions or methods must be chosen in order to examine the case adequately.

Subsequently, a conditional statement is used to determine if the critical buckling load in compression or the tensile strength in tension has been exceeded.

In order to do this, we perform a force-controlled analysis of the diagrid system until the member strength or capacity is exceeded, whilst we linearly and uniformly increase the lateral force applied to the diagrid system by a specified chosen value, which in this study is 0.1 N in order to create a balance of sufficient accuracy and computational speed, allowing us to complete our calculations accurately and in an efficient manner. This process corresponds to moving along the linear branch shown in Figure 56. At which time the axial force in the member reaches its critical value in compression, then the following ratio defines the first critical load λ , causing the instability behavior in the structure for the applied force to the critical force. Also suitable to note, at this point, the most heavily loaded member in the entire system is identified by element and module number, thus, two important inputs to our next analysis, critical load and critical member, are given.

The second aim of this thesis is to model the progressive collapse of the diagrid structure due to the buckling instability of its members. To achieve this, the two outputs from the previous analysis, the critical load and the critical member, are used as inputs. More specifically, once the critical load has been determined, it is multiplied by the lateral force to create the critical structural condition for instability and capacity.

Following the hypothesis outlined in Chapter 6.1, the critical member is considered as unstable and is therefore excluded from further analysis, hence, no additional load increments are applied, and the behavior of the critical member is no longer evaluated.

To take into account these considerations, the geometry of the diagrid system is updated, reducing the degree of hyperstaticity. The area of the critical member is also set to zero. Hence, we can calculate a new stiffness matrix to find the new equilibrium in the structure, allowing us to calculate the new displacements and axial forces in the remaining members.

After a critical member is removed, a linear static analysis is performed again under the same critical load, and a new critical member appears. This process continues until one of the stability conditions defined in Chapter 6.2 is no longer met. Each time a new critical member is found, a plot of the structure is generated, and the critical member is highlighted in the plots so that it is easy to visualize the output from an iteration. In addition to the plot, an Excel sheet is created as an output table that contains the displacements in the x, y, and z directions, and the torsional rotation of each member; this output represents the performance of the overall structure. The table also contains the axial force (tension or compression) present in

6. CRITICAL LOAD ANALYSIS AND PROGRESSIVE COLLAPSE OF DIAGRID SYSTEMS

each member to identify, if calculated, the associated Demand-to-Capacity Ratio (DCR) for each critical member.

The outputs, displacements, DCRs and reductions in the degree of hyperstaticity will represent the global stability analysis of the diagrid system.

There will be an instantaneous increase in the displacements and DCR of the remaining members during the process of removing critical members. Therefore, if the system, or the degree of hyperstaticity, becomes isostatic, or less hyperstatic, the structure's global stability should still be checked to confirm the system does not become unstable in the iterative processes of removing critical members. The stability conditions outlined in Chapter 6.2 were used to validate this process.

For uniform-angle diagrid systems, the limit for the DCR remains 2, and for non-uniform-angle diagrid systems, the limit is 1.5. As for displacements, for both uniform-angle and non-uniform-angle diagrid systems, the limit for maximum allowable displacement is $H/500$, where H is the height of the structure. These two conditions, with non-lability, are maintained during the reduction of the degree of hyperstaticity, and as soon as one condition is no longer satisfied, the iterative process will stop, and the structure can be considered stable from this iterative analysis.

The entire iterative process is illustrated in Figure 57, which presents a flowchart divided into three main sections, including the definition of input parameters, the critical load factor determination step, and the progressive collapse analysis step, each representing a key phase of the methodology.

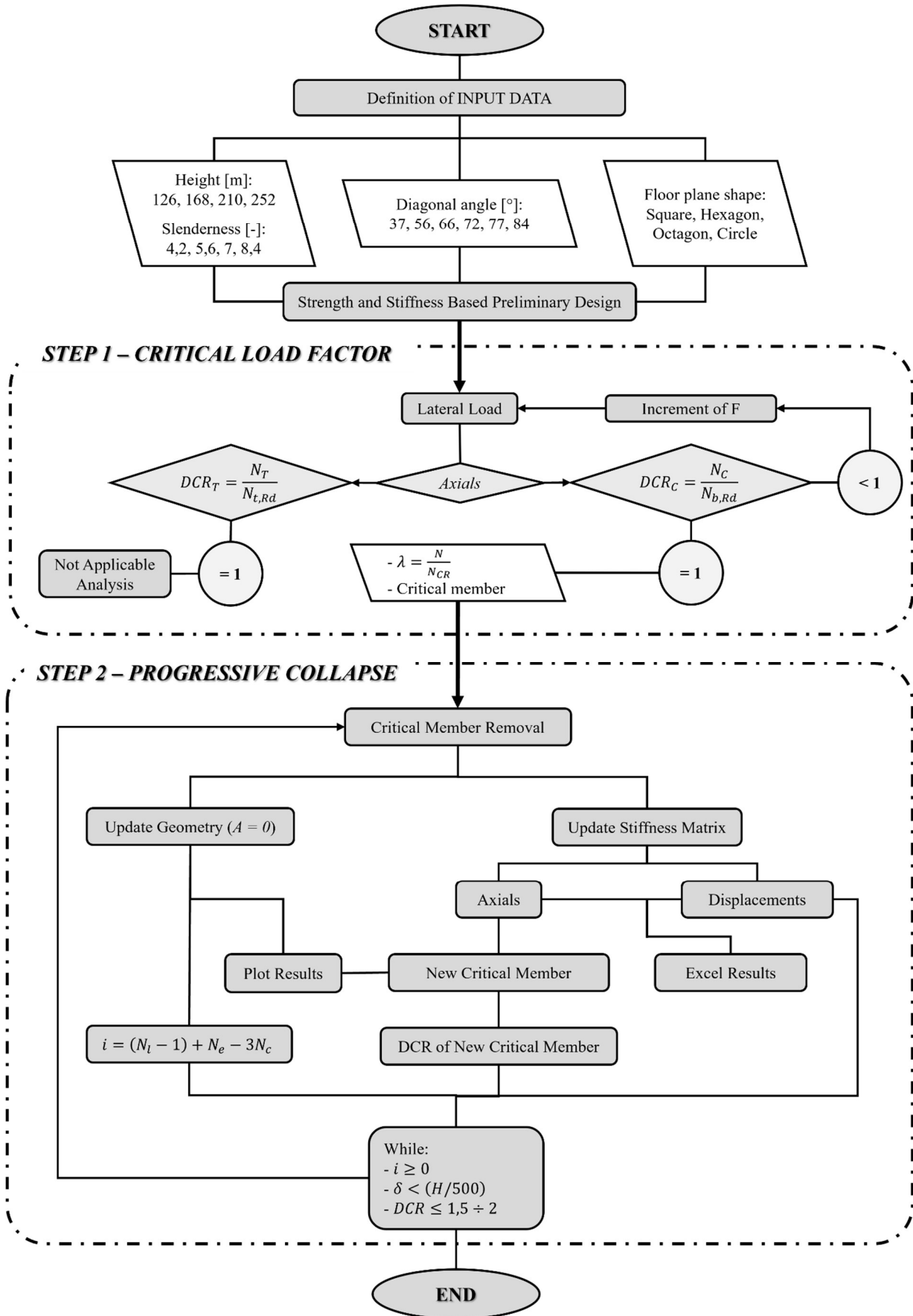


Figure 57: Flowchart of the iterative procedure for the buckling and progressive collapse analysis of the diagrid system; λ = Critical Load Factor, DCR = Demand-to-Capacity Ratio, δ = Top Lateral Displacement, i = Degree of Hyperstaticity

6. CRITICAL LOAD ANALYSIS AND PROGRESSIVE COLLAPSE OF DIAGRID SYSTEMS

6.4. Validation of the Methodology

This chapter validates the proposed methodology of the MATLAB code analysis by comparing it to a Finite Element Method (FEM) analysis. The goal of the validation is to confirm the accuracy of the methodology in finding the critical load factor, the critical members, and the axial forces in the members. The top lateral displacement of the structure is also analyzed to confirm agreement with the results as well.

The chapter is organized as follows: Section 6.4.1 which includes a description of the FEM analysis setup, including modeling assumptions, boundary conditions, and the iterative procedure for validating the MATLAB methodology. Section 6.4.2 provides a comparative analysis of the results, to confirm that the members considered critical by the MATLAB analysis agree with the members deemed critical by the FEM approach, in terms of axial forces in the critical members and the lateral top displacements of the entire structure.

6.4.1. FEM Analysis Model and Assumptions

To validate the MATLAB code analysis, a Finite Element Method (FEM) analysis was conducted using a simplified diagrid structure with a height of 126 meters, consisting of six modules, each composed of 24 elements. The structure features a square floor plan, with each member inclined at 76° . The FEM model was defined with the same geometry, cross-sectional areas, and material properties for each member as specified in Table 13(a). A rigid shell surface was incorporated to simulate the rigidity of the intra-module floors, with its geometry and material properties defined in Table 13(b). The applied loads were identical to those used in the MATLAB code, including a constant lateral force applied at each extremities node along one edge of the structure in order to have an eccentricity that simulates the same torque moment applied on each floor in the MATLAB model.

For the first goal, the critical load, as well as the most critical member, were determined using a linear buckling analysis of the FEM model. This falls in line with the linear elastic assumptions that were taken in the MATLAB analysis. Once that this was done, to start on the second goal, the most critical member was removed from the FEM analysis and a new static analysis was conducted with only the critical load applied (all loads were multiplied by the buckling critical load factor). In the FEM model, the axial force which the removed

member had previously carried was redistributed to the nodes it was connected to so that the physical presence of the member was considered, but it no longer had load-bearing capacity. Since the MATLAB did not allow any further increments of axial force in the removed member, this solution reflects that approach.

Diagonal Member		Rigid Floor	
Cross-Sectional Area [m ²]	0,27395	Thickness [m ²]	0,05
Diameter [m ²]	0,04		
Young Modulus [Mpa]	210 E6	Young Modulus [Mpa]	210 E10
Weight [ton/m ³]	7,8		
(a)		(b)	

Table 13: Geometric and material properties of the diagrid structure for FEM validation; (a) diagonal members; (b) rigid floor)

The iterative process continued until one of the stability conditions specified in the study was not met consecutively for a member. The process in the FEM analysis replicated the process that was used in the MATLAB code in an iterative manner, further validating the results.

6.4.2. Results Comparison

In this section, the results obtained from the MATLAB code analysis are compared with those derived from the Finite Element Method (FEM) analysis to validate the accuracy and reliability of the proposed methodology. The comparison focuses on three key aspects: first and foremost, verifying that the critical elements and their order of identification are consistent between the MATLAB analysis and the FEM analysis. Additionally, the axial forces in the most critical members and the global lateral displacements of the structure are evaluated. The MATLAB analysis is fully detailed in Figure 58, while Figures 59 through 65 present the FEM results, specifically the identification and order of the critical elements along with their corresponding axial forces. Finally, a comparison is made between the axial force values and the top lateral displacement, as shown in the graphs in Figures 66(a) and 66(b).

6. CRITICAL LOAD ANALYSIS AND PROGRESSIVE COLLAPSE OF DIAGRID SYSTEMS

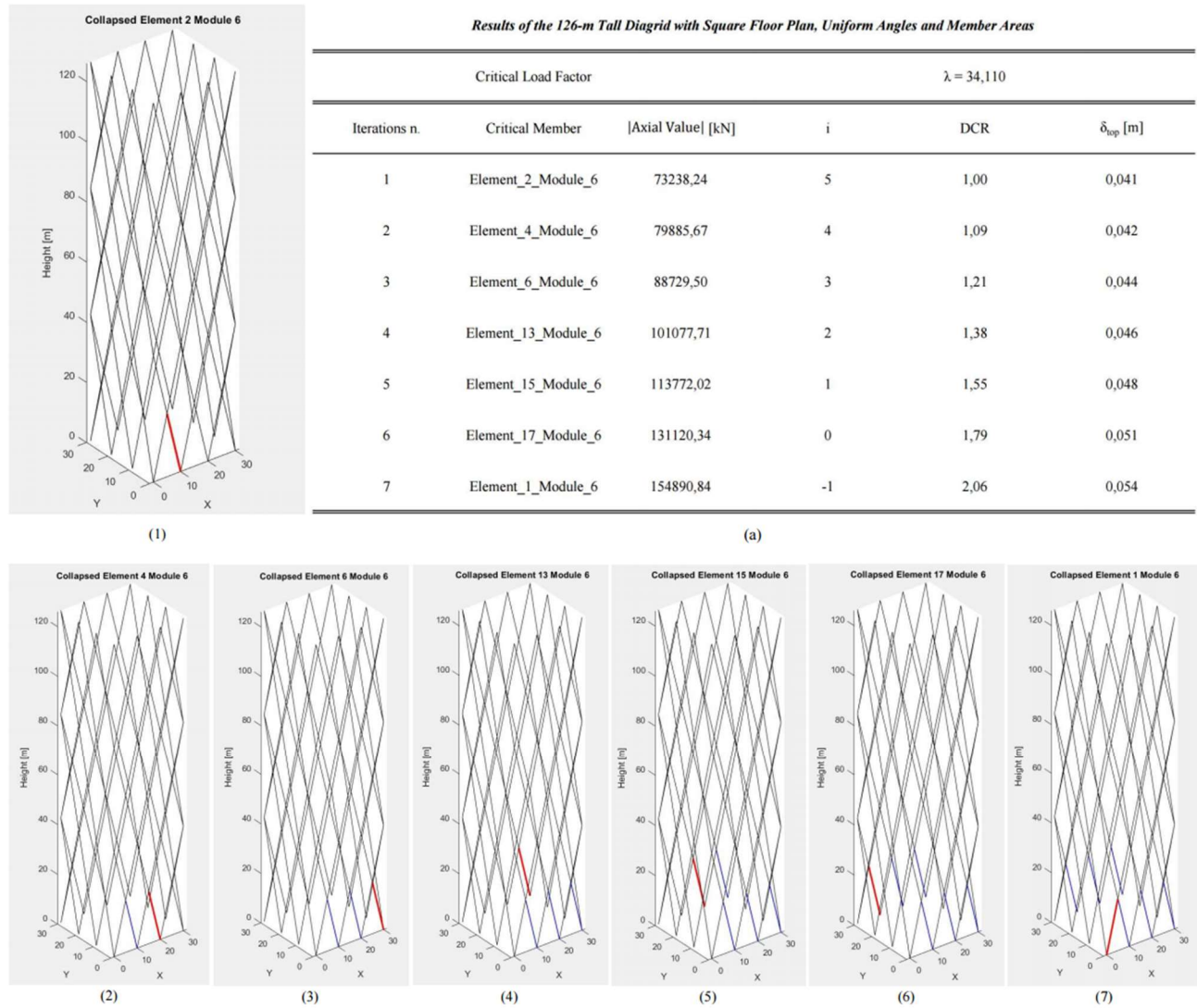


Figure 58: Buckling and progressive collapse analysis of the 126-m tall diagrid system with a square floor shape and uniform angles; (1) initial critical member identification; (a) table summarizing the critical load factor (λ), critical member removed, axial force, degree of hyperstaticity (i), DCR, and top displacement (δ_{top}) for each iteration; (2–7) structural configurations during each progressive collapse iteration, highlighting the removal of the critical member (red) and previously removed members (blue).

6.4. Validation of the Methodology

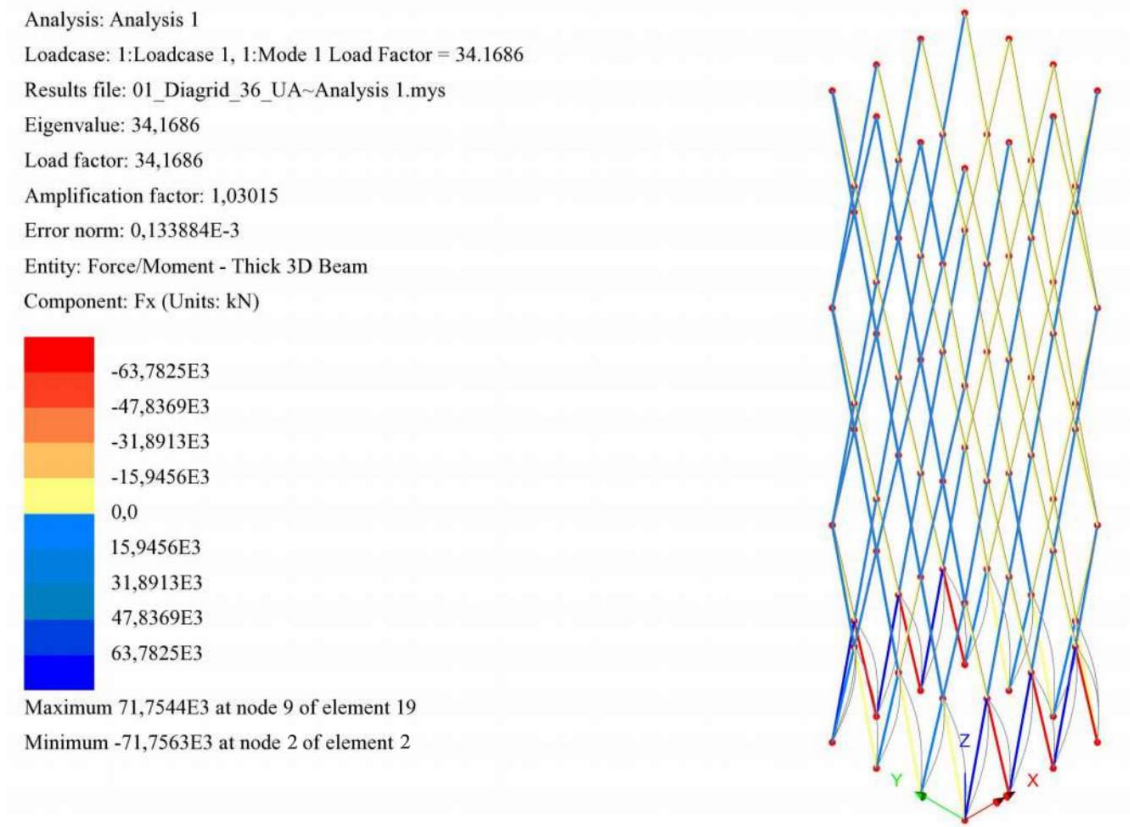


Figure 59: FEM linear buckling analysis of the 126-m tall diagrid system, showing the axial force (F_x) distribution and identification of the critical load factor and first critical member

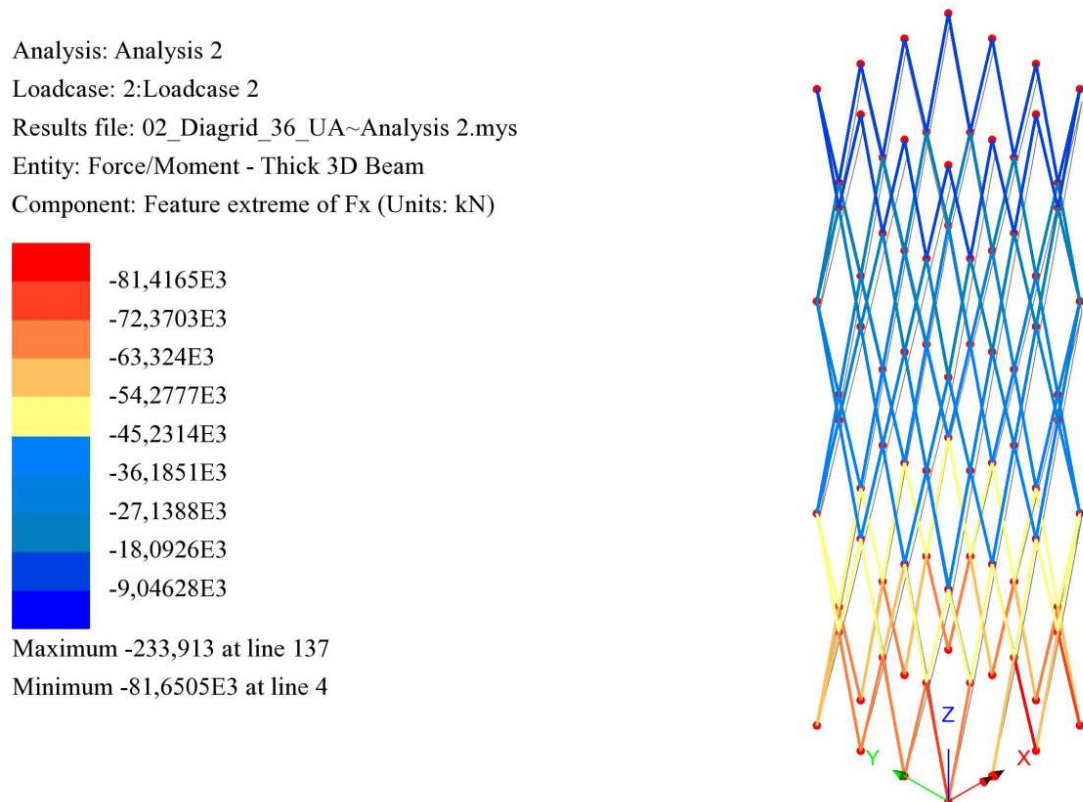


Figure 60: First static analysis after the removal of the first critical member, highlighting the axial force redistribution and identification of subsequent critical member

6. CRITICAL LOAD ANALYSIS AND PROGRESSIVE COLLAPSE OF DIAGRID SYSTEMS

Analysis: Analysis 3
 Loadcase: 4:Loadcase 3
 Results file: 02_Diagrid_36_UA~Analysis 3.mys
 Entity: Force/Moment - Thick 3D Beam
 Component: Feature extreme of Fx (Units: kN)

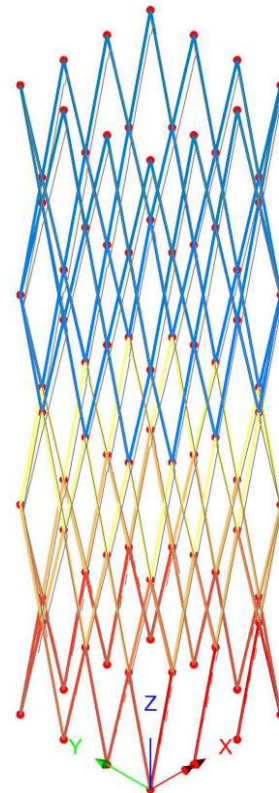
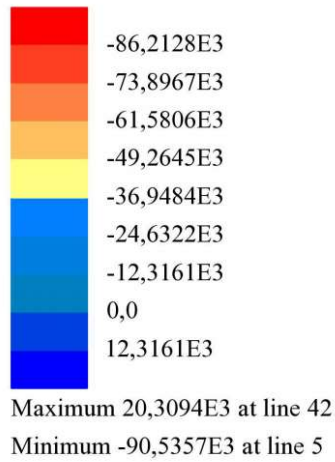


Figure 61: Second static analysis after the removal of the second critical member, highlighting the axial force redistribution and identification of subsequent critical member

Analysis: Analysis 4
 Loadcase: 5:Loadcase 4
 Results file: 02_Diagrid_36_UA~Analysis 4.mys
 Entity: Force/Moment - Thick 3D Beam
 Component: Feature extreme of Fx (Units: kN)

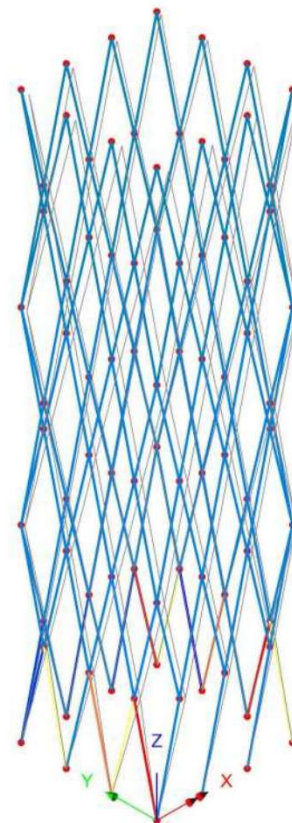
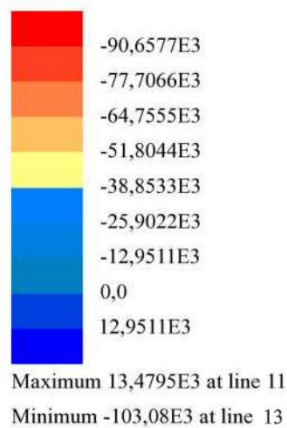


Figure 62: Third static analysis after the removal of the third critical member, highlighting the axial force redistribution and identification of subsequent critical member

6.4. Validation of the Methodology

Analysis: Analysis 5
 Loadcase: 6:Loadcase 5
 Results file: 02_Diagrid_36_UA~Analysis 5.mys
 Entity: Force/Moment - Thick 3D Beam
 Component: Feature extreme of Fx (Units: kN)

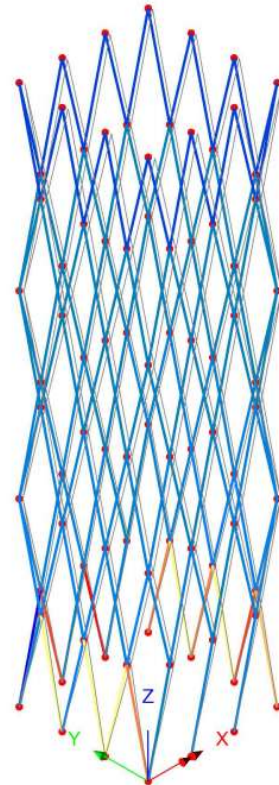
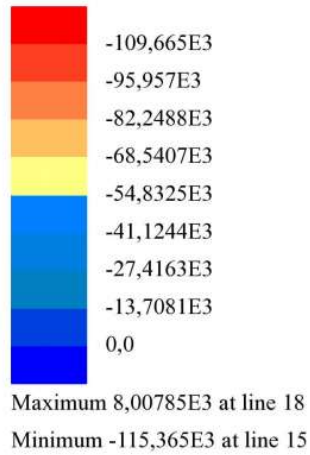


Figure 63: Fourth static analysis after the removal of the fourth critical member, highlighting the axial force redistribution and identification of subsequent critical member

Analysis: Analysis 6
 Loadcase: 7:Loadcase 6
 Results file: 02_Diagrid_36_UA~Analysis 6.mys
 Entity: Force/Moment - Thick 3D Beam
 Component: Feature extreme of Fx (Units: kN)

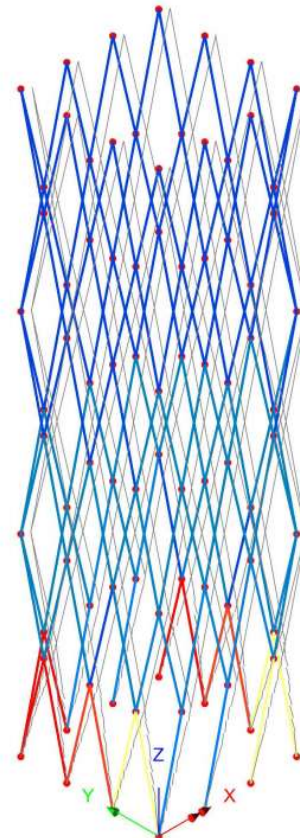
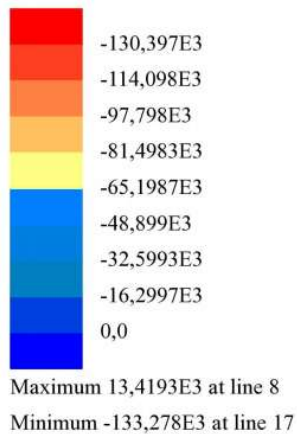


Figure 64: Fifth static analysis after the removal of the fifth critical member, highlighting the axial force redistribution and identification of subsequent critical member

6. CRITICAL LOAD ANALYSIS AND PROGRESSIVE COLLAPSE OF DIAGRID SYSTEMS

Analysis: Analysis 7
 Loadcase: 2:Loadcase 2
 Results file: 01_Diagrid_36_UA~Analysis 7.mys
 Entity: Force/Moment - Thick 3D Beam
 Component: Feature extreme of Fx (Units: kN)

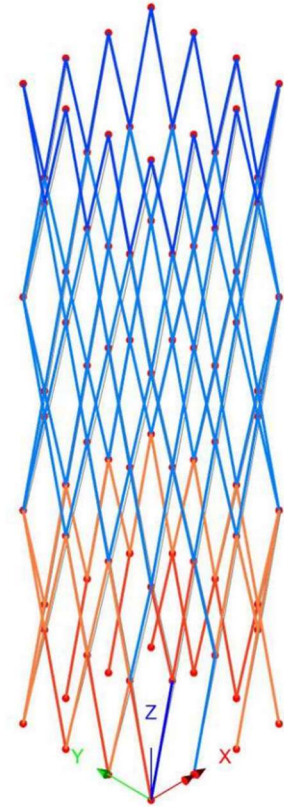
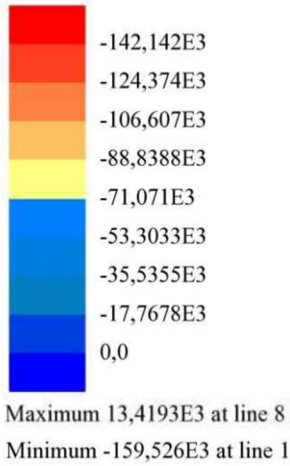


Figure 65: Sixth static analysis after the removal of the sixth critical member, highlighting the axial force redistribution and identification of subsequent critical member

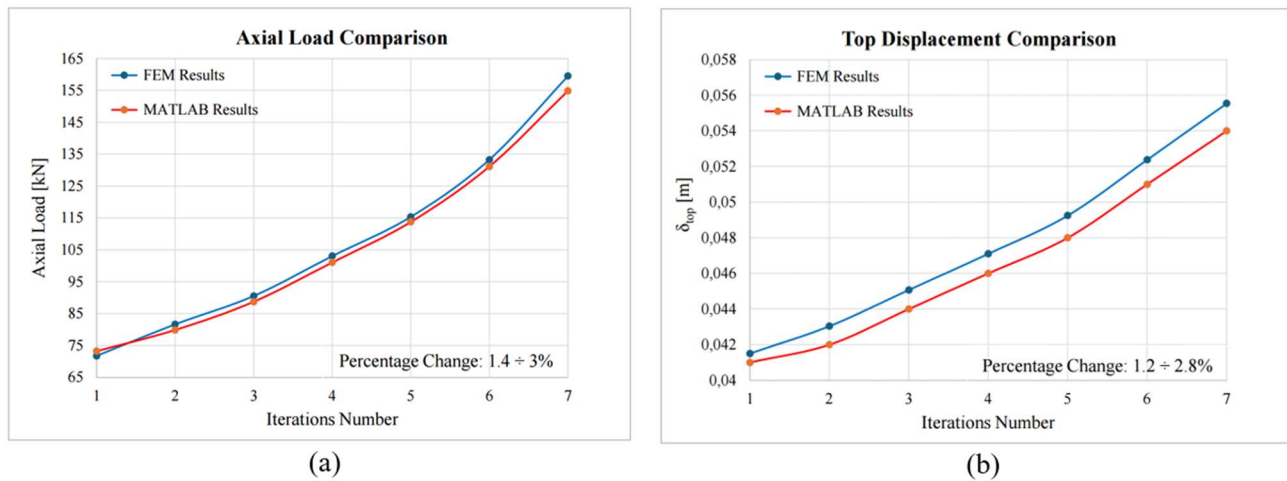


Figure 66: Comparison of results between FEM and MATLAB analyses for the 126-m tall diagrid system; (a) Axial load values across iterations; (b) Top lateral displacement (δ_{top}) across iterations

The FEM analysis validates that the most critical members identified in the MATLAB analysis were in fact those obtained via the FEM analysis. It has been shown that the critical load factor produced through the linear buckling analysis matches the critical load factor of the MATLAB analysis with a percentage change of 0.17%. Additionally, the results of the comparison show a strong level of congruence between the MATLAB and FEM analyses because the percentage change between the axial forces of the most critical members as well

as the top lateral displacements is less than 3%, in both cases. These two percentages needed to be assessed because it was important to ensure that any differences between the two analyses had minimal deviation from one another. In this case, the findings confirmed the functionality of the MATLAB method, and the ability to capture the structural response of the diagrid system. In addition, the close alignment of results also provided further confidence in the assumptions and simplifications employed while conducting the MATLAB analysis and consequently helped ensure the assumptions did not compromise the outcomes. In the next Chapter, the final outcomes of this thesis will be presented and discussed in further detail.

7. RESULTS

7.1. Results Introduction

This chapter presents the results obtained through the methodology described previously, developed within the MATLAB environment. The diagrid systems analyzed in this study are based on the solutions identified by Albitos et al. in [38]. These solutions were selected due to their optimal performance in terms of structural efficiency, torsional stiffness, and construction feasibility, as outlined in the multi-response framework discussed earlier. By focusing on these configurations, the analysis ensures consistency with the established methodological framework.

A total of sixty diagrid systems, including both uniform-angle and varying-angle configurations, were analyzed in detail. However, only eight of these systems, four uniform-angle and four varying-angle, were fully represented in terms of plotted results. These eight systems, one for each building height (126 m, 168 m, 210 m, and 252 m), were chosen from Tables 1 – 4 as the ones yielding the best results in the study. For these configurations, the results are comprehensively presented, including both the identification of the critical load factor and the progressive collapse analysis, as explained in detail in the previous chapter.

For the remaining configurations, while they were analyzed in detail, only a comparison of the Demand-to-Capacity Ratio (DCR), the most critical parameter defining instability during the progressive collapse analysis, is plotted. This comparison is presented separately for all uniform-angle diagrids from Tables 1 – 4 and for all varying-angle diagrids from the same tables.

Regarding displacements, it is important to note that they never emerged as a driving parameter for identifying instability conditions. Differently from the DCR, displacement values were always verified and remained within acceptable limits throughout the analysis. Consequently, there is no interest in plotting displacement results, as they do not provide additional insights into the structural behavior or stability of the diagrid systems.

7.2. Results for Uniform-Angle Diagrid Systems

The following section presents the detailed plots for the four uniform-angle diagrid systems selected from Tables 1 – 4. These configurations represent the optimal solutions for each building height, as identified in the study. The selected solutions are the following:

- 126-m tall diagrid: Solution 4908 (O3)
- 168-m tall diagrid: Solution 23936 (C2)
- 210-m tall diagrid: Solution 41107 (O2)
- 252-m tall diagrid: Solution 46370 (H2)

For each solution, the results are organized into two main figures in order to provide a comprehensive understanding of the structural behavior of the selected uniform-angle diagrid systems, identifying the critical load factor and highlighting their performance under progressive collapse conditions and the critical parameters influencing their stability:

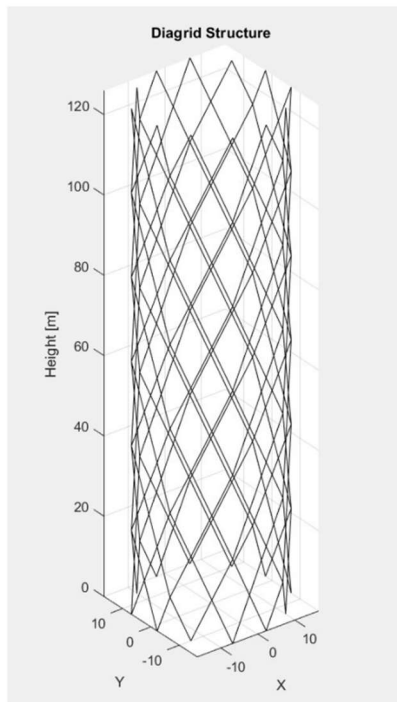
1. Structural Overview and Member Properties:

The first figure provides an overview of the diagrid structure configuration (subfigure a) and a table (subfigure b), summarizing key geometric and structural properties, such as the slenderness ratio, the number of intra-module floors, and, for each module, the member inclination and cross-sectional area.

2. Critical Load Factor and Progressive Collapse Analysis:

The second figure focuses on the progressive collapse analysis. Subfigure (1) highlights the first critical member identified during the analysis, while subfigure (a) presents a table summarizing the critical load factor (λ) and the results of each iteration. The table includes the iteration number, the critical member removed, the corresponding axial force, the decrement in the degree of hyperstaticity, the DCR value, and the top displacement. Below the table, subfigures (2 – n. of iterations) illustrate the diagrid configurations with the progressive removal of the most critical members, providing a visual representation of the structural changes during each iteration.

7. RESULTS



(a)

Solution 4908 (03) – 126-m Tall Diagrid with Octagonal Floor Shape

Slenderness Ratio		4,2
Number of Intra-Module		12
Module n.	Member Inclination	Member Area [m ²]
1	66°	0,2739
2	66°	0,2739
3	66°	0,2739
4	66°	0,2739
5	66°	0,2739
6	66°	0,2739
7	66°	0,2739
8	66°	0,2739
9	66°	0,2739
10	66°	0,2739
11	66°	0,2739
12	66°	0,2739

(b)

Figure 67: Structural overview and member properties of the 126-m tall diagrid system (Solution 4908 (03)) with octagonal floor shape; (a) Diagrid structure configuration; (b) Table of the properties, including slenderness ratio, number of intra-module, member inclination, and cross-sectional area for each module

7.2. Results for Uniform-Angle Diagrid Systems

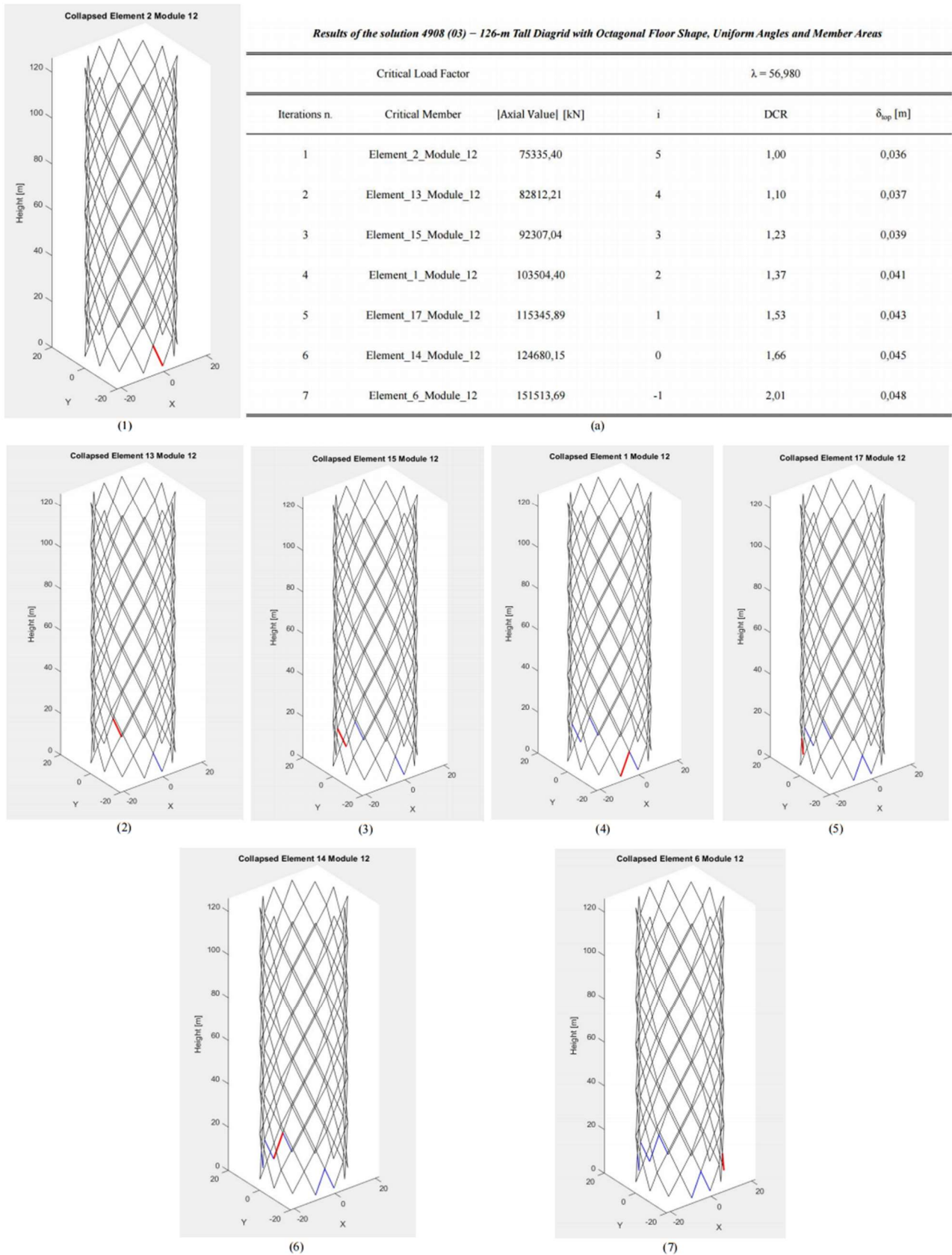
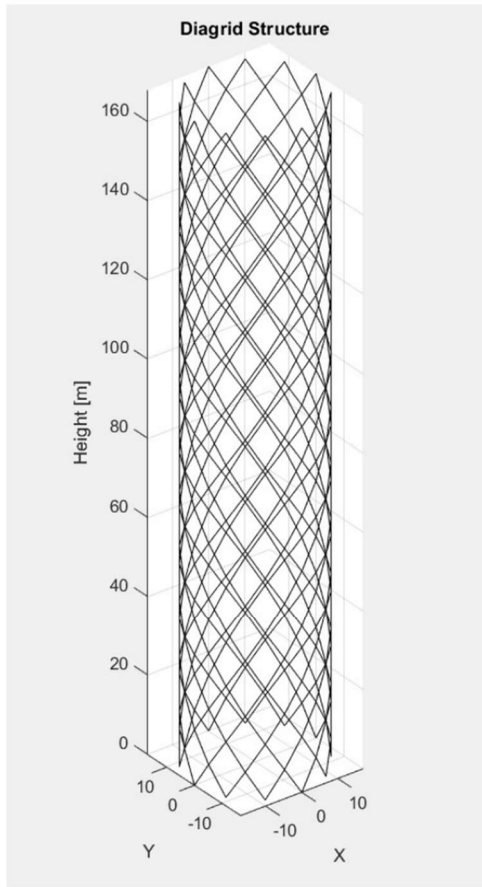


Figure 68: Buckling and progressive collapse analysis of the 126-m tall diagrid system (Solution 4908 (03)) with octagonal floor shape and uniform angles; (1) initial critical member identification; (a) table summarizing the critical load factor (λ), critical member removed, axial force, degree of hyperstaticity (i), DCR, and top displacement (δ_{top}) for each iteration; (2–7) structural configurations during each progressive collapse iteration, highlighting the removal of the critical member (red) and previously removed members (blue).

7. RESULTS



(a)

Solution 23936 (C2) – 168-m Tall Diagrid with Circular Floor Shape		
Slenderness Ratio	5,6	
Number of Intra-Module	24	
Module n.	Member Inclination	Member Area [m ²]
1	56°	0,2739
2	56°	0,2739
3	56°	0,2739
4	56°	0,2739
5	56°	0,2739
6	56°	0,2739
7	56°	0,2739
8	56°	0,2739
9	56°	0,2739
10	56°	0,2739
11	56°	0,2739
12	56°	0,2739
13	56°	0,2739
14	56°	0,2739
15	56°	0,2739
16	56°	0,2739
17	56°	0,2739
18	56°	0,2739
19	56°	0,2739
20	56°	0,2739
21	56°	0,2739
22	56°	0,2739
23	56°	0,2739
24	56°	0,2739

(b)

Figure 69: Structural overview and member properties of the 168-m tall diagrid system (Solution 23936 (C3)) with circular floor shape; (a) Diagrid structure configuration; (b) Table of the properties, including slenderness ratio, number of intra-module, member inclination, and cross-sectional area for each module

7.2. Results for Uniform-Angle Diagrid Systems

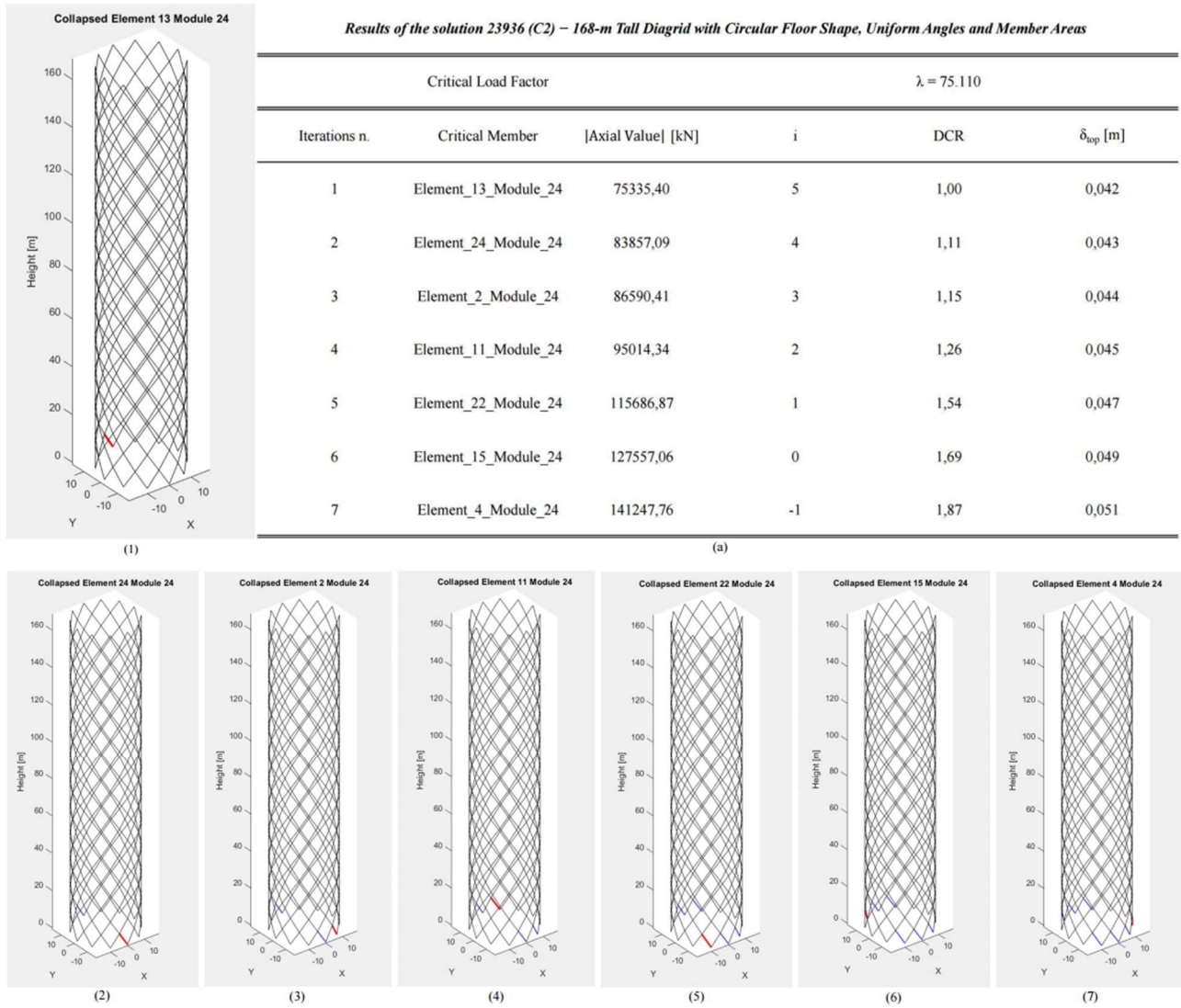


Figure 70: Buckling and progressive collapse analysis of the 168-m tall diagrid system (Solution 23936 (C3)) with circular floor shape and uniform angles; (1) initial critical member identification; (a) table summarizing the critical load factor (λ), critical member removed, axial force, degree of hyperstaticity (i), DCR, and top displacement (δ_{top}) for each iteration; (2–7) structural configurations during each progressive collapse iteration, highlighting the removal of the critical member (red) and previously removed members (blue).

7. RESULTS

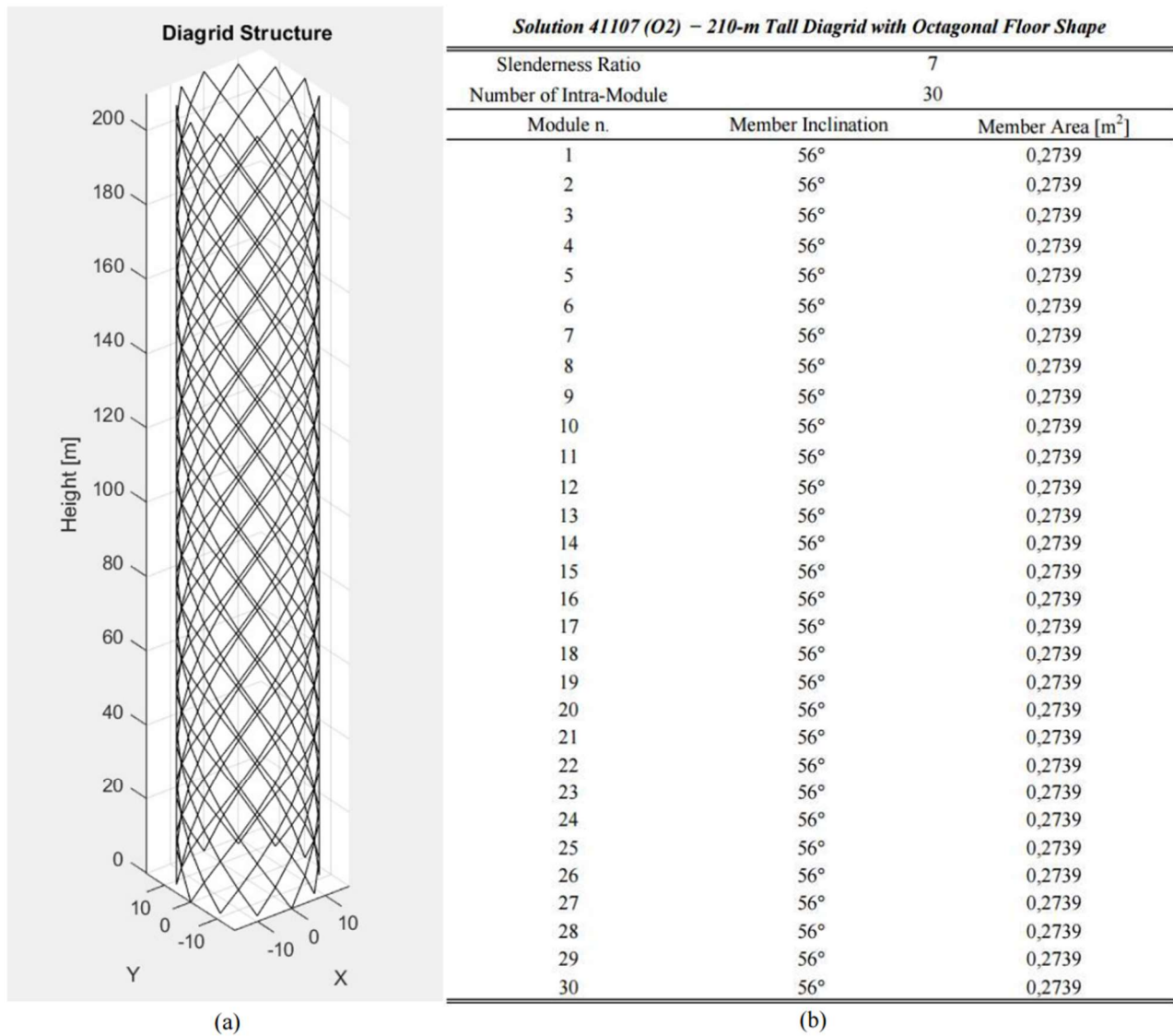


Figure 71: Structural overview and member properties of the 210-m tall diagrid system (Solution 41107 (O2)) with octagonal floor shape; (a) Diagrid structure configuration; (b) Table of the properties, including slenderness ratio, number of intra-module, member inclination, and cross-sectional area for each module

7.2. Results for Uniform-Angle Diagrid Systems

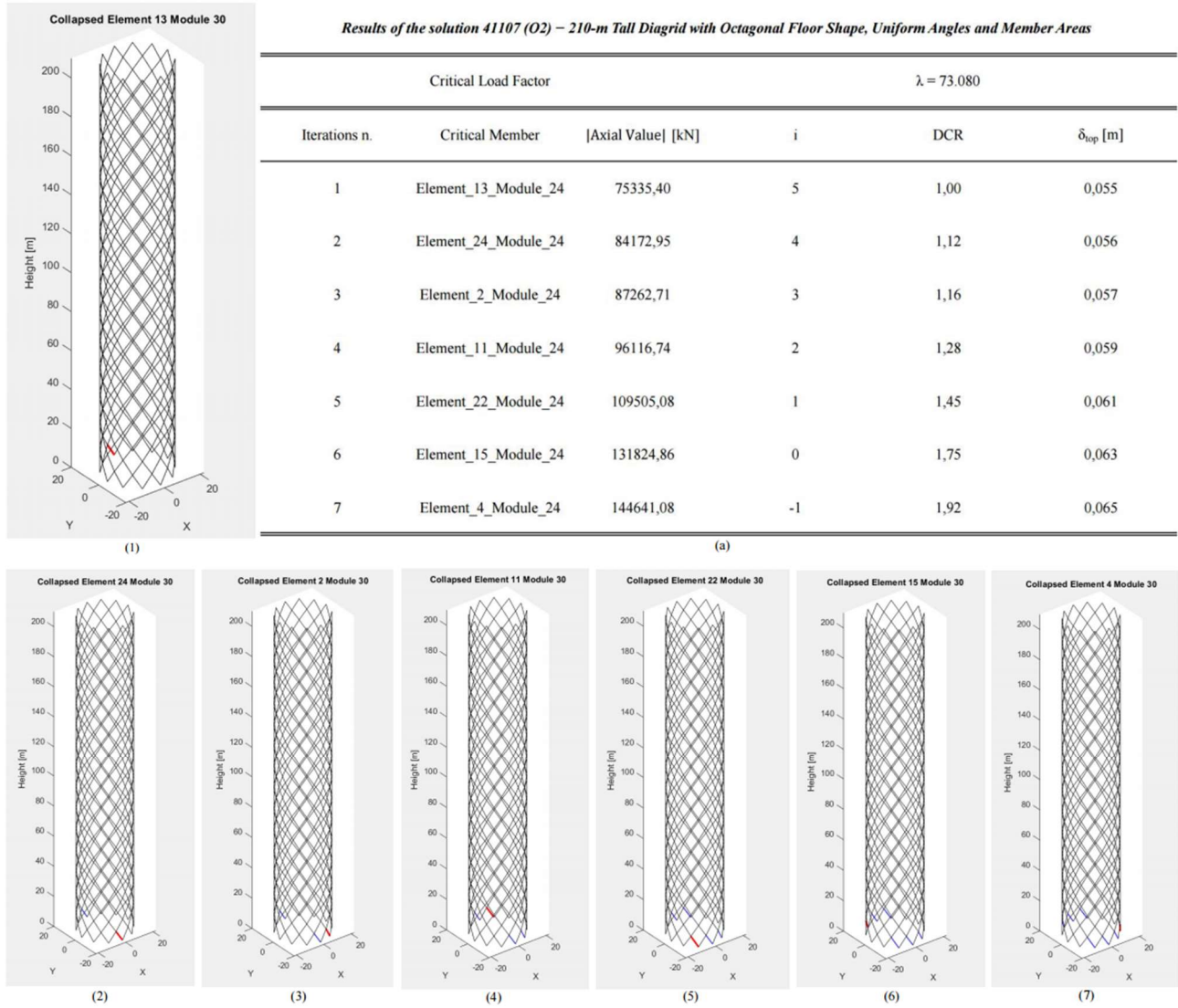
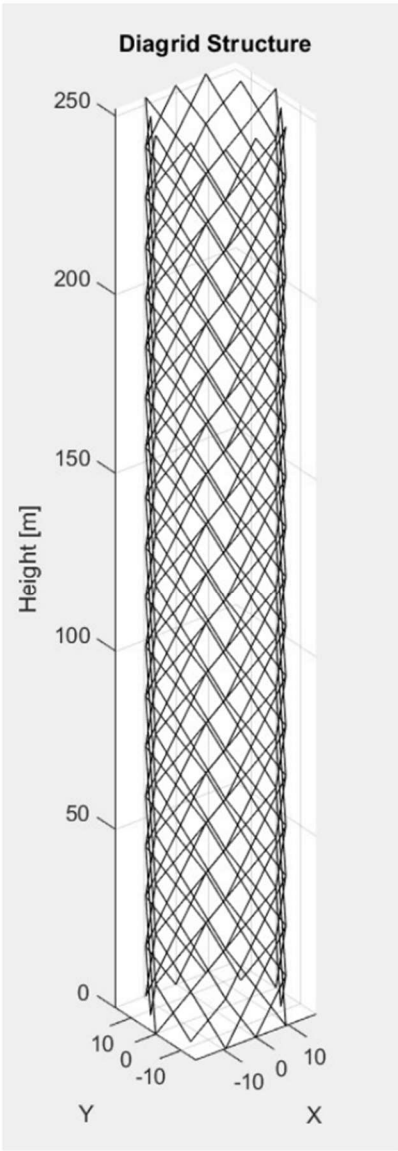


Figure 72: Buckling and progressive collapse analysis of the 210-m tall diagrid system (Solution 41107 (O2)) with octagonal floor shape and uniform angles; (1) initial critical member identification; (a) table summarizing the critical load factor (λ), critical member removed, axial force, degree of hyperstaticity (i), DCR, and top displacement (δ_{top}) for each iteration; (2–7) structural configurations during each progressive collapse iteration, highlighting the removal of the critical member (red) and previously removed members (blue).

7. RESULTS



(a)

Solution 46370 (H2) – 252-m Tall Diagrid with Hexagonal Floor Shape		
Slenderness Ratio	8,4	
Number of Intra-Module	36	
Module n.	Member Inclination	Member Area [m ²]
1	56°	0,2739
2	56°	0,2739
3	56°	0,2739
4	56°	0,2739
5	56°	0,2739
6	56°	0,2739
7	56°	0,2739
8	56°	0,2739
9	56°	0,2739
10	56°	0,2739
11	56°	0,2739
12	56°	0,2739
13	56°	0,2739
14	56°	0,2739
15	56°	0,2739
16	56°	0,2739
17	56°	0,2739
18	56°	0,2739
19	56°	0,2739
20	56°	0,2739
21	56°	0,2739
22	56°	0,2739
23	56°	0,2739
24	56°	0,2739
25	56°	0,2739
26	56°	0,2739
27	56°	0,2739
28	56°	0,2739
29	56°	0,2739
30	56°	0,2739
31	56°	0,2739
32	56°	0,2739
34	56°	0,2739
35	56°	0,2739
36	56°	0,2739

(b)

Figure 73: Structural overview and member properties of the 252-m tall diagrid system (Solution 46370 (H2)) with octagonal floor shape; (a) Diagrid structure configuration; (b) Table of the properties, including slenderness ratio, number of intra-module, member inclination, and cross-sectional area for each module

7.2. Results for Uniform-Angle Diagrid Systems

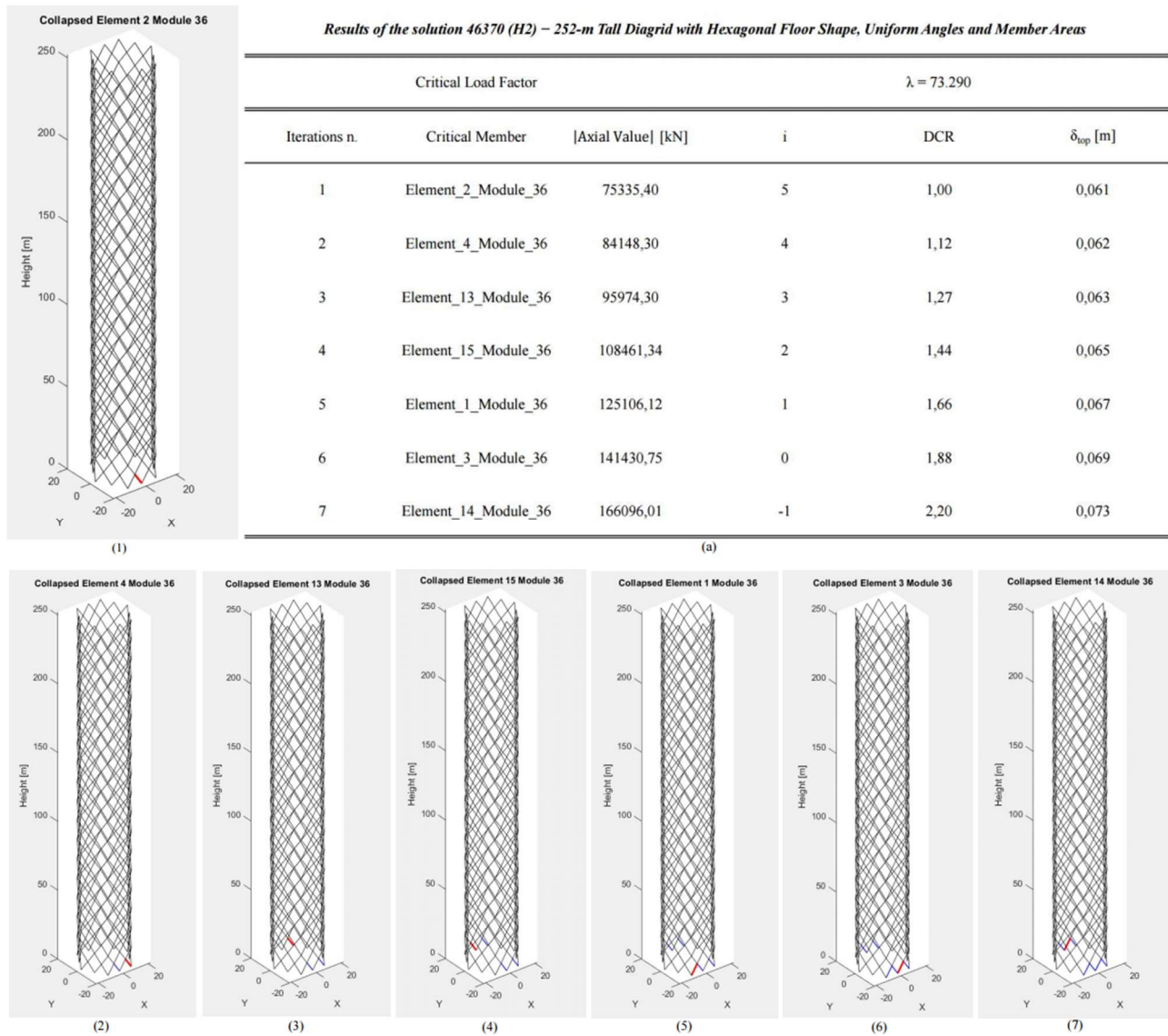


Figure 74: Buckling and progressive collapse analysis of the 252-m tall diagrid system (Solution 46370 (H2)) with octagonal floor shape and uniform angles; (1) initial critical member identification; (a) table summarizing the critical load factor (λ), critical member removed, axial force, degree of hyperstaticity (i), DCR, and top displacement (δ_{top}) for each iteration; (2–7) structural configurations during each progressive collapse iteration, highlighting the removal of the critical member (red) and previously removed members (blue).

From the results, it is interesting to observe that the driving parameter defining the instability of the system is the Demand-to-Capacity Ratio (DCR). For uniform-angle diagrids, the DCR limit value is assumed to be equal to 2. Instability occurs when this limit is exceeded, or, alternatively, when the lability condition of the system is reached.

Furthermore, additional insights into the behavior of the DCR in uniform diagrid members will be presented in Figure 83, where a comparison of all other uniform configurations resulting from Tables 1 – 4 is provided.

7. RESULTS

7.3. Results for Varying-Angle Diagrid Systems

The following section presents the detailed plots for the four varying-angle diagrid systems selected from Tables 1 – 4. These configurations represent the optimal solutions for each building height, as identified in the study. The selected solutions are as follows:

- 126-m tall diagrid: Solution 7554
- 168-m tall diagrid: Solution 654
- 210-m tall diagrid: Solution 41098
- 252-m tall diagrid: Solution 46361

For each solution, the results are organized in the same way of the uniform-angle diagrid systems.

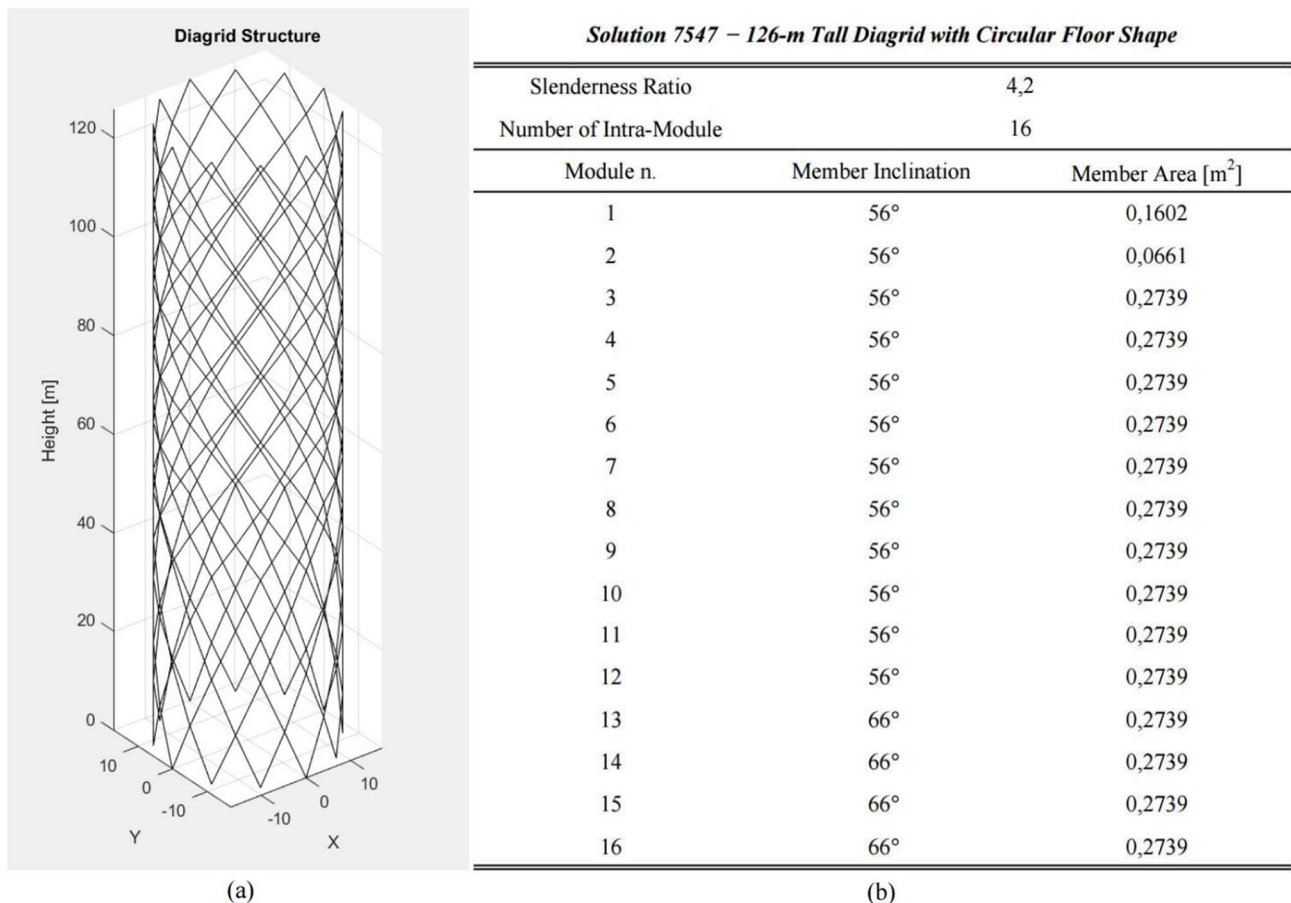


Figure 75: Structural overview and member properties of the 126-m tall diagrid system (Solution 7547) with circular floor shape; (a) Diagrid structure configuration; (b) Table of the properties, including slenderness ratio, number of intra-module, member inclination, and cross-sectional area for each module

7.3. Results for Varying-Angle Diagrid Systems

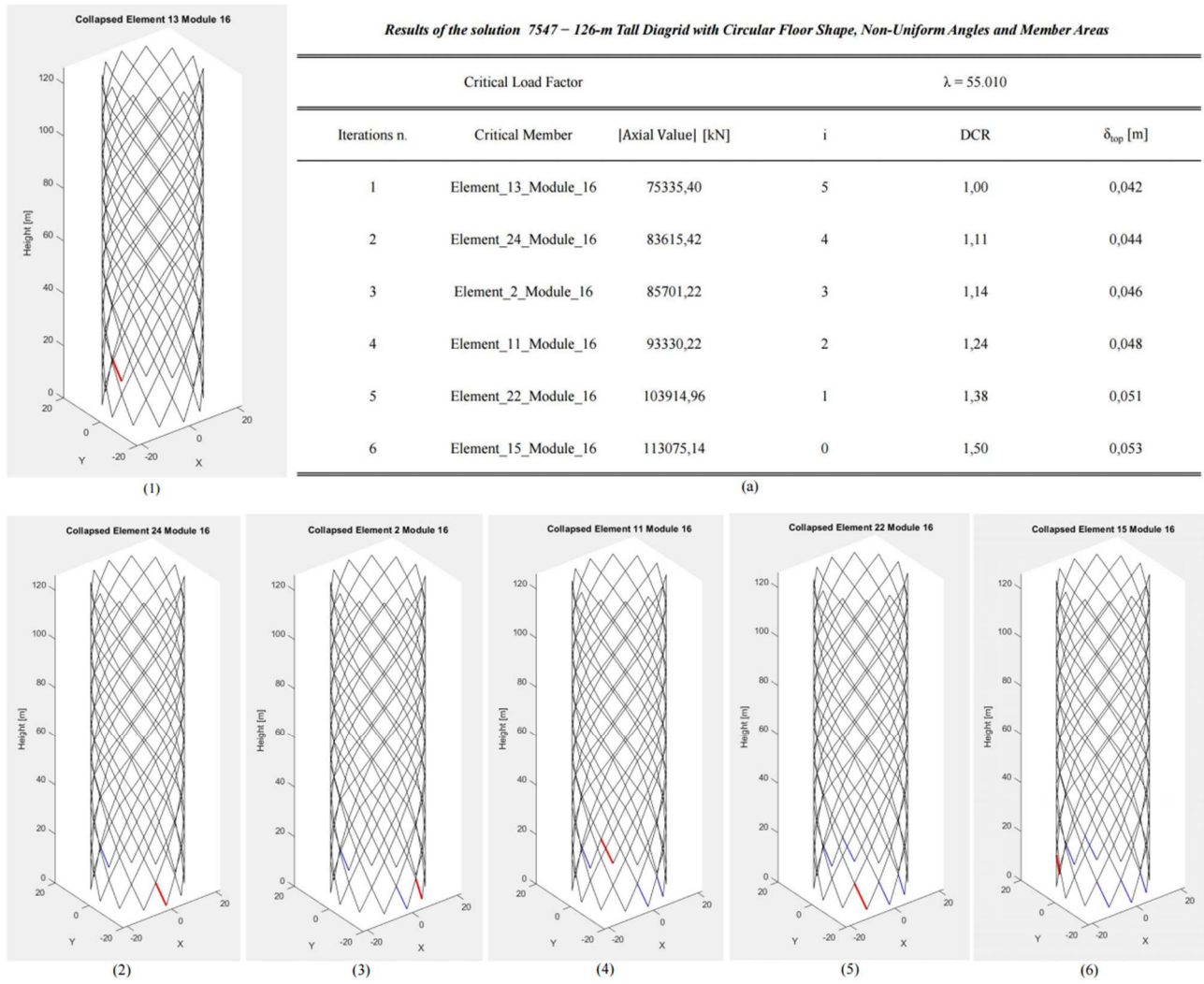
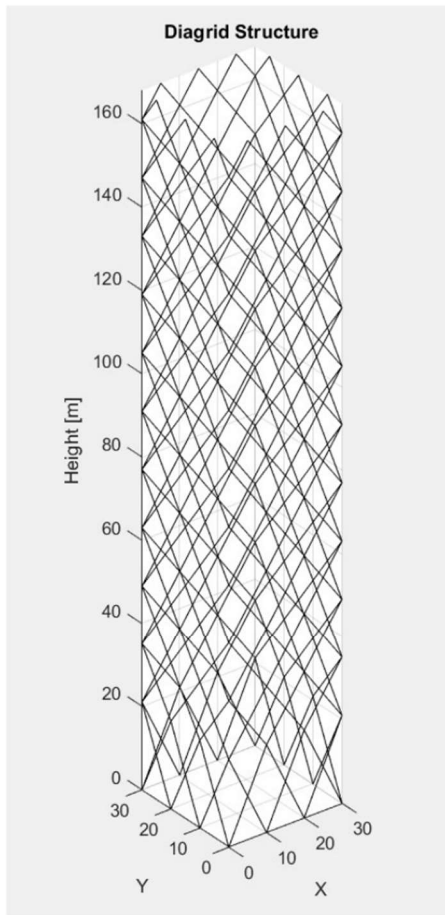


Figure 76: Buckling and progressive collapse analysis of the 126-m tall diagrid system (Solution 7547) with circular floor shape and uniform angles; (1) initial critical member identification; (a) table summarizing the critical load factor (λ), critical member removed, axial force, degree of hyperstaticity (i), DCR, and top displacement (δ_{top}) for each iteration; (2–7) structural configurations during each progressive collapse iteration, highlighting the removal of the critical member (red) and previously removed members (blue).

7. RESULTS



<i>Solution 654 – 168-m Tall Diagrid with Square Floor Shape</i>		
Slenderness Ratio	5,6	
Number of Intra-Module	23	
Module n.	Member Inclination	Member Area [m ²]
1	56°	0,0703
2	56°	0,1602
3	56°	0,2739
4	56°	0,2739
5	56°	0,2739
6	56°	0,2739
7	56°	0,2739
8	56°	0,2739
9	56°	0,2739
10	56°	0,2739
11	56°	0,2739
12	56°	0,2739
13	56°	0,2739
14	56°	0,2739
15	56°	0,2739
16	56°	0,2739
17	56°	0,2739
18	56°	0,2739
19	56°	0,2739
20	56°	0,2739
21	56°	0,2739
22	66°	0,2739
23	66°	0,2739

(b)

Figure 77: Structural overview and member properties of the 168-m tall diagrid system (Solution 654) with square floor shape; (a) Diagrid structure configuration; (b) Table of the properties, including slenderness ratio, number of intra-module, member inclination, and cross-sectional area for each module

7.3. Results for Varying-Angle Diagrid Systems

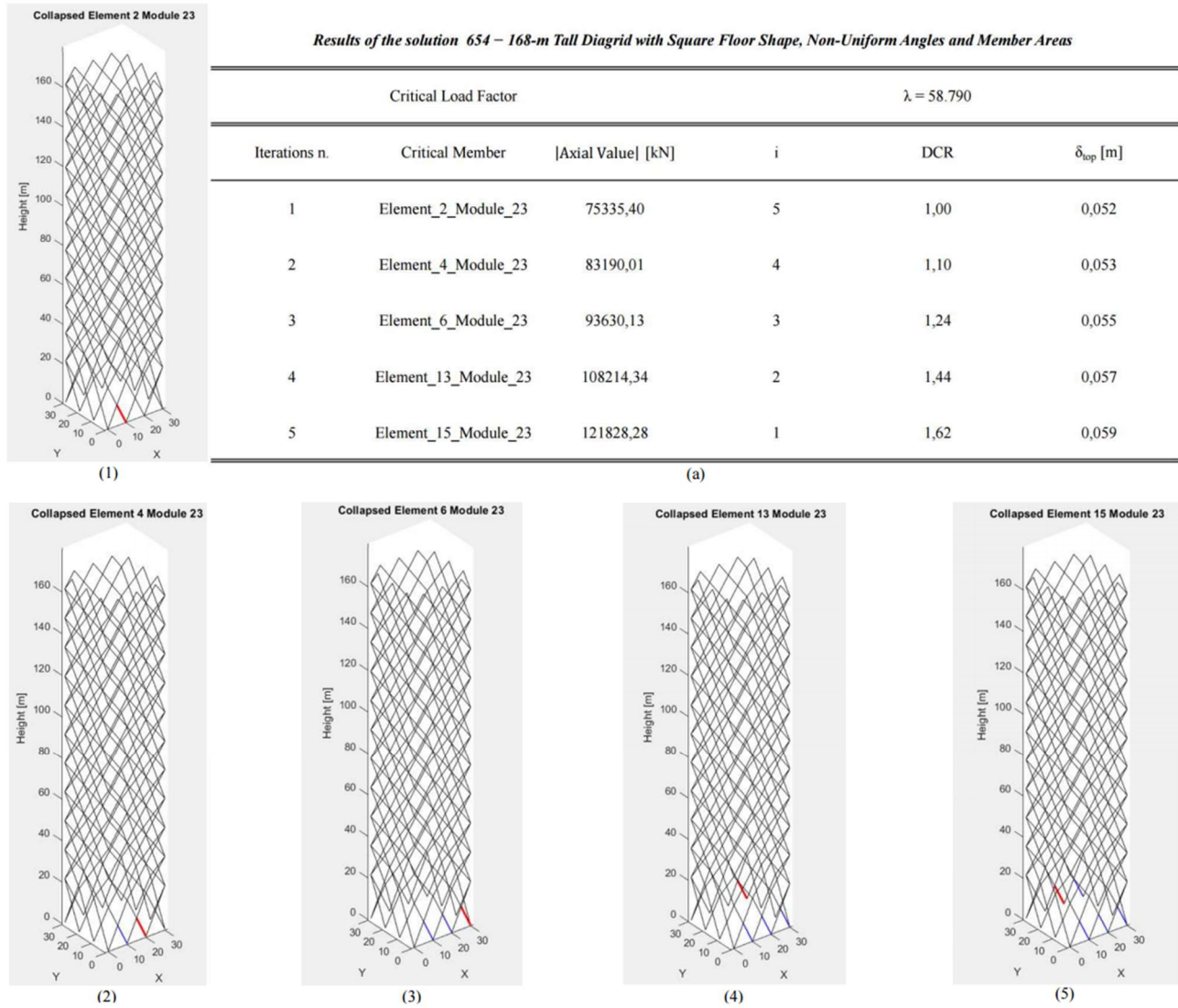


Figure 78: Buckling and progressive collapse analysis of the 168-m tall diagrid system (Solution 654) with circular floor shape and uniform angles; (1) initial critical member identification; (a) table summarizing the critical load factor (λ), critical member removed, axial force, degree of hyperstaticity (i), DCR, and top displacement (δ_{top}) for each iteration; (2–7) structural configurations during each progressive collapse iteration, highlighting the removal of the critical member (red) and previously removed members (blue).

7. RESULTS

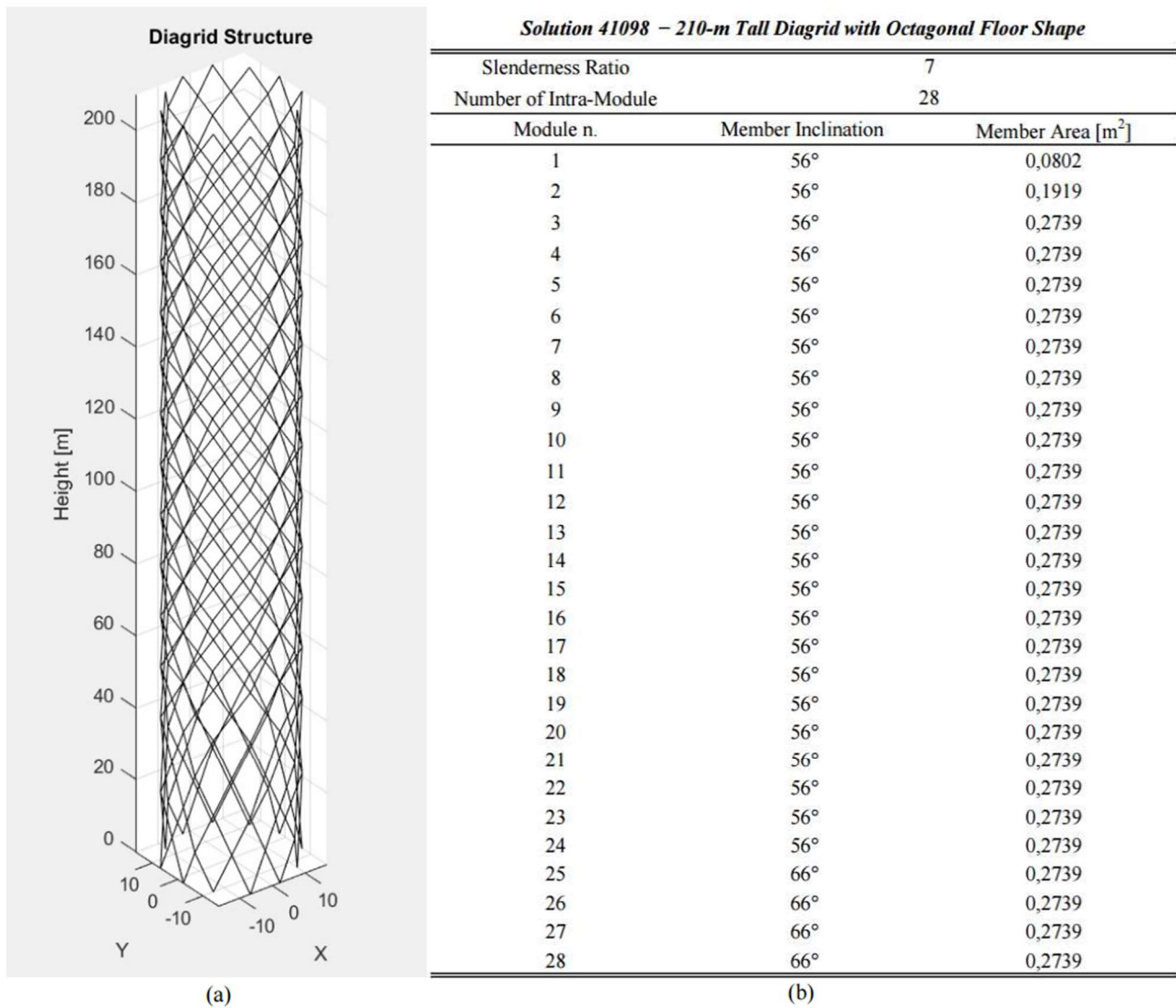


Figure 79: Structural overview and member properties of the 210-m tall diagrid system (Solution 41098) with octagonal floor shape;
 (a) Diagrid structure configuration; (b) Table of the properties, including slenderness ratio, number of intra-module, member inclination, and cross-sectional area for each module

7.3. Results for Varying-Angle Diagrid Systems

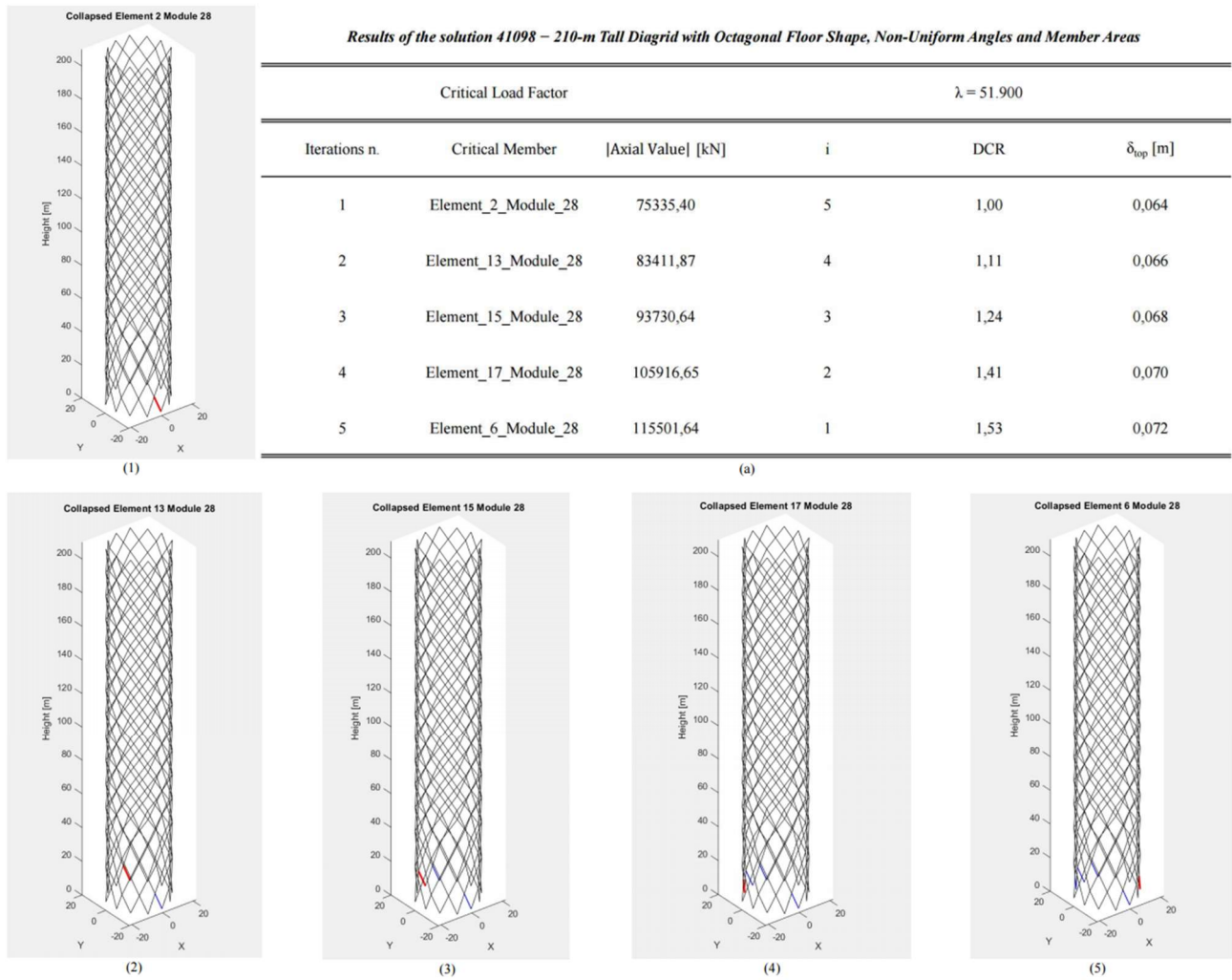


Figure 80: Buckling and progressive collapse analysis of the 210-m tall diagrid system (Solution 41098) with octagonal floor shape and uniform angles; (1) initial critical member identification; (a) table summarizing the critical load factor (λ), critical member removed, axial force, degree of hyperstaticity (i), DCR, and top displacement (δ_{top}) for each iteration; (2–7) structural configurations during each progressive collapse iteration, highlighting the removal of the critical member (red) and previously removed members (blue).

7. RESULTS

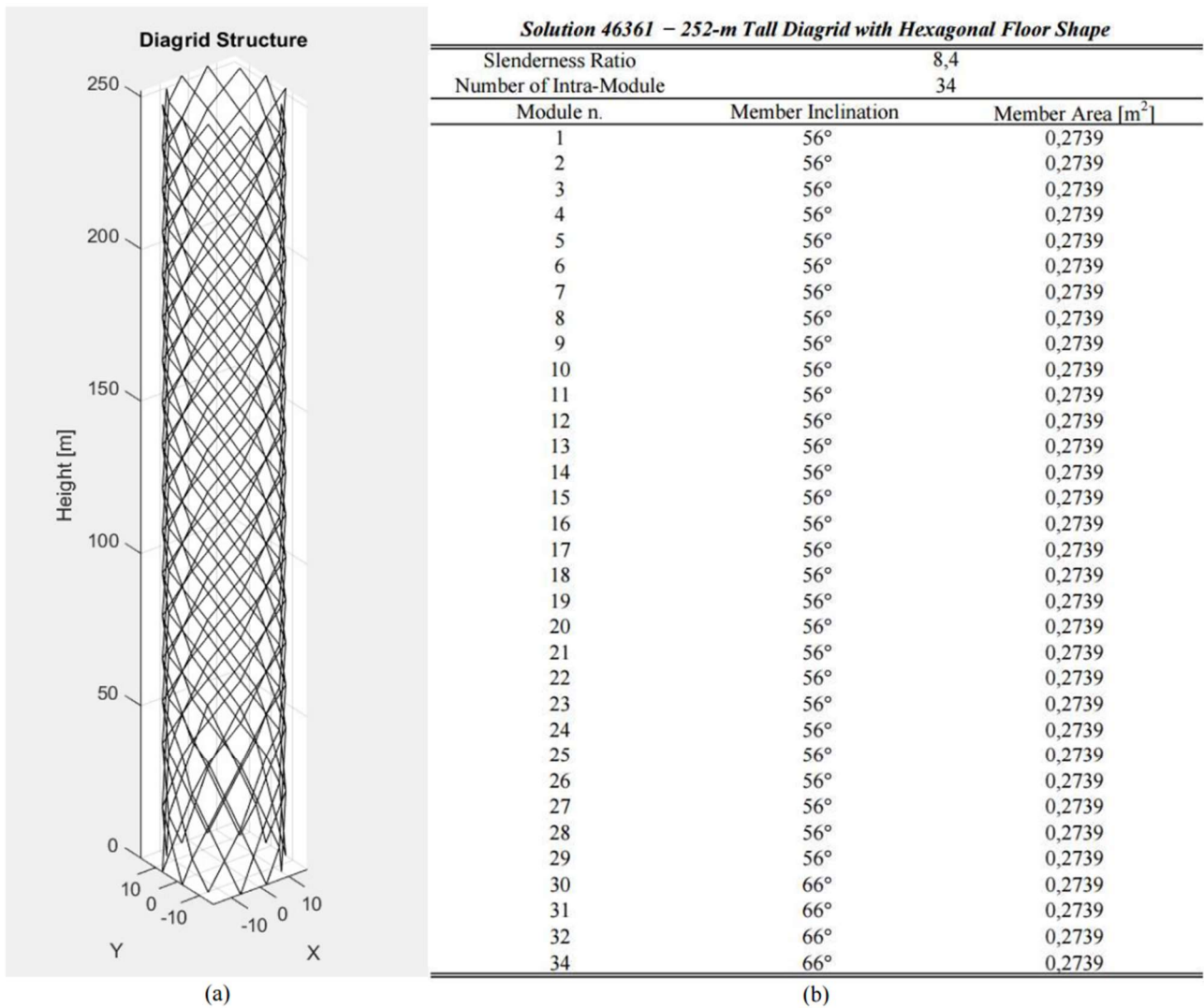


Figure 81: Structural overview and member properties of the 252-m tall diagrid system (Solution 46361) with hexagonal floor shape;
 (a) Diagrid structure configuration; (b) Table of the properties, including slenderness ratio, number of intra-module, member inclination, and cross-sectional area for each module

7.3. Results for Varying-Angle Diagrid Systems

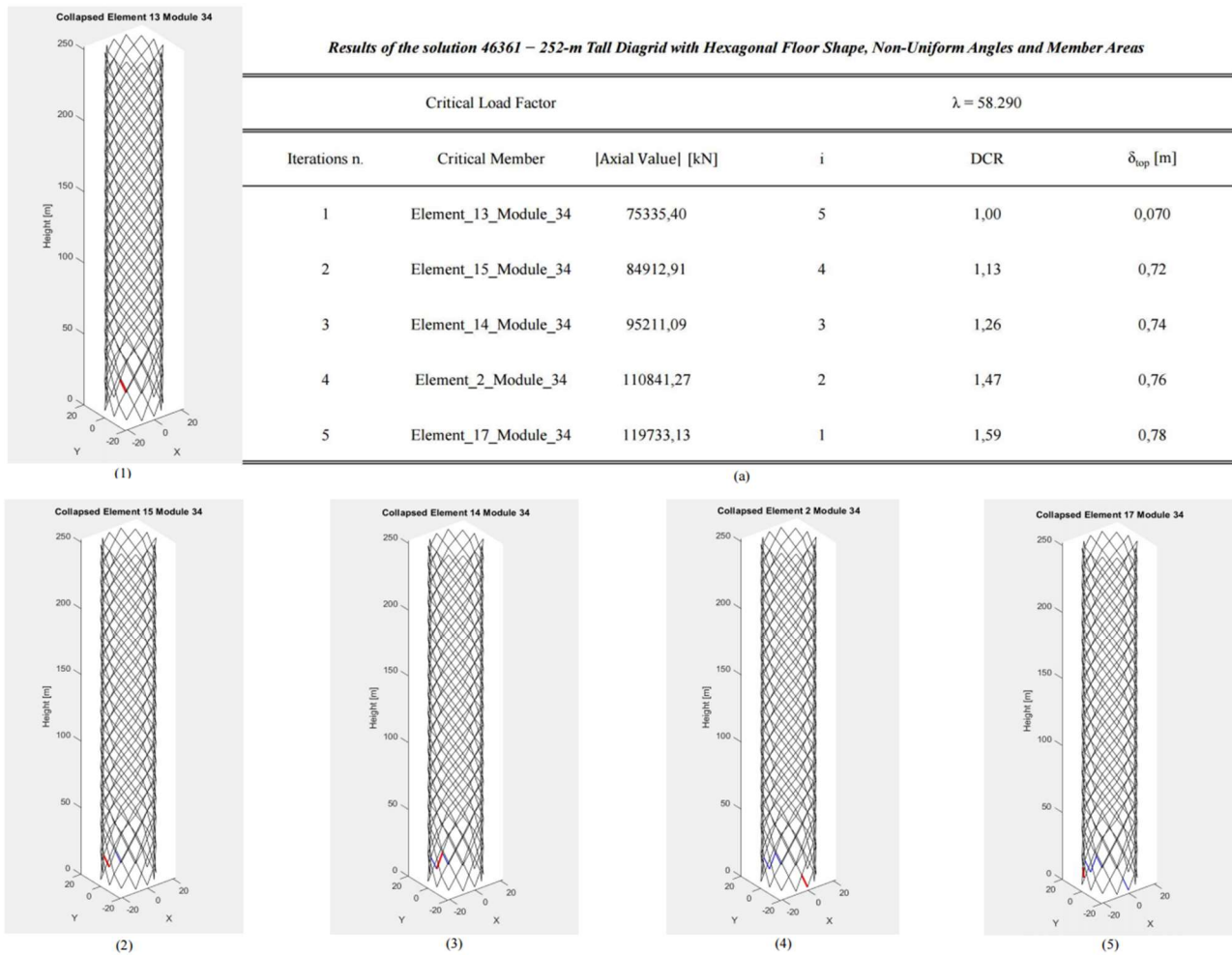


Figure 82: Buckling and progressive collapse analysis of the 252-m tall diagrid system (Solution 46361) with hexagonal floor shape and uniform angles; (1) initial critical member identification; (a) table summarizing the critical load factor (λ), critical member removed, axial force, degree of hyperstaticity (i), DCR, and top displacement (δ_{top}) for each iteration; (2–7) structural configurations during each progressive collapse iteration, highlighting the removal of the critical member (red) and previously removed members (blue).

As seen from the results for the different angle diagrid systems, the driving parameter defining instability of the system is the Demand-to-Capacity Ratio. For the angles defined, the DCR limit is assumed to be equal to 1.5 (atypical structure). Instability will occur if the established limit is exceeded or if the state of lability is true. In comparing the results for uniform-angle and varying-angle diagrid systems, it is interesting to note how there were fewer iterations before stating instability occurred for the different angle cases when the DCR limit of 1.5 is defined for the different angle systems is comparatively low, especially in the case of diagrid heights over 126 m. The primary reason is that the defined DCR limit for the varying-angle cases was defined for atypical structures that resulted in an early arrival of instability. The same difference is shown in comparing all the varying-angle configurations in Figure 84, and also shows how the DCR limit varies the progressive collapse response of diagrid systems.

7. RESULTS

7.4. Progressive Collapse Behavior of Uniform- and Varying-Angle Diagrid Systems: Insights from DCR Analysis

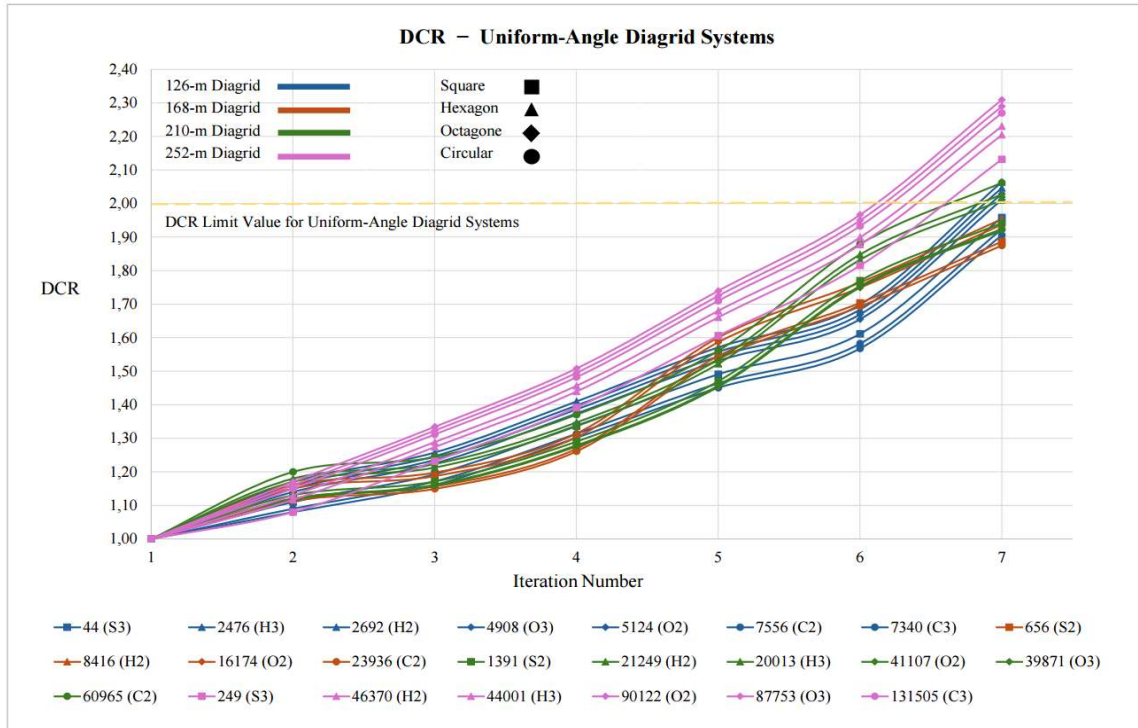


Figure 83: Comparison of the Demand Capacity Ratio for the progressive collapse behavior of uniform-angle diagrid systems for various building heights (126-, 168-, 210-, and 252-m) and floor shapes (square, hexagonal, octagonal, and circular).

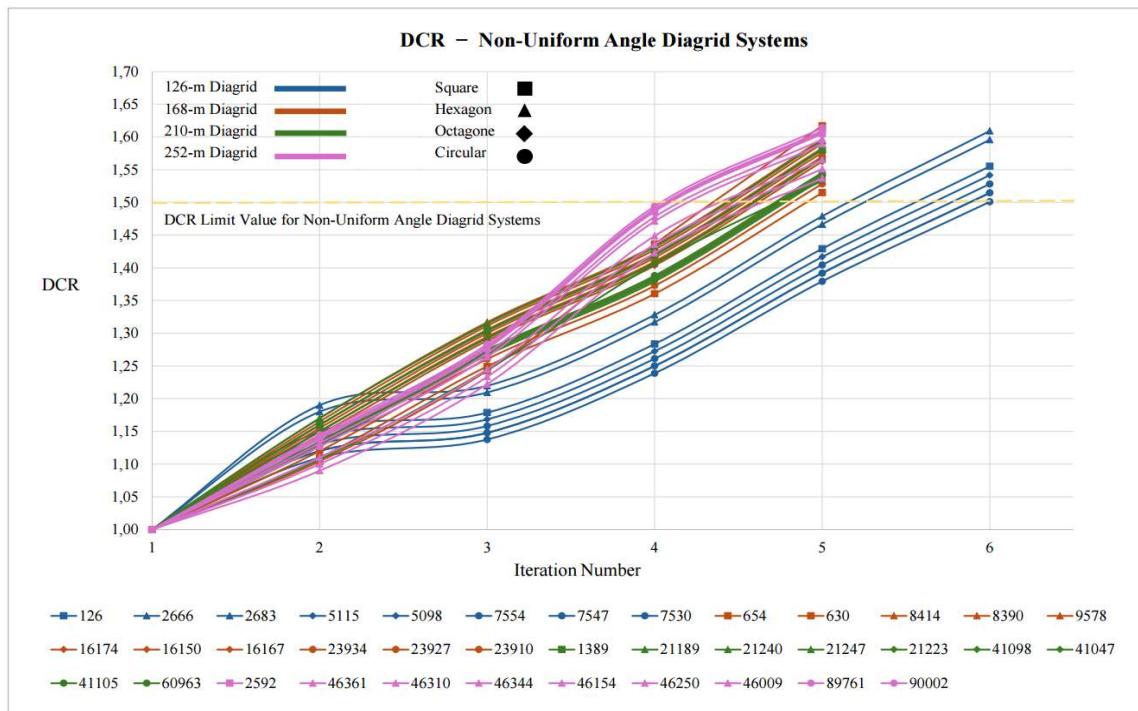


Figure 84: Comparison of the Demand Capacity Ratio for the progressive collapse behavior of varying-angle diagrid systems for various building heights (126-, 168-, 210-, and 252-m) and floor shapes (square, hexagonal, octagonal, and circular).

7.4. Progressive Collapse Behavior of Uniform- and Varying-Angle Diagrid Systems: Insights from DCR Analysis

These two Figures (83 – 84) provide valuable insights into the progressive collapse behavior of uniform and non-uniform angle diagrid systems across different building heights (126 m, 168 m, 210 m, and 252 m) and floor shapes (square, hexagonal, octagonal, and circular). In each is described the evolution of the DCR values across iterations until the limit, 2 for uniform-angle diagrids and 1.5 for non-uniform angle diagrids, is reached or surpassed.

It is important to point out that, consistently with what occurred with all configurations, for the DCR, it starts from 1.0, meaning that the system is stable and below the identified limits, and subsequently continues to grow with each iteration, which reflects the axial stresses were growing in members and, thus the system has a lower level of stability as critical members are taken out of the analysis. In the case of uniform-angle diagrid (Figure 83), with regard to the height of the building, taller diagrid systems (252 m type) had greater DCR values at earlier iterations than shorter diagrids (126 m type), indicating that taller diagrid systems are more prone to being unstable under progressive collapse conditions. Further to this, the increasing rate of DCR is steeper after members are taken out of analysis in taller diagrid systems, indicating that the contribution of higher axial stress is a great contributor to overall stability loss. An additional consideration is with regard to the floor shape, specifically, circular (C) floor shapes had greater DCR values than other shapes (square, hexagon, octagon) with the same building height type. In fact, this may suggest that circular floor shape configurations may be more susceptible to progressive collapse conditions. Further to this, octagonal (O) and hexagonal (H) floor shapes showed more gradually-steep increases in DCR, suggesting more stable configurations with respect to progressive collapse conditions. For varying-angle diagrids (Figure 84), the direction of either building height or floor shape with DCR trend was similar to that of the uniform-angle configurations. In fact, similar to uniform-angle systems, the main difference is the more severe design rule (DCR) of 1.5, which meant DCR-based instability occurred with fewer iterations, particularly pertaining to building layouts that were taller. Also, if the diagrid types with 126 m were considered, the overall number of iterations resulted in fewer iterations for varying-angle systems.

It is important to recognize that the difference in the number of iterations between uniform-angle and varying-angle diagrid systems is strictly related to the assumptions on the limits made for this study. Most importantly, the limit DCR for uniform-angle systems is at 2.0 and for varying-angle systems, there is a stricter DCR of 1.5, as they are considered atypical

7. RESULTS

structural systems. This difference with respect to the DCR limits elements had a significant impact on the overall results, particularly the number of iterations until identified instability. However, if uniform-angle and non-uniform angle diagrid systems were treated as atypical structural systems, they would all experience the same limit of DCR 1.5, and this difference would not be as noticeable. In this case, the number of iterations to identify instability would be similar for either system and, further, the demonstrated advantage of uniform-angle systems with respect to resilient configurations would be far less apparent and incidental. This example demonstrates the fact that the results are sensitive to the assumptions made in defining the classification and DCR limits of the structural systems.

8. CONCLUSIONS

In conclusion, this thesis has presented a numerical model based on the Matrix-Based Method (MBM), examining the structural response of diagrid systems with a focus on critical load factor for buckling and progressive collapse analysis. The intention was to build and expand upon the MBM and provide a more thorough understanding of the behavior of diagrid structures subjected to extreme loading situations.

The identification of ideal diagrid systems created using a multi-response framework approach using MBM methodology reinforced the adopted methodology for this research. Thus, an added level of consistency was also applied in examining the diagrid structural response. Overall, the extension of the MBM methodology illustrates its feasibility and competency in accurately representing critical load factors and progressive collapse behavior. Assessment of uniform-angle and varying-angle diagrid systems by pursuing optimal configurable diagrids also solidified many pre-existing notions and discoveries regarding any geometric configuration of diagrid systems, but also building heights, and floor shapes. More precisely, in the case study assessments of both the uniform and non-uniform-angle diagrid systems, more importance must be given to the design considerations because the greater height and circular floor shape of the diagrid system appear to increase the potential for instability. Moreover, the progressive collapse analysis revealed that the Demand-to-Capacity Ratio (DCR) is the driving parameter defining the instability of diagrid systems, and its definition has to be carefully considered due to the analysis sensitivity of the results to the assumed DCR limits. In fact, for uniform-angle diagrids, a DCR limit of 2.0 was assumed, while for varying-angle diagrids, a stricter limit of 1.5 was applied due to their classification as atypical structural systems resulting in fewer iterations before instability was reached, particularly for taller structures.

This analysis additionally illustrated the resilience of a diagrid structure in critical circumstances, even when critical members were removed, stability was still maintained. Hopefully, the outcome of this analysis, if imagined into the real world, can lead to even more safe and effective use of diagrid structures. By evaluating which members are most critical in a progressive collapse in diagrid structural performance, this would provide the structural designers some advance clue in what members, would be worth taking action on beforehand, so to increase their structural performance and reduce the potential for a structural failure. Therefore, using the results of the progressive collapse analysis both in the design stage and

the planning phase, gives designers and engineers a way to develop and evaluate structures within a more resilient framework, ensuring better performance under standard use conditions.

The analyses used in the study follow the Matrix-Based Method (MBM), this method provides a simpler and faster approach to the building modelling methods available to the designer and engineer, that imply a higher computational cost. To this end, the MBM was helpful for determining the number of diagrid configurations quantitatively to be more efficient in the development of the diagrid structure, with relatively careful and confident estimates of the performance of individual members or an overall lateral capacity assessment. Therefore, MBM research provides the designer and engineer with an easy and useful way to create more risk aversion in some areas of tracking and optimizing diagrid structures, which is easy to adapt to, especially in the early stages of the design phase, or for quickly evaluating how a diagrid structural system performs.

The MBM model considers any possible shape of diagrid space structure in which the elements exhibit linear elastic behavior and are subjected only to axial forces, considering that the floors remain planar after deformation, behaving as rigid bodies with six degrees of freedom, neglecting the floors within the diagonal modules.

However, to analyze the high-rise building, the MBM has been embedded to the General Algorithm, simplifying the problem, reducing the degrees of freedom to three, (two lateral displacements and one torsional rotation).

The applicable loads include vertical distributed loads and horizontal nodal loads, both used to perform linear static analyses to determine the critical load factor and identify critical members subject to buckling. Furthermore, progressive collapse scenarios can be simulated by iteratively removing critical members and recalculating the structural response. However, not considering the phenomena of plasticity or geometric non-linearity greatly simplifies the analysis; moreover, this method does not include dynamic effects of loads and does not take into account any geometric or manufacturing imperfections, which could affect the overall stability of the structure.

For this reason, there are further opportunities to extend this study and expand the framework of analysis available in MBM methodologies.

In summary, the overall area of structural engineering is slowly moving toward more and more effective and resilient solutions to address the difficulties of modern-day urban spaces, continuing to assess and develop diagrid systems with advanced numerical analysis.

ACKNOWLEDGEMENTS

Ever since I was a child, I have dreamed of achieving this goal, probably because I wanted to follow and surpass my father, whom I have always considered an idol. Or, perhaps, because I loved playing with bricks, and this passion was combined with the fascination that engineering has always exerted on me. The fact is that engineering, in all its forms, has always fascinated me, but civil engineering in particular. The possibility of contributing to the construction of something that can last and become a symbol for a country, like the Colosseum for Italy or the Eiffel Tower for France, has always fueled my dreams. Of course, I admit, it is probably also the fault of my delusions of grandeur and egocentricity.

In fact, those who have known me for a long time know that, even as a child, I used to firmly exclaim: *“When I grow up, I will be the best civil engineer in the world!”* This phrase still echoes in my mind today and continues to push me over my limits whenever I feel on the point of giving up.

During my course of study, several people did not take me seriously: some did not believe in me at all and told me that I would never become anybody, simply because, in their opinion, I did not put enough effort into my studies. However, my not being serious about studying was also fueled by the thought that, sooner or later, I would have to do it once I got into university, so I was mainly trying to enjoy life as much as possible.

On 4 October 2020, after failing the entrance test several times and finally narrowly passing it, my university journey began. With it, also began my time to prove to everyone wrong that I was, in fact, capable of achieving my goals, giving a moral slap in the face to those who had not believed in me or seen me as incapable. However, with the beginning of this new phase of my life, many of the things that had accompanied me up to that point also ended: friends, sport, family time and general free time.

I was ready to give up everything to achieve my goals. I knew the reputation of *“engineering”*, but my hunger was greater. I spent day and night taking courses, arranging notes, completing assignments and studying, never stopping, not even on holidays. However, like everyone else, I had limits. Perhaps because I had never studied so much, or probably because of the few hours of sleep or the loneliness caused by Covid, I was reaching my limit. Engineering was eating me up. I was no longer anything but notes, deadlines, study and exams. I had become a freshman with grades on my transcript. Everything seemed so heavy. I was beginning to hate what, since childhood, I had always wanted. And as I went on, the

phrase that had always pushed me to overcome my limitations became smaller and smaller in my mind: it was turning from a battle scream into a whisper.

And yet, thanks to what was taking everything away from me, I got to know Livia, an extraordinary girl, who was in the same situation as me, with the same ambitions, and with whom I fell madly in love. She is the first person I want to thank wholeheartedly, because without her, I would not have my degree today.

My second thanks go to the University, mainly because it allowed me to meet her, but also because, in addition to having taught me many important notions and introduced me to special people and professors, in recent years, it has opened my eyes to a concept that I had never considered, namely, the error of comparison.

It may sound trivial, but many, because of this mistake, judge themselves as “*failures*” and self-declare themselves “*not enough*”, comparing themselves to those few who manage to finish their studies with top marks in the minimum time. I would like to open their eyes as the university did to me, and I begin to do so with a quote:

“Are all human beings truly equal? Nowadays, wherever you go, people talk about fighting for equality. But although we are all equal at birth, things soon begin to change. Academic efforts are an example of what distinguishes some people, allowing them to rise above others. Furthermore, human beings change over time based on their actions. In the end, equality is just a fantasy, and most of us go through life denying the fact that we live in a meritocracy” (Shōgo Kinugasa, Classroom of the Elite).

My answer is no! Looking back, who is lucky enough to know from an early age who they want to be? Who has the privilege of enjoying life during adolescence without having to think much about studying? Who is lucky enough to meet their soul mate and walk the university path together? And above all, who is lucky enough to be able to study in a perfect context? I'm talking about a context in which you have a brother whose patience you test just to get rid of the stress caused by the hours spent studying, a perfect context in which you have a mother who is always present and supportive, who worries more than you do when you have to take an exam, and a perfect context in which a father, whom you have always seen as an idol, advises and guides you in everything without ever letting you lack anything. That's why I was able to focus on my goals and give my all to achieve them, and for that I want to thank my family, for always being there and supporting me in all aspects, thank you Ale, thank you Mom, thank you Dad. Without you this journey would not have been the same.

I love you all so much.

REFERENCES

- [1] K. S. Moon, J. J. Connor and J. E. Fernandez, “Diagrid structural systems for tall buildings: characteristics and methodology for preliminary design,” *The Structural design of tall and Special Buildings* 16.2, pp. 205-230, 2007.
- [2] Mir M. Ali, Kheir Al-Kodmany, “Tall Buildings and Urban Habitat of the 21st Century: A Global Perspective” *Buildings* 2012, 2, 384-423.
- [3] MELE, Elena, et al. Ruolo dell'acciaio ed esigenze di ricerca nelle grandi architetture. *COSTRUZIONI METALLICHE*, 2010, 62.5: 59-69.
- [4] SARKISIAN, Mark. *Designing tall buildings: structure as architecture*. Routledge, 2016.
- [5] Prasad, “Tall Building Design and Construction”. Structural Guide Civil & Structural Engineering Knowledge Base, 2018.
<https://www.structuralguide.com/tall-building-design-and-construction/>
- [6] “Norme Tecniche per le costruzioni”. Ministero delle Infrastrutture e dei Trasporti, 2018.
- [7] E. Mele. “Ruolo dell'acciaio ed esigenze di ricerca nelle grandi architetture”. In: *Costruzioni metalliche* 2010.
- [8] Prasad, “14 Types of Structural Forms for Tall Buildings”. Structural Guide Civil & Structural Engineering Knowledge Base, 2018.
<https://www.structuralguide.com/structural-forms-for-tall-buildings/>
- [9] BOAKE, Terri Meyer. *Diagrid structures: systems, connections, details*. Walter de Gruyter, 2014.
- [10] LABO, Simone, et al. Esoscheletri tipo diagrid per la riqualificazione degli edifici esistenti in ottica ciclo vita. *COSTRUZIONI METALLICHE*, 2019, 2019.9-10: 24-35.
- [11] MELE, Elena, et al. Non-conventional structural patterns for tall buildings: from diagrid to hexagrid and beyond. *Fratt ed Integrità Strutt*, 2016, 47: 186-208.
- [12] Asadi, E.; Adeli, H. Diagrid: An innovative, sustainable, and efficient structural system. *Struct. Des. Tall Spec. Build.* 2017, 26, e1358.

- [13] Angelucci, G.; Mollaioli, F. Diagrid structural systems for tall buildings: Changing pattern configuration through topological assessments. *Struct. Des. Tall Spec. Build.* 2017, 26, e1396.
- [14] NAIK SWARAL, R.; GANDHI DIPESH, A.; SARVAIYA HIMMAT, K. Structural Investigations on Diagrid Node: A Review, 2024.
- [15] Shi Q., Ying Y. and Wang B., Experimental investigation on the seismic performance of concrete-filled steel tubular joints in diagrid structures, *Structures*, 31, 230–247, (2021).
- [16] Jeong I., Jeong I., Ju Y.K. and Kim S., Experimental and Analytical Investigation of Web-transferred Diagrid Node under Seismic Condition, *International Journal of High-Rise Buildings* 1(1), 29-36 (2012)
- [17] Liu C., Li Q., Lu Z. and Wu H., A review of the diagrid structural system for tall buildings, *Structural Design of Tall and Special Buildings*, 27(4), (2018).
- [18] SCARAMOZZINO, Domenico; LACIDOGNA, Giuseppe; CARPINTERI, Alberto. New trends towards enhanced structural efficiency and aesthetic potential in tall buildings: The case of diagrids. *Applied Sciences*, 2020, 10.11: 3917.
- [19] MOON, Kyoung-Sun; CONNOR, Jerome J.; FERNANDEZ, John E. Diagrid structural systems for tall buildings: characteristics and methodology for preliminary design. *The structural design of tall and special buildings*, 2007, 16.2: 205-230.
- [20] MOON, Kyoung Sun. Sustainable structural engineering strategies for tall buildings. *The Structural Design of Tall and Special Buildings*, 2008, 17.5: 895-914.
- [21] MOON, Kyoung Sun. Optimal grid geometry of diagrid structures for tall buildings. *Architectural Science Review*, 2008, 51.3: 239-251.
- [22] ZHANG, Chonghou; ZHAO, Feng; LIU, Yansheng. Diagrid tube structures composed of straight diagonals with gradually varying angles. *The Structural Design of Tall and Special Buildings*, 2012, 21.4: 283-295.
- [23] ZHAO, Feng; ZHANG, Chonghou. Diagonal arrangements of diagrid tube structures for preliminary design. *The Structural Design of Tall and Special Buildings*, 2015, 24.3: 159-175.

REFERENCES

- [24] MIRNIAZMANDAN, Seyedehaida, et al. Mutual effect of geometric modifications and diagrid structure on structural optimization of tall buildings. *Architectural science review*, 2018, 61.6: 371-383.
- [25] LACIDOGNA, G.; SCARAMOZZINO, D.; CARPINTERI, A. Influence of the geometrical shape on the structural behavior of diagrid tall buildings under lateral and torque actions. *Developments in the built environment*, 2020, 2: 100009.
- [26] SCARAMOZZINO, Domenico, et al. Selection of the optimal diagrid patterns in tall buildings within a multi-response framework: Application of the desirability function. *Journal of Building Engineering*, 2022, 54: 104645.
- [27] Theory Profile Library Checked Sections – Nemetschek Scia Engineer, 2010. https://help.scia.net/download/16.0/en/Cross-sections_Theory_enu.pdf
- [28] MONTUORI, Giovanni Maria, et al. Design criteria for diagrid tall buildings: Stiffness versus strength. *The Structural Design of Tall and Special Buildings*, 2014, 23.17: 1294-1314.
- [29] MONTUORI, Giovanni Maria, et al. Secondary bracing systems for diagrid structures in tall buildings. *Engineering Structures*, 2014, 75: 477-488.
- [30] LACIDOGNA, Giuseppe; SCARAMOZZINO, Domenico; CARPINTERI, Alberto. A matrix-based method for the structural analysis of diagrid systems. *Engineering Structures*, 2019, 193: 340-352.
- [31] MELE, Elena, et al. Diagrid structures for tall buildings: case studies and design considerations. *The Structural Design of Tall and Special Buildings*, 2014, 23.2: 124-145.
- [32] LIU, Chengqing; MA, Kaiqiang. Calculation model of the lateral stiffness of high-rise diagrid tube structures based on the modular method. *The structural design of tall and special buildings*, 2017, 26.4: e1333.
- [33] CARPINTERI, Alberto; CARPINTERI, Andrea. Lateral loading distribution between the elements of a three-dimensional civil structure. *Computers & structures*, 1985, 21.3: 563-580.

- [34] LACIDOGNA, Giuseppe, et al. Diagrid systems coupled with closed-and open-section shear walls: Optimization of geometrical characteristics in tall buildings. *Procedia Manufacturing*, 2020, 44: 402-409.
- [35] BERNUZZI, Claudio. Progetto e verifica delle strutture in acciaio: secondo le Norme Tecniche per le Costruzioni 2018 e l'Eurocodice 3. 2018.
- [36] MENDIS, Priyan, et al. Wind loading on tall buildings. *Electronic Journal of Structural Engineering*, 2007.
- [37] ASCE, Minimum Design Loads for Buildings and Other Structures, American Society of Civil Engineers.
- [38] ALBITOS, Bonierose. *Analysis of the optimal diagrid geometry for tall buildings based on the desirability function*. 2021. Master Thesis. Politecnico di Torino.
- [39] CARPINTERI, Alberto. *Advanced structural mechanics*. CRC Press, 2017.
- [40] Vincenzo Franciosi, *Scienza delle Costruzioni Vol. III, Tomo II (Teoria delle Strutture)*, Liguori editore, Napoli 1971.
- [41] PASQUALE, Luca. Comportamento post-critico di strutture reticolari saldate, Tesi 2011-12.
- [42] PORTLAND CEMENT ASSOCIATION, et al. An Engineer's Guide to: Concrete Buildings and Progressive Collapse Resistance. 2005.
- [43] Ricardo Liberato, "All Gizah Pyramids", photography [Online]. Available: https://en.wikipedia.org/wiki/File:All_Gizah_Pyramids.jpg. [Accessed: Apr. 3, 2025].
- [44] Hardnfast, "Ancient ziggurat at Ali Air Base Iraq", photography [Online]. Available: https://en.m.wikipedia.org/wiki/File:Ancient_ziggurat_at_Ali_Air_Base_Iraq_2005.jpg. [Accessed: Apr. 3, 2025].
- [45] John R. Chapin, "The Great Chicago Fire, an artists rendering, *Chicago in Flames -- The Rush for Lives Over Randolph Street Bridge*", photography [Online]. Available: <https://it.m.wikipedia.org/wiki/File:Chicago-fire1.jpg>. [Accessed: Apr. 3, 2025].

REFERENCES

- [46] Chicago Architectural Photographing Company, "Exterior of the Home Insurance Building by architect William Le Baron Jenney in Chicago, Illinois", photography [Online]. Available: https://it.m.wikipedia.org/wiki/File:Home_Insurance_Building.JPG. [Accessed: Apr. 3, 2025].
- [47] Nepenthes, "Burj Khalifa in 2025", photography [Online]. Available: https://www.wikiwand.com/File:Burj_Khalifa.jpg. [Accessed: Apr. 3, 2025].
- [48] "Havemeyer Building, Photographic Plate Dey, Church and Cortlandt Street, 1895", photography [Online]. Available: <https://old.skyscraper.org/tenandtaller/havkv.jpg>. [Accessed: Apr. 3, 2025].
- [49] Dave Burk © SOM, "One Maritime Plaza in 2023", photography [Online]. Available: https://www.som.com/wp-content/uploads/2017/10/516209_000_N2_large-1687894807-scaled.jpg. [Accessed: Apr. 3, 2025].
- [50] Photo © Hedrich Blessing, "Dewitt Chestnut Apartments", photography [Online]. Available: https://www.som.com/wp-content/uploads/2021/07/dewittchestnutapts_788x900_hedrichblessing_01jpg.jpg. [Accessed: Apr. 3, 2025].
- [51] "Shanghai Tower", photography [Online]. Available: <https://www.buildingcue.it/wp-content/uploads/2020/12/shangai-tower-ctbuh.jpg>. [Accessed: Apr. 3, 2025].
- [52] Jeffmock, "Aerial view of World Trade Center, and surrounding area of New York, with Downtown Manhattan in the foreground, looking north easterly", photography [Online]. Available: [https://en.m.wikipedia.org/wiki/File:World_Trade_Center,_New_York_City_-_aerial_view_\(March_2001\).jpg](https://en.m.wikipedia.org/wiki/File:World_Trade_Center,_New_York_City_-_aerial_view_(March_2001).jpg). [Accessed: Apr. 3, 2025].
- [53] Bernt Rostad, "John Hancock Center in Chicago, Illinois", photography [Online]. Available: https://it.m.wikipedia.org/wiki/File:John_Hancock_Center_in_mist.jpg. [Accessed: Apr. 3, 2025].

- [54] jberginc, "Sears Tower", photography [Online]. Available:
https://as2.ftcdn.net/jpg/00/03/54/81/1000_F_3548107_7vtZxpQGu6ULhVsB1Jvt2tglrOhISKYQ.jpg. [Accessed: Apr. 3, 2025].
- [55] Dreamword, "Photograph of Hearst Tower in Manhattan taken from the 24th floor of a nearby building", photography [Online]. Available:
[https://commons.wikimedia.org/wiki/File:Hearst_Tower_\(August_2024\).jpg](https://commons.wikimedia.org/wiki/File:Hearst_Tower_(August_2024).jpg).
[Accessed: Apr. 3, 2025].
- [56] "Shabolovka Radio Tower, Moscow", photography [Online]. Available:
https://images.skyscrapercenter.com/building/shukhovtower_ext-overall_publicdomain.jpg. [Accessed: Apr. 3, 2025].
- [57] Paste, "30St Mary Axe is a skyscraper in London's main financial district", photography [Online]. Available:
https://en.m.wikipedia.org/wiki/File:30_St_Mary_Axe,_%27Gherkin%27.JPG.
[Accessed: Apr. 3, 2025].
- [58] CEphoto, Uwe Aranas, "Beijing, China: National Stadium, also known as "birds nest"", photography [Online]. Available:
https://commons.wikimedia.org/wiki/File:Beijing_China_Beijing-National-Stadium-01.jpg. [Accessed: Apr. 3, 2025].
- [59] Charlie fong, "The night view of Beijing National Aquatics Center", photography [Online]. Available:
<https://it.wikipedia.org/wiki/File:%E5%9B%BD%E5%AE%B6%E6%B8%B8%E6%B3%B3%E4%B8%AD%E5%BF%83%E5%A4%9C%E6%99%AF.jpg>. [Accessed: Apr. 3, 2025].